

ENERGY LABORATORY

MASSACHUSETTS INSTITUTE
OF TECHNOLOGY

ULTRASONIC FLOWMETERING WITH
REFLECTED PULSES

by

David C. Hoyle
Leon R. Glicksman
Carl R. Peterson

Energy Laboratory
Report No. MIT-EL-84-016

September 1984



Ultrasonic Flowmetering with Reflected Pulses

by

David C. Hoyle
Leon R. Glicksman
Carl R. Peterson

Abstract

A transit time type ultrasonic flowmeter was tested with two different reflected pulse trajectories in flowing air at ambient conditions against an orifice meter. The flowmeter was designed to be highly accurate, to require minimal excavation for installation (both transducers to be placed on the upper surface of the pipe), and to require no service shutdown for installation or calibration. The two trajectories were two successive tilted diameters with a single reflection, and three successive tilted midradius chords with two reflections. High frequency (100 kHz) narrowband pulses were used. Both ultrasonic flowmetering configurations were tested in 12 inch pipe in fully developed turbulent flow, and in the abnormal flow downstream of a 90 degree elbow. The velocity range was 5.5 fps - 25 fps. The triple midradius chord configuration performed extremely well, with maximum errors of 1.3, and 2.0 percent of reading, in the normal and abnormal flows, respectively. The double tilted diameter configuration gave maximum errors of 7.2, and 9.3 percent of reading in the normal and abnormal flows, respectively. Recommendations for field testing of the two ultrasonic configurations are made.

A numerical simulation of ultrasonic flowmetering in an abnormal flow using single, double, and triple midradius chords, and a double tilted diameter was conducted prior to the experimental tests. The simulation showed that the triple midradius chord and double tilted diameter were, respectively, the most accurate and second most accurate of the four trajectories.

An amplitude difference between the acoustic signals received at the upstream and downstream transducers, in flowing air, was measured. This amplitude difference is believed to be caused by flow effects. A two-dimensional model was developed to explain the amplitude difference in terms of focusing of the downstream ultrasonic beam and defocusing of the upstream beam, due to velocity gradients. The focusing and defocusing predicted by the model was found to be too small to explain the amplitude difference, however.

Table of Contents

	<u>Page</u>
Title Page	1
Abstract	2
List of Figures	6
List of Tables	9
Acknowledgements	10
Chapter 1 Introduction	11
Chapter 2 Background	15
2.1 Design Specifications for the New Flowmeter	15
2.1.1 Functional Requirements	15
2.1.2 Installation and Service Requirements	16
2.2 The Dynamic Head Device Presently Employed - The Annubar	16
2.3 Selection of an Appropriate Alternative Flowmeter	17
2.3.1 Initial Phases of the Present Research	18
2.4 Past and Present Ultrasonic Flowmetering Techniques	21
2.4.1 Direct Pulse Ultrasonic Flowmeters for Gases	21
2.4.2 Reflected Pulse Ultrasonic Flowmeters	25
Chapter 3 Derivation of the Ultrasonic Flowmetering Equations	32
3.1 Calculating Cross Sectional Average Velocity from Ultrasonic Measurements	32
3.2 Self-Calibration Technique	34
3.3 Ultrasonic Flowmetering under Abnormal Conditions	36
3.3.1 Ultrasonic Flowmetering in Flow with Axisymmetric Swirl	36

Chapter 4	Numerical Simulation of Ultrasonic Flowmetering Downstream of an Elbow	39
4.1	Objectives of the Simulation	39
4.2	Simulation Techniques	40
4.3	Results and Conclusions	42
Chapter 5	Experimental Hardware and Procedure	47
5.1	The Test Rig	47
5.2	Ultrasonic Flowmetering Hardware	49
5.2.1	Panametrics' Model C508R (Modified Model 6000)	50
5.2.1.1	Pulsing and Receiving	50
5.2.1.2	Timing Method	51
5.2.1.3	The Non-Fluid Transit Time Component t_w	52
5.2.1.4	Cycle Jumping and Pulse Timing	52
5.2.1.5	Data Output Format	53
5.2.2	The Transducers	53
5.2.2.1	Transducer Mounting	55
5.2.2.2	Application of Plastic Wrap to Transducers	55
5.2.2.3	Coaxial Transducer Cables	56
5.3	Reference Instrumentation	57
5.4	Experimental Methods	58
5.4.1	Preparations for Data Acquisition	58
5.4.1.1	Electronics Adjustments	59
5.4.2	Data Acquisition	60
5.4.2.1	Making an Ultrasonic Velocity Measurement	61
5.4.2.2	A Comparison of Triple Midradius Chord and Double Tilted Diameter Cycle Jumping	63
5.5	Data Analysis and Reduction	64
5.5.1	Reduction of Ultrasonic Data	65
5.5.2	Accuracy of Ultrasonic Velocity Measurements	66
5.5.3	Orifice Meter Data Reduction	67
5.5.4	Accuracy of Orifice Meter Measurements	69

Chapter 6	Ultrasonic Flowmetering Results	84
6.1	Triple Midradius Chord Results	85
6.2	Double Tilted Diameter Configuration Results	86
Chapter 7	Conclusions and Recommendations	95
7.1	Conclusions	95
7.2	Recommendations	96
Appendix A	An Experimental Investigation into Factors Affecting Received Signal Amplitude	98
A.1	Introduction	98
A.2	Objectives	99
A.3	Methods	100
A.4	Results and Conclusions	100
Appendix B	The Effect of Velocity Gradients on Ultrasonic Beam Angle	107
Appendix C	Ultrasonic Flowmetering Data	111
References		135

List of Figures

<u>Figure</u>		<u>Page</u>
Figure 2.1	Schematic of Annubar Installation	26
Figure 2.2	a. Double Tilted Diameter Trajectory (One Reflection)	27
	b. Single Tilted Diameter Trajectory (No Reflection)	
Figure 2.3	Triple Midradius Chord Trajectory	28
Figure 2.4	Panometrics-Exxon Direct Pulse Trajectories	29
Figure 2.5	Accuracy of Panometrics-Exxon Ultrasonic Flowmeter Versus Venturi Meter	30
Figure 2.6	Schematic of British Gas Four-Chord Ultrasonic Flowmeter	31
Figure 3.1	Ultrasonic Pulses Traversing a Uniform Flow at an Arbitrary Angle	38
Figure 3.2	Profile Correction Factor for a Midradius Chord	38
Figure 3.3	Axial View of Ultrasonic Interrogation in a Duct with Axisymmetric Swirl	38
Figure 4.1	Ultrasonic Trajectories Tested in the Simulation	44
Figure 4.2	Simulation Geometry	45
Figure 4.3	Chords of Ultrasonic Interrogation and Simulated Abnormal Velocity Profile	46
	a. Single Midradius Chord b. Profile	
	c. Single Diameter d. Profile	
Figure 5.1	Schematic of M.I.T. Test Facility	71
Figure 5.2	Photograph of Ultrasonic Test Section	72
Figure 5.3	Photograph of Blower Outlet	73
Figure 5.4	a. Oscillogram of "Sync" Signal	74
	b. Oscillogram of Received Signals	

Figure 5.5	Oscillogram of Received Signal (Expanded)	74
Figure 5.6	Oscillogram of Received Signal and Filtering Window	75
Figure 5.7	Oscillograms: a. Integration Level b. Integrated Threshold	76
Figure 5.8	Oscillograms: a. Integrated Threshold b. Zero Cross Signal c. "Stop" Signal	76
Figure 5.9	a. Histogram of Typical Downstream Transit Time Distribution b. Histogram of Typical Upstream Transit Time Distribution c. Histogram of Typical Transit Time Difference Distribution	77
Figure 5.10	Sample Flowmeter Data Printout	78
Figure 5.11	Schematic of Transducer	79
Figure 5.12	l. Double Tilted Diameter Transducer Saddle r. Triple Midradius Chord Transducer Saddle	79
Figure 5.13	a. Transducer with Locking Collar and Fittings b. Transducer Mounted in Saddle	80
Figure 5.14	a. Transducer with Plastic Collar Removed b. Transducer and Plastic Collar with Plastic Wrap in Place	81
Figure 5.15	Triple Midradius Chord and Double Tilted Diameter Data Rejection Versus Velocity in Fully Developed Flow	82
Figure 5.16	Triple Midradius Chord and Double Tilted Diameter Data Rejection Versus Velocity in the Abnormal Flow 6D from Elbow	83
 Figures Chapter 6: Area Averaged Velocity Measurements, Ultrasonic Flowmeter Versus Orifice		
Figure 6.1	Triple Midradius Chord Ultrasonic Flowmeter in Fully Developed Flow	89

Figure 6.2	Triple Midradius Chord Ultrasonic Flowmeter 10D from Elbow	90
Figure 6.3	Triple Midradius Chord Ultrasonic Flowmeter 6D from Elbow	91
Figure 6.4	Double Tilted Diameter Ultrasonic Flowmeter in Fully Developed Flow	92
Figure 6.5	Double Tilted Diameter Ultrasonic Flowmeter 6D from Elbow	93
Figure 6.6	Double Tilted Diameter Ultrasonic Flowmeter, Pulses Reflected from Roofing Material	94
Figure A.1	Zero-Flow Received Signal Amplitude Minus Received Signal Amplitude with Flow Versus Flow Velocity	105
Figure A.2	Standard Deviation of Received Signal Amplitude Versus Flow Velocity	106
Figure B.1	Schematic Showing Convergence of Downstream Ultrasonic Beam (Convergence Greatly Exaggerated)	109
Figure B.2	Wave Element Rotation Diagram	110

List of Tables

<u>Table</u>		<u>Page</u>
Table 4.1	Numerical Simulation Results	43
Table 5.1	Uncertainties Associated with Δt Measurements and Ultrasonic Velocity Measurements at Maximum and Minimum Flowrates	70
Table 6.1	Ultrasonic Flowmetering Results: Triple Midradius Chord Configuration	87
Table 6.2	Ultrasonic Flowmetering Results: Double Tilted Diameter Configuration	88
Table A.1	Upstream and Downstream Received Signal Amplitude Measurements at Maximum Flowrate	103
Table A.2	Upstream Received Signal Amplitude Measurements at Different Flowrates	104

Acknowledgements

The authors are very grateful to Consolidated Edison of New York for their financial support of this project. Special thanks are due to Costas Continos and Hans Mertens of Gas Systems, and to Ben Lee of Research and Development, for their advice and assistance.

Larry Lynnworth, and others at Panametrics were an invaluable source of technical assistance throughout the course of the project. We wish to thank Mr. Lynnworth for all his help, which included correcting a portion of the manuscript. Thanks are also due to Panametrics for the loan of the flowmetering package used in the experimental phases of this project.

Chapter 1 Introduction

Consolidated Edison of New York City has expressed the need for a new gasmeter for accurately monitoring large diameter interdistrict gas transmission lines for loss due to theft or leakage. The present paper describes the successful continuation - to the point of making recommendations for field testing - of a previous research effort aimed at developing a new flowmeter for Con Edison.

The new flowmeter uses ultrasonic flowmetering technology in a novel way to meet Con Edison's four major design specifications¹: the flowmeter should be accurate to 0.5 percent of totalized flow over one year; it should be much simpler to install than a conventional flowmeter, essentially meaning that excavation be limited to that necessary to expose the upper surface of a buried main; its installation must not require service shutdown; and, the flowmeter should not require zero-flow calibration once installed in the gas main.

The new flowmeter described here offers accuracy of 1.3 percent of reading (compared to an orifice meter) in fully developed flow, and accuracy of 2.0 percent of reading at any orientation relative to an elbow as close as six pipe diameters upstream. Installation of the flowmeter requires less circumferential access to the pipe exterior than any other ultrasonic flowmeter offering comparable accuracy. Like many contemporary ultrasonic flowmeters, the new flowmeter can be inserted into a live gas main by a process known as "hot-tapping," and it requires no zero-flow calibration.

The task of developing the new flowmeter was first approached by Bender¹, who began by developing a set of design requirements for the replacement flowmeter in conjunction with Con Edison, the four most important of which have been presented above. Bender considered a number of candidate flowmetering schemes before ultimately choosing the ultrasonic transit time method on the basis of its "mechanical simplicity

and potential for high accuracy."

A transit time ultrasonic flowmeter measures flow velocity by sending acoustic pulses upstream and downstream in the flowing fluid between two transducers, each of which acts alternately as sender and receiver. This process will be referred to as "ultrasonic interrogation." An acoustic pulse always propagates relative to a fluid at the velocity of sound in the fluid, regardless of the motion of the fluid. However, the absolute velocity of an acoustic pulse, i.e., relative to stationary points, in a flowing fluid is the vector sum of the sonic velocity and the flow velocity. An upstream traveling pulse travels between stationary points in a flowing fluid at an absolute velocity less than the speed of sound, and a downstream traveling pulse travels between stationary points in a flowing fluid at a velocity greater than the speed of sound. For ultrasonic flowmetering, this means that there is a difference between the upstream and downstream pulse flight times between transducers. The average velocity of the fluid flowing through the path traveled by the ultrasonic pulses can be calculated either from a combination of the individual transit times, or from the transit time difference. The path traveled by the ultrasonic pulses in the flowing fluid will be referred to as the "ultrasonic trajectory." The ultrasonic trajectory can be direct, in which case the pulses propagate along an unbroken straight line path between the two transducers, or reflecting, in which case the the pulses are reflected from the pipe wall as they travel between the transducers. The combination of an ultrasonic trajectory and the placement of the transducers to initiate that trajectory will be referred to as an "ultrasonic configuration." Typical direct and reflecting trajectories are shown in Figure 2.2.

Because the at the time Bender was doing his work ultrasonic flowmeters were of the direct type,^{5,17} and required that transducers be placed on opposite sides of the pipe - clearly violating the Con Edison requirement of top-insertability - Bender developed an ultrasonic flowmeter

in which the shock pulses used to interrogate the flow were reflected off of the bottom of the pipe at a point midway between two top-mounted transducers. This "double tilted diameter" trajectory is shown schematically in Figure 2.2a.¹ Bender built a laboratory prototype in which the shock pulses were generated by a starter's pistol, and tested it against an orifice meter. Bender's prototype met the design requirements of being top-insertable; with proper shock generators it would also have been insertable without service interruption. The prototype used a novel self-calibration technique which meant that it needed no zero-flow calibration. The prototype failed to meet the accuracy requirement, however. Furthermore, it was not clear that a suitable shock pulse generator would be easily found or developed.

The present research project picked up where Bender left off with the immediate goal of developing a shock pulse generator, but shock pulse interrogation of the gas was soon abandoned in favor of interrogation using conventional high frequency narrowband pulses which are much easier to generate. In preparation for further laboratory testing of reflected pulse ultrasonic flowmetering using high frequency pulses, an ultrasonic flowmetering electronics package, containing pulsing and receiving circuitry, timing circuitry, and a microprocessor for data averaging was borrowed from Panametric's, Inc., of Waltham, Mass. Two ultrasonic transducers were purchased from Panametrics.

Prior to conducting ultrasonic flowmetering tests in the laboratory, a numerical study was done to see which pulse trajectories were worth testing, based on the ability of each trajectory to accurately measure the average velocity of both simulated normal and abnormal flows in a circular duct. The interest in accurate performance under distorted flow conditions is motivated by a desire to ease the very stringent requirement for undistorted flow associated with some meters. Flow interrogation and velocity averaging over an extended pathlength offers the potential to overcome abnormal profile

induced errors. Two reflected pulse trajectories were chosen for lab testing based on the results of this study. One was Bender's (Figure 2.2a), and the other was a double reflection trajectory in which the pulses traveled along three successive midradius chords (Figure 2.3).²

Tests of the two ultrasonic flowmetering trajectories were conducted in the M.I.T. flowmeter test facility in fully developed flow, and in the abnormal flow downstream of a 90 degree elbow, using an orifice meter as standard. Part of the testing involved investigations into the effects of flow turbulence on the amplitude of the electrical signal generated at the receiving transducer (upstream and downstream). The received signal amplitude played an important part in pulse timing.

The M.I.T. flowmetering tests showed the triple midradius chord trajectory to be more accurate than the double tilted diameter trajectory in both types of flow. It is recommended that field tests be conducted using the triple midradius trajectory.

Chapter 2 Background

The purpose of the ultrasonic flowmeter described in this thesis is to provide an accurate and reliable flowmeter to be used by Consolidated Edison to monitor interdistrict natural gas lines for loss and theft. The design specifications for the new flowmeter are described. The characteristics of the dynamic head device presently employed are given. The decisions made by Bender in electing to use ultrasonic flowmetering technology are discussed. The preliminary phases of the present research work are presented. The chapter concludes with a brief review of contemporary ultrasonic flowmetering technology.

2.1 Design Specifications for the New Flowmeter

2.1.1 Functional Requirements

Consolidated Edison has expressed a desire for accuracy from the flowmeter of plus or minus 0.5 percent of total volumetric flow. Bender translated this figure into a minimum resolveable flowrate equal to one percent of the flowrate in an interdistrict line averaged over one year. The minimum resolveable flowrate can be represented as a band of constant vertical width on a graph of volumetric flowrate plotted against time, representing the magnitude of the tolerance on the measurement of any flowrate. The minimum resolveable flowrate dictates the fineness of resolution of the flowmeter, or, said in another way, the lowest flowrate the meter must be able to detect.

The velocity range over which the new flowmeter must operate was specified to Bender as 0-30 feet per second, with flow reversals. It was subsequently mentioned, during the course of the present work, that the meter might have to handle velocities as high as 100 feet per second.²⁶ The line size at the site chosen for the first tests was to be 24

inches.

Because service in the interdistrict gas lines can at no time be interrupted, and hence no zero point can be set, the flowmeter must either be able to calibrate itself in flowing gas or require no in-pipe calibration.¹

2.1.2 Installation and Service Requirements

Since line service also cannot be interrupted for installation, the line must be hot-tapped for meter insertion, a widely-practiced procedure. To lessen excavation costs meter placement has been restricted to the upper surface of the gas main.

Finally, the flowmeter must offer long life and high reliability in the 160 psig, corrosive environment of the gas main.¹

2.2 The Dynamic Head Device Presently Employed - The Annubar

The Annubar is best envisioned as an array of four pitot tubes spaced along a diameter such that the impact ports interrogate equal annular areas of the pipe in which velocity is to be measured. Physically the Annubar is a hollow tube of square cross section which is inserted into the pipe along a diameter, oriented with a sharp corner facing upstream. A schematic of an Annubar installation is shown in Figure 2.1. The impact ports located on the upstream edge open into the interior of the square body from which an "interpolating tube" carries an average impact pressure reading to the outside of the pipe. A suction port, located at the pipe centerline on the downstream edge of the Annubar is connected to the outside of the pipe by a tube running through the Annubar body. The average velocity over the pipe cross section is proportional to the square root of the pressure differential between the two Annubar outputs.

The manufacturer claims accuracy of plus or minus one percent of reading for a properly installed Annubar. Correct Annubar installation for high accuracy requires a minimum of

eleven diameters of straight pipe between the Annubar and an out-of-plane elbow, and minimum of thirty diameters between the Annubar and a partially open valve. A peculiar feature claimed for the Annubar is that, when installed in-plane two diameters downstream of the centerline of an elbow, it will provide a velocity reading accurate to plus or minus three percent of value and, after individual calibration, to plus or minus one percent of value. Four to five diameters of straight pipe are required downstream of the Annubar.³

Installation of an Annubar requires access to only one side of the pipe, and mounts are available which allow hot-tapping of the pipe. Annubars are rated to 2000 psig. The Annubar has a fairly limited useful flow range of approximately 3.5:1 when used with standard differential pressure instrumentation.³

The Annubar has the obvious disadvantage that the upstream impact ports are subject to fouling. Another disadvantage of the Annubar is that because it interrogates the flow only along a single chord of the duct - in this case, a diameter - it is subject to profile abnormality errors. Tests of an Annubar in the M.I.T. facility six pipe diameters downstream of a 90 degree elbow showed variations of up to 4.6 percent between Annubar velocity measurements made in the plane of the elbow and those made out of the plane of the elbow.

2.3 Selection of an Appropriate Alternative Flowmeter

Bender considered a total of nine flowmetering techniques as candidates for the new flowmeter, including hot wire and pitot tube arrays, an internally assembled turbine meter, pressure drop over a known length of tubing inserted into the main, and a variable diameter orifice plate whose area would change to maintain a constant pressure drop. The most promising candidates, according to Bender, were an internally assembled turbine meter with counterrotating blades and the ultrasonic techniques. The turbine meter would have been

installed in the main by first inserting and anchoring a centerbody, and then sequentially inserting the blades into two spindles on the centerbody. Whereas counterrotating turbine meters have been used successfully to accurately measure velocity in the presence of swirl, such a device was deemed too complex, mechanically. Bender ultimately chose to pursue ultrasonic technology "on the basis of its mechanical simplicity and potential for higher accuracy."¹

In designing his ultrasonic flowmeter Bender made two fundamental decisions. The first was to use a reflected-pulse trajectory so that both transducers could be located on the same side of the gas main, in accordance with the design specification of top-insertability. This transducer configuration was a major change from the opposed transducer configuration used in two contemporary ultrasonic flowmeters,^{5,17} which clearly rendered them unsuitable for Con Edison's application. The reflected-pulse and opposed transducer configurations are shown schematically in Figure 2.2. The second of Bender's decisions was to use shock pulses to interrogate the gas flow rather than high frequency pulses - a decision based primarily on the reasoning that acoustic noise and roughness of the reflecting surface on the order of the pulse wavelength would distort or mask the high frequency acoustic signals.

Bender's flowmeter used a novel technique for self-calibration in flowing gas, which will be explained in section 3.2. Contemporary ultrasonic flowmeters were not completely self-calibrating once installed in the gas main.

2.3.1 Initial Phases of the Present Research

The present research project began as direct follow-up of Bender's work, with the initial goal of developing a highly reliable shock pulse generator suitable for field testing. Bender had generated shock pulses using a starter's pistol. The redirection of the research away from shock pulse flow interrogation to the present high frequency interrogation came

as the result of experimental work and further literature studies.

It was decided to investigate the possibility of generating mild shocks using piezoelectric transducers or other transducers normally used to generate high frequency tone bursts. A telephone conversation with a manufacturer of piezoelectric transducers for rangefinding indicated that piezoelectric transducers were simply not suitable for shock generation because of their tendency to "ring."⁴ The experiments in shock generation were therefore focused, initially, on the Polaroid ultrasonic transducer.

Attempts were made to generate shock pulses with a Polaroid transducer by pulsing it with a 500 volt peak-to-peak square wave. These pulses were created by switching a 500 V power supply on and off using a high voltage transistor. The output of the transducer was, unfortunately, nothing more than the 50 kHz pulse it was designed to produce. The transducer output was measured using a Bruel and Kjaer one-eighth inch microphone with a frequency response of up to 120 kHz.

Although the Polaroid transducers failed as shock generators, reflected pulse experiments performed with a pair of Polaroid transducers - one connected to a Polaroid rangefinding circuit and acting as the sender, and the other connected to a biasing voltage and monitored on an oscilloscope - were more successful. Clean signals were received with the transducers mounted in a configuration similar to Bender's, 40 inches apart in an 11 inch diameter plastic pipe. A layer of five-sixteenths inch nuts and bolts scattered on the pipe bottom at the point of reflection caused signal attenuation, but did not seem to distort the received signal.

This success with reflected high frequency pulses prompted a meeting with Mr. Larry Lynnworth of Panametrics, Inc., Waltham, MA, co-author of a 1977 paper on ultrasonic flowmetering of natural gas using non-reflecting high frequency pulses.¹⁷ Based on the favorable results obtained

with reflected high frequency pulses mentioned above, on Lynnworth's success with similar experiments,²⁷ and on information Lynnworth provided on the use of reflected high frequency pulses in liquid flow measurements, it was decided to abandon broadband shock pulses in favor of narrowband high frequency pulses.

Having been brought up to date by Lynnworth on the state of the art of ultrasonic flowmetering in gases, it became clear that two years after Bender began his work contemporary ultrasonic flowmeters were still not suitable for Con Edison's application. A brief review of the evolution of the state of the art of ultrasonic flowmetering in gases follows in Section 2.4. It will suffice here to state that contemporary ultrasonic flowmeters using the opposed-transducer configuration were not top-insertable, nor were they completely self-calibrating once installed in the gas main, disadvantages acknowledged by Bender. The additional Consolidated Edison requirement of high accuracy, not met by Bender's prototype, also came into question: ultrasonic flowmeters interrogating the flow along a "tilted diameter" were, like the Annubar, unable to measure off-diameter profile abnormalities such as those existing downstream of an elbow. A simple numerical study was done to aid in the selection of reflected pulse trajectories to be tested in the laboratory. The accuracy of Bender's trajectory in the simulated flow downstream of an elbow was compared with that of trajectories in which the pulses traveled along two, and three successive midradius chords (Figure 4.1). This study is discussed in Chapter 4. It was decided that the present research program should focus on evaluating the performance of the double tilted diameter and triple midradius chord reflected-pulse flowmetering configurations, both of which would be top-insertable and self-calibrating. Bender's trajectory, although it was found to be subject to small errors caused by profile asymmetry in the numerical simulation, was chosen for its simplicity. The triple midradius trajectory was chosen

because of its potential for providing accurate velocity measurements in abnormal flows. This potential for high accuracy, inferred from the large portion of the duct interrogated by this configuration, was verified by the numerical study. Both configurations would be tested in fully developed flow, and in the abnormal flow downstream of a 90 degree elbow, using an orifice meter as the standard.

2.4 Past and Present Ultrasonic Flowmetering Techniques

Examples of past and current ultrasonic flowmeter designs are presented under two broad categories. "Direct Pulse Ultrasonic Flowmeters" are those in which the pulses propagate along an unbroken straight line path between the two transducers. "Reflected Pulse Ultrasonic Flowmeters" are those in which the pulses are reflected from the pipe wall (or from a plate suspended in the flow) as they travel between the two transducers. The intent is not to give a complete history, nor a complete review of the state of the art, but to provide an idea of the context in which the present research project has evolved.

2.4.1 Direct Pulse Ultrasonic Flowmeters for Gases

The ultrasonic flowmeters described below offer the following advantages over orifice or venturi meters:

- Virtually zero pressure drop across the meter.
 - Ability to measure flowrate over a wide range, 50:1 or more.
 - Most can be installed in live mains by "hot tapping," which means lower installation cost.
 - All measure bi-directional flow, and indicate flow direction.
- In addition, all claim accuracy comparable to, or superior to orifice or venturi meters. All are designed to withstand the corrosive environment of a natural gas main, and line pressures on the order of 1000 psig.

These meters also possess the following disadvantages, making most of them unsuitable for Consolidated Edison's application:

- Most use the opposed transducer configuration, meaning that they are not top insertable.
- Most interrogate the gas flow along only a single chord, making them subject to error caused by abnormal flow profiles.
- None is known to be self-calibrating once installed in the gas main.

Specific advantages and disadvantages are listed under each flowmeter. The specifications given represent actual field or laboratory test conditions, and not theoretical limits.

Hamilton Standard Sonimeter 1350.⁵ Original design 1965, redesign 1973.

Description: Contrapropagation type, transit time type. Interrogated flow along tilted diameter using shock pulses generated by a fast-acting valve. Shown schematically in Figure 2.2b.

Line Size: Tested in 8, 20, 24, and 30 inch lines.

Flow Range: One installation experienced 5-60 fps.

Pulse Repetition Rate: 10 upstream-downstream pairs every 3 minutes.

Accuracy: One installation gave plus or minus 0.44 percent repeatability versus an orifice for one day totalized flow.

Advantages: Easily installed by two men; portable.

Disadvantages: Low pulse repetition rate - unsuitable for measuring pulsating or otherwise unsteady flow. Complex mechanical pulse generator of questionable reliability. Installation required access to more than 180 degrees of pipeline exterior. Interrogation along a single tilted diameter subject to flow profile abnormality errors.

Panametrics' Tests with Columbia Gas.¹⁶ Model 7000 Flowmeter.
 Description: Transit time type. Sealed piezoelectric transducers with impedance matchers pulsed with a modulated 100 khz signal. Tilted diameter trajectory.
 Figure 2.2b.

Line Size: 24 inches.

Flow Range: 1 - 50 fps.

Line Pressure: Not specified.

Pulse Repetition Rate: 250 pulses per second, in one direction only. Pulsing direction reversed every 4 seconds.

Accuracy: Agreement with multiple run orifice station within plus or minus 0.5 percent (whether this means percent of reading or percent of full scale is not stated).

Advantages: High pulse repetition rate. No mechanical pulse generator.

Disadvantages: Installation requires access to more than 180 degrees of pipeline exterior. Single diametral interrogation subject to profile abnormality errors.

Panametrics - Exxon Flare Gas Meter Model 7100.⁶

Description: Transit time type. Sealed piezoelectric transducers with impedance matchers pulsed with 100 kHz bursts. The following direct trajectories were used at different locations: Full, and one-half tilted diameters, and full, and one-half midradius chords; these configurations are illustrated in Figure 2.4. The impedance matchers and one-half midradius chords are covered by Panametrics' patents.

Line Sizes: 6 inches to 30 inches.

Flow Range: 0.1 - 30 fps in flare gas; up to 85 fps in 10 inch diameter lab test rig.

Line Pressure: Up to 450 psig.

Repetition Rate: Interrogation direction reversed approximately 100 times per second.

Accuracy: Presented graphically in terms of agreement with venturi meters. See Figure 2.5.

Advantages: High pulse repetition rate allows accurate measurement of unsteady flow. No mechanical pulse generator. One-half tilted diameter, and one-half midradius chord trajectories mean that only approximately 90 degrees of the pipe exterior must be accessible for meter installation.

Disadvantages: Tilted diameter and single midradius chord trajectories subject to profile abnormality errors. Single midradius chord sensitive to swirl. The amount of pipe exterior that must be accessible for installation not yet minimized.

British Gas Multipath Ultrasonic Flowmeter.⁷

Description: Patented 4-chord, 8 transducer interrogation method, similar to Gaussian quadrature (Figure 2.6). Piezoelectric transducers with interface layer. Prototype tested in fully developed and abnormal flows.

Line Size: 150mm (approx. 6 inches). Transducers mounted in specially fabricated spool piece.

Line Pressure: 24 - 52 bar.

Flow Range: 0.2 - 25 m/s.

Pulse Repetition Rate: Mean velocity calculated from 12-second averages, representing 200 measurements on each chord.

Accuracy: Within one percent of reading for most flow situations, compared with critical nozzles.

Advantages: High accuracy in swirling and other abnormal flows.

Disadvantages: Installation requires access to entire outside of pipeline, and flow shutoff. Accurately machined spoolpiece with eight transducer ports must be spliced into pipeline. The eight transducers and machined spoolpiece imply high cost. No data available for line pressures near atmospheric where acoustic signal strength is low.

2.4.2 Reflected Pulse Ultrasonic Flowmeters

Reflecting - or "zig-zag" - trajectories have been widely used in ultrasonic flowmetering of liquid flows, primarily to increase the length of the ultrasonic path and thereby increase the transit times and transit time difference. The speed of sound in liquids is high as compared to gases, and small duct diameters are common in many liquid flowmetering applications, such as water flow in small pipes, and cryogenic liquid flow.²⁷ These two factors combine to give ultrasonic transit time differences two orders of magnitude smaller than those encountered in ultrasonic interrogation of large diameter gas mains.

The earliest known use of a zig-zag trajectory was by Petermann in 1959.²⁷ His intention was to increase the axial pathlength of a beam-drift type flowmeter. Prior to the present reflected pulse ultrasonic flowmetering in gases at M.I.T., Lynnworth has demonstrated the double tilted diameter, single reflection configuration in still air in an 18 inch diameter duct.²⁷ Lynnworth also holds a patent on the triple midradius chord,² two reflection configuration, which he has tested in still air.⁸ Lynnworth believes that the M.I.T. tests of these two configurations against an orifice in fully developed and abnormal flows are the first of their kind.⁸

Testing of an ultrasonic flowmeter using two direct pulse trajectories located at and near the midradius has been conducted in flowing gas by Baker and Thompson.¹⁸ There is no indication that their tests involved a triple midradius chord trajectory such as that tested in the present work. Panametrics and Exxon have conducted field tests of direct pulse midradius chord trajectories in flowing gas.^{6,8}

To Differential Pressure Instrumentation

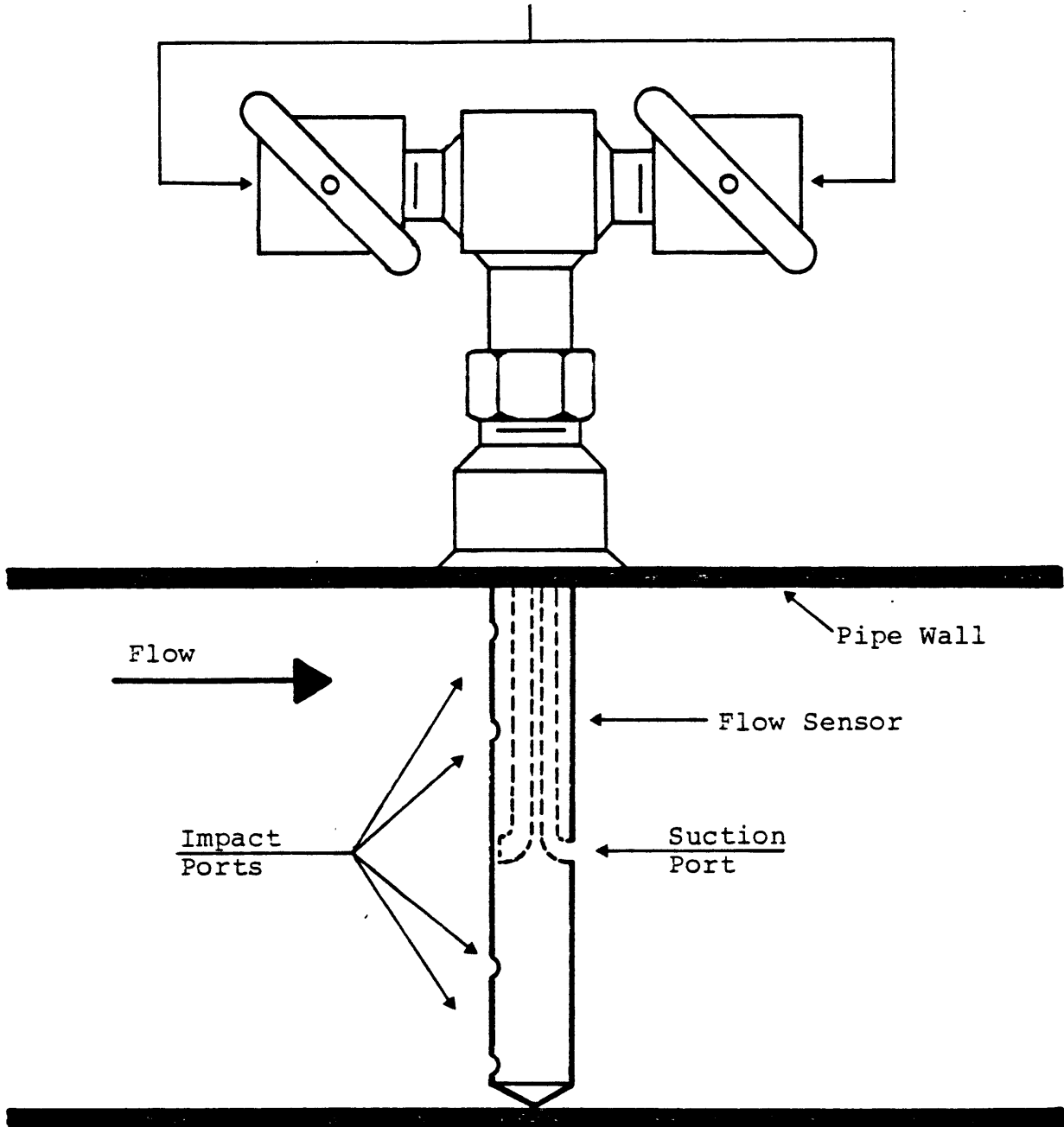
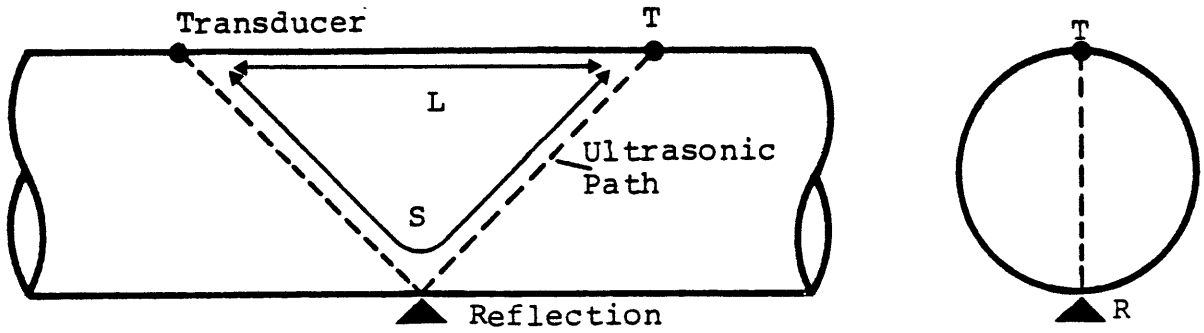


Figure 2.1: Schematic of Annubar Installation³



a. Double Tilted Diameter Trajectory (One Reflection)

b. Single Tilted Diameter Trajectory (No Reflection)

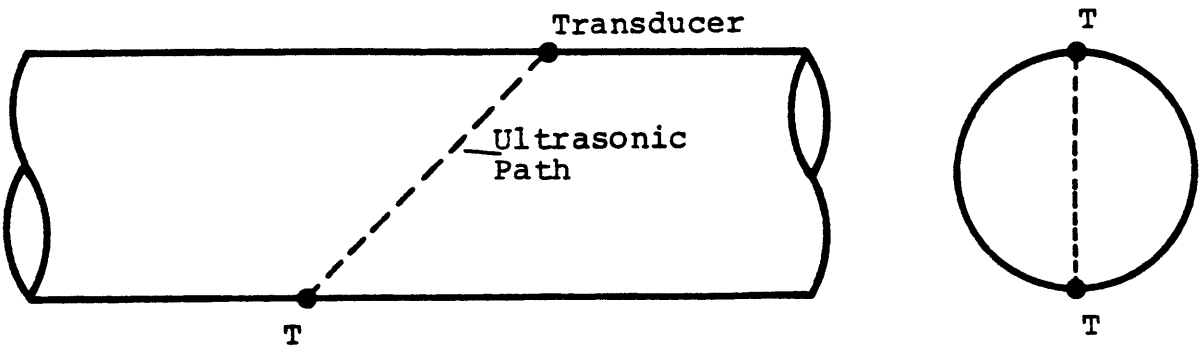


Figure 2.2: Single and Double Tilted Diameter Ultrasonic Trajectories

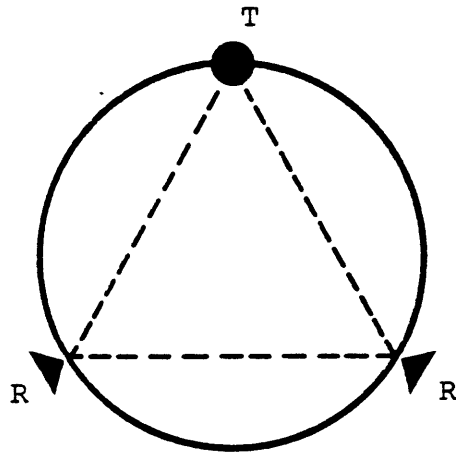
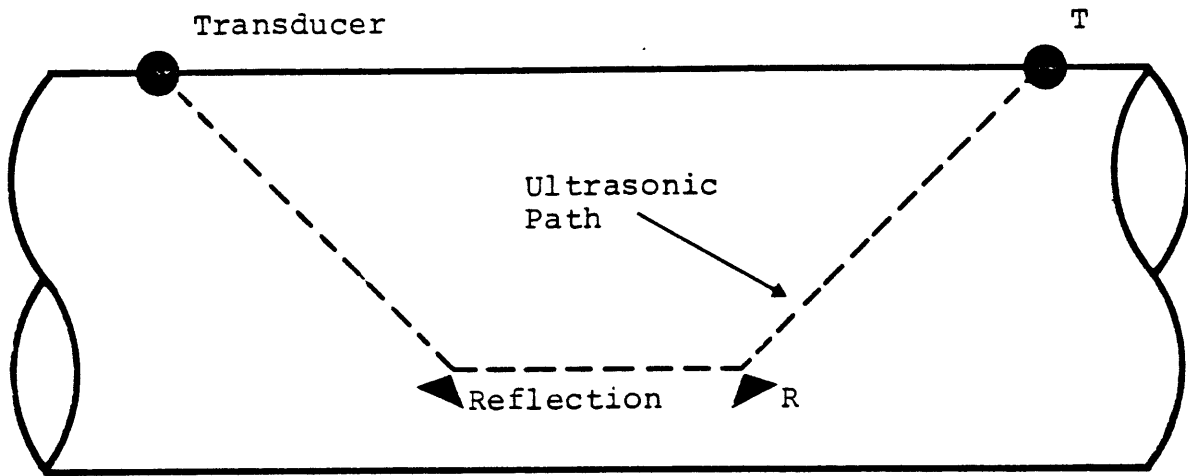


Figure 2.3: Triple Midradius Chord Trajectory

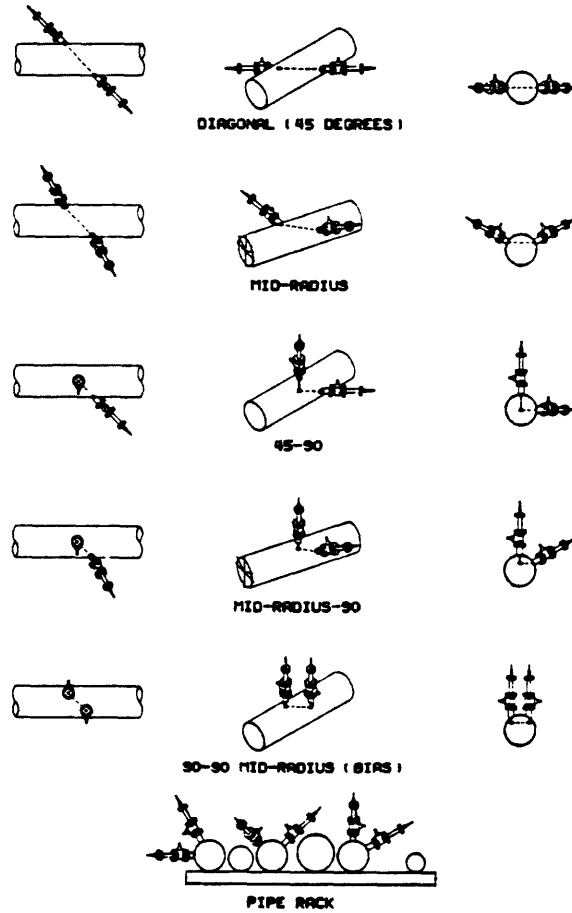


Figure 2.4: Panametrics-Exxon Direct Pulse Trajectories ⁶

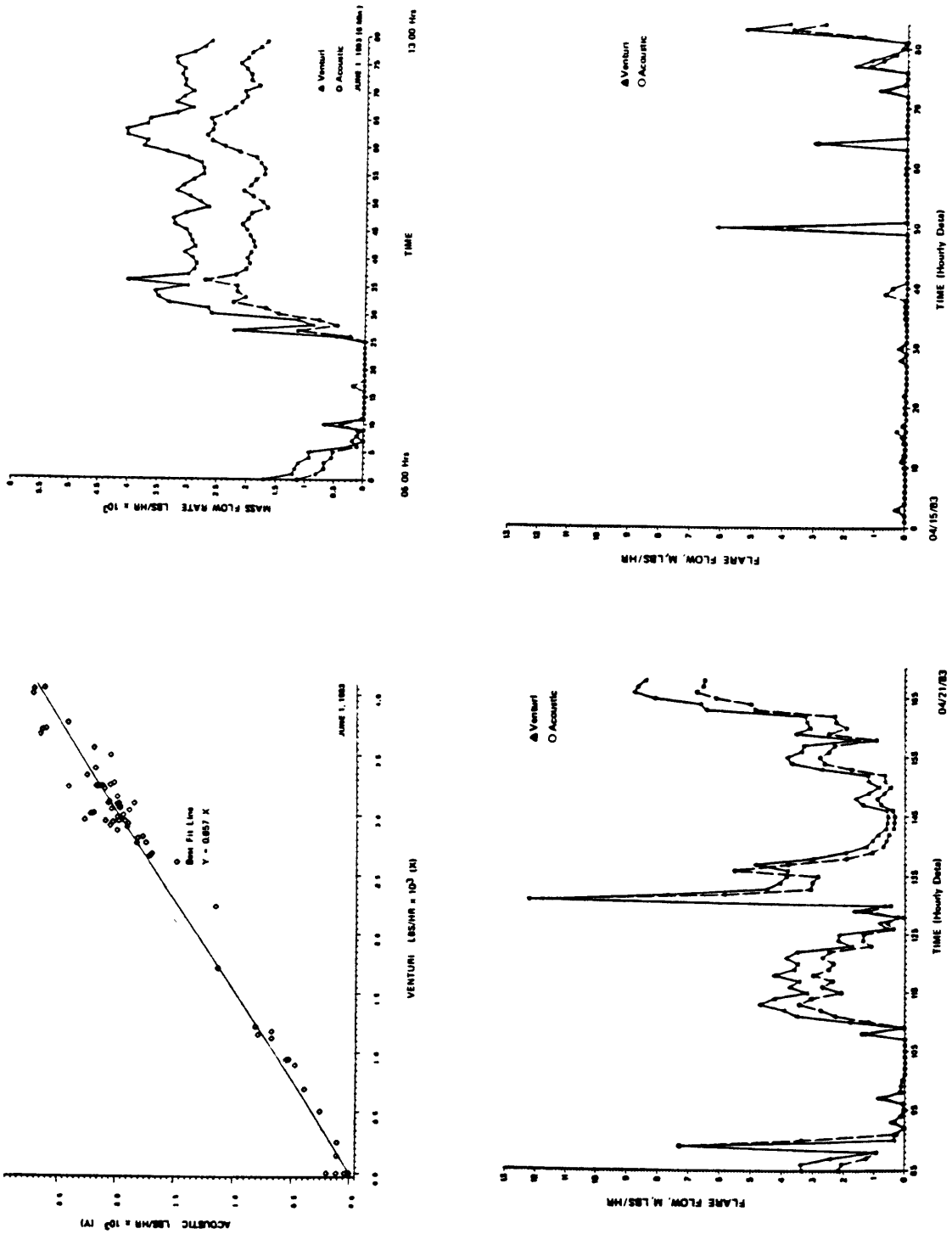


Figure 2.5: Accuracy of Panametrics-Exxon Ultrasonic Flowmeter Versus Venturi Meter (Ref. 6)

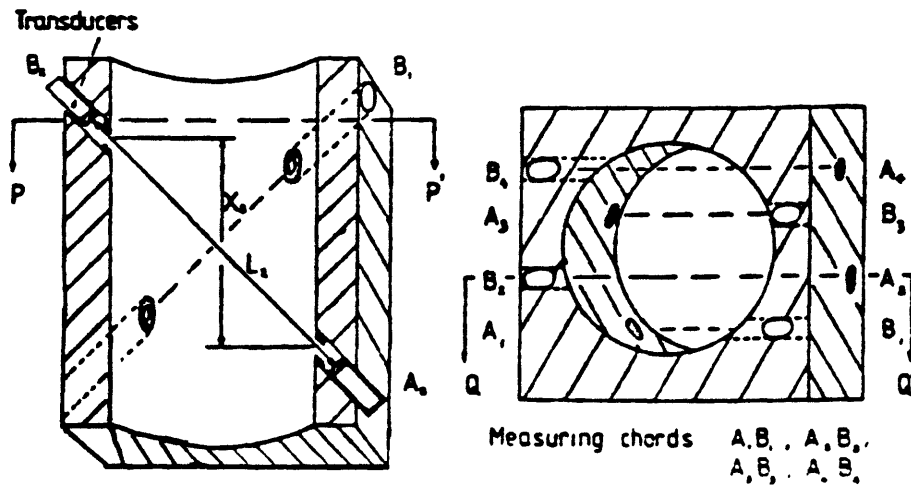


Figure 2.6: Schematic of British Gas Four-Chord Ultrasonic Flowmeter (Ref. 7)

Chapter 3

Derivation of the Ultrasonic Flowmetering Equations

It was stated in the Introduction that an ultrasonic transit time flowmeter calculates the average velocity of the fluid flowing through the acoustic path using measurements of upstream and downstream pulse flight times. The equation used to calculate the average velocity over the cross section of a duct from ultrasonic measurements is derived. The self-calibration technique is presented. Special cases of ultrasonic flowmetering in abnormal flows are discussed.

3.1 Calculating Cross Sectional Average Velocity from Ultrasonic Measurements

An acoustic pulse (ultrasonic or weak shock) propagates through a fluid at the speed of sound in the fluid, c . In a fluid flowing with uniform velocity V a pulse propagating downstream at an angle θ with respect to the direction of motion of the fluid will travel between fixed points at speed $c+V\cos\theta$; for an upstream traveling pulse the speed would be $c-V\cos\theta$ (See Figure 3.1). In the case of ultrasonic interrogation of nonuniform flow in a duct without swirl, a downstream traveling pulse will travel between any two points in the duct in time t_d :²⁴

$$t_d = \frac{S}{c + \left(\frac{L}{S}\right) V_{1n}} \quad (3.1)$$

where:

- S = Total ultrasonic pathlength.
- L = Axial component of the ultrasonic path.
- V_{1n} = Line-averaged velocity of the fluid traversed by the acoustic path.

Similarly, the transit time of an upstream traveling pulse

will be t_u :

$$t_u = \frac{S}{c - \left(\frac{L}{S}\right) V_{1n}} \quad (3.2)$$

The transit time difference between upstream and downstream pulses is thus

$$\Delta t = \frac{2LV_{1n}}{c^2 - \left(\frac{L}{S}\right)^2 V_{1n}^2} \quad (3.3)$$

from which it follows that

$$V_{1n} = \frac{S^2}{L\Delta t} \left[\left(1 + \left(\frac{c\Delta t}{S} \right)^2 \right)^{1/2} - 1 \right] \quad (3.4)$$

The above derivation is based on several simplifications. One is that the Mach number of the flowing fluid, V_{avg}/c , be low enough that convection does not cause the ultrasonic path to deviate significantly from a straight line. The derivation also assumes that the upstream and downstream pulses "see" the same line-averaged velocity, V_{1n} . As a numerical example, if V_{1n} as seen by the upstream pulse is 23 fps, and V_{1n} as seen by the downstream pulse is 27 fps, Equation 3.4 gives $V_{1n} = 24.94$ fps as the average. The error compared to the true mean V_{1n} of 25 fps is 0.25 percent. The equation used by Bender to compute V_{1n} did not rely on the assumption of equal upstream and downstream V_{1n} values:¹

$$V_{1n} = \frac{S^2}{2L} \left(\frac{t_u - t_d}{t_u + t_d} \right) \quad (3.5)$$

Using the numerical values from the above example, Equation 3.5 gives $V_{1n} = 25.002$ fps.

It is convenient when describing an ultrasonic trajectory in a circular duct to view the duct in axial projection. The ultrasonic trajectory appears in projection as a full or

partial chord of the circle representing the duct cross section, and V_{ln} is the line-averaged axial velocity of the fluid through which this chord passes. As illustrated in Figures 2.2a and 2.3 of Chapter 2, of special interest in this work will be ultrasonic trajectories which project onto a diameter and those which project onto one or more midradius chords.

Because the desired output of a flowmeter is most often volumetric flowrate, or mass flowrate, it is necessary to have a relation between the line-averaged axial velocity V_{ln} , and the average axial velocity over the entire cross section of the pipe, V_{avg} . This relation is well established for fully developed, axisymmetric flow for two particular chords of ultrasonic interrogation: the diameter and the midradius. Kivilis and Reshetnikov⁹ derived a Reynolds number dependent factor, m , for fully developed axisymmetric flow, relating velocity measured ultrasonically along a tilted diameter to the average velocity over the cross section:

$$V_{avg} = V_{ln} \left(\frac{1}{m} \right) \quad (3.6)$$

where:

$$- m = 1.119 - 0.011(\log(Re)). \quad (3.7)$$

- Re = Reynolds number of the turbulent flow, $4 \cdot 10^3 - 3 \cdot 10^6$.

The velocity measured ultrasonically by interrogation along a path projecting onto a midradius chord has been found, for a fully developed axisymmetric flow, to correspond almost exactly to the cross sectional average velocity, independently of Reynolds number, as shown in Figure 3.2.^{10,18} The profile correction factors are derived from numerical calculations of the line averaged velocity across empirical velocity profiles.

3.2 Self-Calibration Technique

The self-calibration of the M.I.T. reflected pulse ultrasonic flowmetering configurations consists of self-measurement of the total ultrasonic pathlength, S , shown

in Figure 2.2a. While the L pathlength (See Figure 2.2a) is easily computed from external measurements of the distance between the transducer mounts, the S pathlength would be difficult to compute accurately from external measurements. While the S pathlength only enters into the calculation of V_{1n} as a second order term, and can be ignored with little effect on the accuracy of the calculation (See Section 5.5.2), the ability to measure the S pathlength in a gas main is important for two other reasons. First, ultrasonic measurements of the S pathlength give information about the amount of scale and other deposits on the pipe wall at the point(s) of reflection. Upon installation, this information can be combined with external measurements of the pipe diameter and circumference when computing the cross sectional area of the pipe. The pipe cross sectional area enters into volume and mass flow calculations, and may introduce the largest uncertainty into these calculations.¹³ Measurements of S made periodically would give a history of pipe deposit formation, which could be used to update the cross sectional area measurement. A second reason for the importance of periodic S measurements is that deviations of the L pathlength from the initial value, caused by vibration induced movement or other trauma to the transducers, can be detected.

The S pathlength measurements are made by averaging pairs of upstream and downstream ultrasonic transit time measurements and multiplying the average transit times by the speed of sound in the gas: Equations 3.1 and 3.2 give the downstream and upstream transit times, respectively. Adding these together, and neglecting V_{1n}^2 compared to c^2 , gives:

$$t_u + t_d \approx \frac{2Sc}{c^2}$$

which reduces to:¹

$$S \approx \left(\frac{t_u + t_d}{2} \right) c \quad (3.8)$$

Measurements of S were made in flowing air in the M.I.T. test rig at 25 fps with the double tilted diameter configuration. The S measurements made with flow were in agreement with zero-flow ultrasonic S measurements to within 0.1 percent.

3.3 Ultrasonic Flowmetering under Abnormal Conditions

The profile correction factors, m , are derived from numerical integration of empirical velocity profiles, based on the assumption of an ultrasonic beam of zero width. The error associated with using ultrasonic beams of finite width (See section 5.2.2) is assumed to be small.

Deviations of the flow profile from the fully developed, axisymmetric case can change the relationship between the line-averaged velocity measured along an arbitrarily located diametral or midradius chord and the cross sectional average velocity. That is, the Kivilis m factor and Lynnworth m factor would no longer serve to convert V_{ln} into V_{avg} . The Kivilis m factor for the double tilted diameter was used in the present experimental work, however, because it was felt that once the Reynolds number of an abnormal flow was known (from orifice measurements of V_{avg}), the Kivilis m factor based on that Reynolds number would be correct on average. An m factor of unity was used for the triple midradius chord trajectory because it was felt that the line averaged velocity measurement made along the three successive midradius chords in an abnormal flow would be very close to the line averaged velocity a single midradius chord would measure in an axisymmetric flow, which would be corrected with $m = \text{unity}$.

3.3.1 Ultrasonic Flowmetering in Flow with Axisymmetric Swirl

The motion of a fluid particle in axisymmetric swirling flow can be expressed in terms of an axial component $V_a(r)$ and a tangential component $V_t(r)$. Because only $V_a(r)$ contributes to volumetric and mass flow calculations, the problem is to design an ultrasonic flowmetering scheme capable of rejecting $V_t(r)$. Figure 3.3 depicts schematically an axial view of a

circular duct with swirling flow, being interrogated ultrasonically along an arbitrarily located chord and along a tilted diameter. It is clear from the diagram that pulses propagating along the diametral trajectory will not be affected by $V_t(r)$, because there is no component of $V_t(r)$ parallel to the diametral path. It is also clear that a component of $V_t(r)$ will either increase or decrease the propagation velocity and the transit times of the ultrasonic pulses traveling along all non-diametral paths. The ultrasonic velocity calculation is based on the difference of the upstream and downstream transit times, $t_u - t_d$. Hence, to cancel the effect of $V_t(r)$ on the ultrasonic velocity measurement made along an off-diameter path, $V_t(r)$ must uniformly increase (or decrease) both t_u and t_d . In general terms, this says that the rotational velocity component $V_t(r)$ will be cancelled only if both the upstream and downstream pulses traverse the flow in the same rotational direction, i.e., both clockwise, or both counterclockwise. Thus, $V_t(r)$ cannot be cancelled by reversing the direction of ultrasonic transmission between transducers at opposite ends of a single chord.

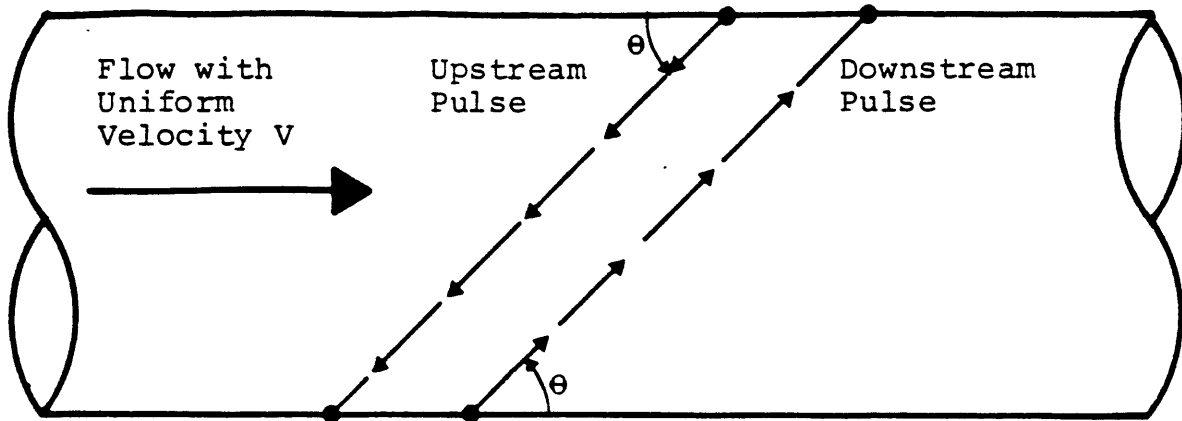


Figure 3.1: Ultrasonic Pulses Traversing a Uniform Flow at an Arbitrary Angle

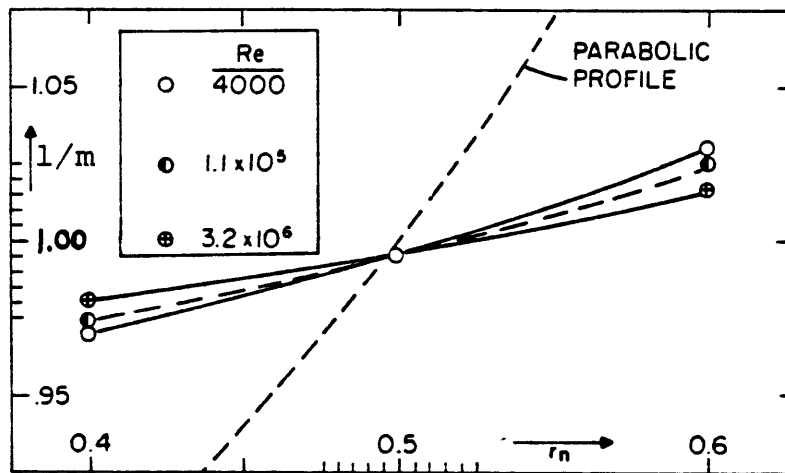


Figure 3.2: Profile Correction Factor for a Midradius Chord (Ref. 10)

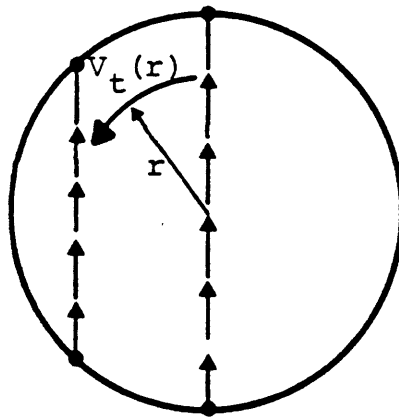


Figure 3.3: Axial View of Ultrasonic Interrogation in a Duct with Axisymmetric Swirl

Chapter 4

Numerical Simulation of Ultrasonic Flowmetering Downstream of an Elbow

4.1 Objectives of the Simulation

Prior to making ultrasonic flow measurements in the M.I.T. test facility, a simple numerical study was done to compare the ability of three different reflected pulse trajectories to give accurate cross sectional average velocity readings (after correction with the turbulent profile correction factor, m , appropriate to the particular trajectory and Reynolds number) when placed at different rotational orientations relative to a simulation of the abnormal flow downstream of an elbow. The tests were also conducted in a power law simulation of an axisymmetric profile, where the three trajectories accurately measured the average flow to two decimal places, the resolution of the simulation. The three trajectories were a double tilted diameter, and two and three successive midradius chords, shown in Figure 4.1. The purpose of comparing these three trajectories numerically was to allow a selection the two best for experimental tests in the laboratory. An intuitive ranking of the three trajectories in terms of perceived ability to reject profile abnormalities placed the triple midradius chord trajectory first because, in axial projection, its ultrasonic path was symmetric and covered - linearly - the largest portion of the flow. Moreover, a quick calculation using a power law profile showed that this trajectory interrogated the highest mass flow per unit beam width of the three trajectories.

The double midradius chord trajectory, although not, strictly speaking, top insertable, was felt to avoid the potential difficulties of the triple midradius chord trajectory of long pathlength through the gas (high acoustic attenuation), and two reflections (greater opportunity for distortion of the acoustic signal because of roughness of the reflecting surface). It was shown that this trajectory

interrogated the second highest mass flow per unit beam width - 66 percent more than interrogated by the double tilted diameter trajectory (viewed in axial projection).

The double tilted diameter trajectory, while it interrogated the smallest mass flow per unit beam width, offered true top-insertability and a shorter pathlength than the triple midradius chord trajectory. It was between these last two trajectories that a choice needed to be made experimentally.

4.2 Simulation Techniques

The velocity measured by an ultrasonic flowmeter has been stated (in Section 3.1) to be equal to the line averaged velocity of the fluid flowing through the axial projection of the ultrasonic trajectory. This line averaged velocity can be expressed as V_{1n} :⁹

$$V_{1n} = \frac{1}{2l_0} \int_0^{2l_0} V(l) dl \quad (4.1)$$

where:

- $V(l)$ = Axial velocity of fluid flowing through a point on the ultrasonic trajectory a distance l from the point of initiation of the ultrasonic pulse.
- $2 \cdot l_0$ = Length of the ultrasonic trajectory in axial projection (length of the ultrasonic "chord").

In an axisymmetric flow the velocity $V(l)$ at any point on the ultrasonic trajectory is simply a function of the radial distance from the center of the duct to that point. In an asymmetric profile, $V(l)$ at a point on the ultrasonic trajectory will depend on the radial distance, r , to that point, and on the angle of rotation, α , of the chord representing the ultrasonic trajectory with respect to the velocity profile. See Figure 4.2.

In the present numerical simulation, an abnormal (non-axisymmetric) velocity profile was generated

mathematically, and interrogated at different angles of ultrasonic chord rotation. The ultrasonic chords were located at the diameter of the duct, and at the midradius. The interrogation geometries, and the abnormal profile (illustrated twice for ease of verification of the simulated ultrasonic velocity measurements by comparison with profile shape) are shown in Figure 4.3a-d. The abnormal velocity profile was created in two steps. First, an axisymmetric profile was generated using the familiar power law:¹¹

$$V(r) = \left(1 - \frac{r}{a}\right)^{1/n} (V_{cl}) \quad (4.2)$$

where:

- a = Radius of duct.
- r = Radial distance from center of duct.
- V(r) = Axial velocity at radial distance, r.
- V_{cl} = Centerline velocity.
- n = Power law exponent (Reynolds number dependent).

An exponent of 10 was chosen, which represents a Reynolds number of 2×10^6 . This corresponds to an average flow velocity of 15.5 fps in a 2 foot diameter gas main at 160 psig - a typical Con Edison flow situation. The second step, to make the velocity profile non-axisymmetric, was accomplished by multiplying the velocity at every point in the flow by the square root of the perpendicular distance from that point to the $d = 0$ axis, according to the geometry shown in Figure 4.2. Figures 4.3b&d show the resulting abnormal profile in the plane of the d -axis. The average velocity of the abnormal profile over the duct cross section was calculated numerically to be 14.9 fps (Reynolds number = 1.92×10^6); the maximum velocity was 19.9 fps.

To perform the integration of Equation 4.1 numerically for diametral and midradius chords rotated at an arbitrary angle, α , with respect to the velocity profile, a relation was needed so that $V(l)$ could be expressed in terms of the variables r , a , h , d , and α . Using the geometry of Figure

4.2, the following relations were established:

$$V(l) = v_{cl} \left(1 - \frac{r}{a}\right)^{.1} \left(d^{1/2}\right) \quad (4.6)$$

$$d = a - \left[r \cos \left(\alpha + \cos^{-1} \frac{l_0 - 1}{r} \right) \right]$$

$$r = \left[(l_0 - 1)^2 + h^2 \right]^{1/2}$$

$$l_0 = (a^2 - h^2)^{1/2}$$

The numerical integration of Equation 4.2, using $V(l)$ as given by Equation 4.6, were done on a hand held calculator to 2 decimal places accuracy. The line averaged velocity measurements were corrected with profile correction factors $m =$ unity for the midradius case, and $m = 0.953$ (calculated from the Kivilis equation, Equation 3.7) for the diametral case.

4.3 Results and Conclusions

The results of the simulation are presented in Table 4.1. The triple midradius chord trajectory gave the most accurate cross sectional velocity readings at all rotations. The second best performance was given by the tilted diameter trajectory. Based on these results, the triple midradius chord and double tilted diameter trajectories were chosen for laboratory testing.

Table 4.1 Numerical Simulation Results
Ultrasonic Measurements of the Cross Sectional Average
Velocity of An Abnormal Flow

Note: Actual cross sectional average velocity is 14.9 f/s.
Maximum ultrasonic errors (percent of true value)
are given in parentheses.

(I) Single Diametral and Midradius Chord Measurements

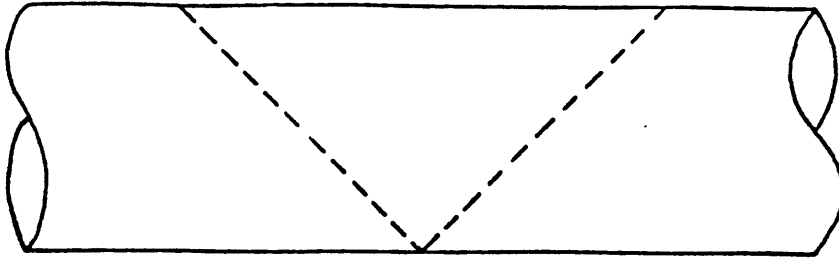
Angle of Rotation (degrees)	Diametral Measurement (f/s)	Midradius Chord Measurement (f/s)
0	14.7 (-1%)	15.0
45	15.2	18.1
90	15.5 (+4%)	19.2 (+29%)
120	15.3	18.6
135	15.2	18.1
165	14.9	16.1
210	15.1	12.9
240	15.3	11.5
285	15.5	11.1 (-26%)
300	15.1	12.9

(II) Measurements Made with Two Successive Midradius
Chords

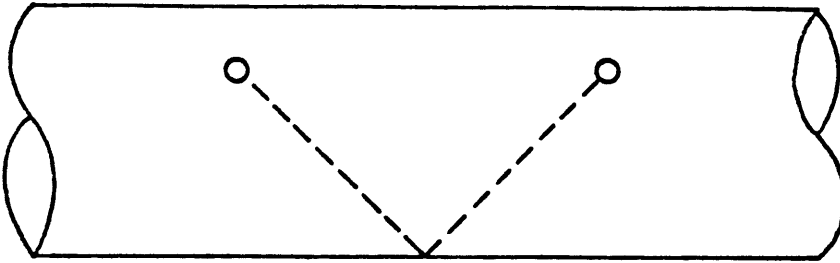
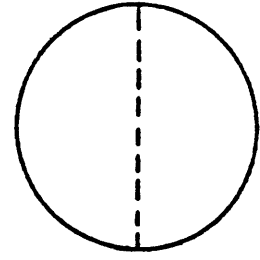
Angles of Chord Rotation (degrees)	Double Midradius Chord Measurement (f/s)
0,120	17.7 (+19%)
90,210	16.1
120,240	15.0
165,285	13.6 (-9%)

(III) Measurements Made with Three Successive Midradius
Chords

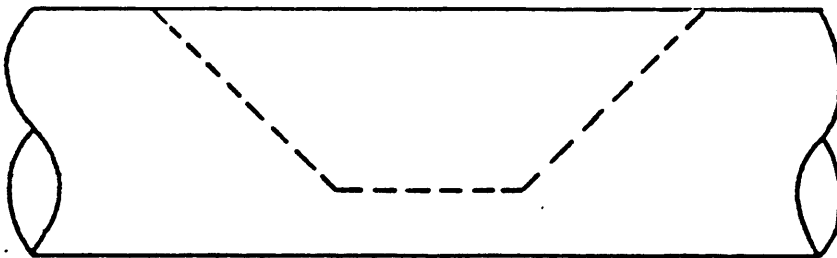
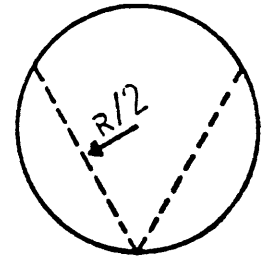
Angles of Chord Rotation (degrees)	Triple Midradius Chord Measurement (f/s)
0,120,240	15.0 (+1%)
45,165,285	15.0
90,210,330	14.9



Double Tilted Diameter Trajectory



Two Successive Midradius Chords



Triple Midradius Chord Trajectory

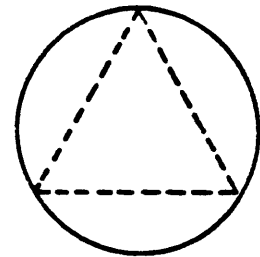


Figure 4.1: Ultrasonic Trajectories Tested in the Simulation

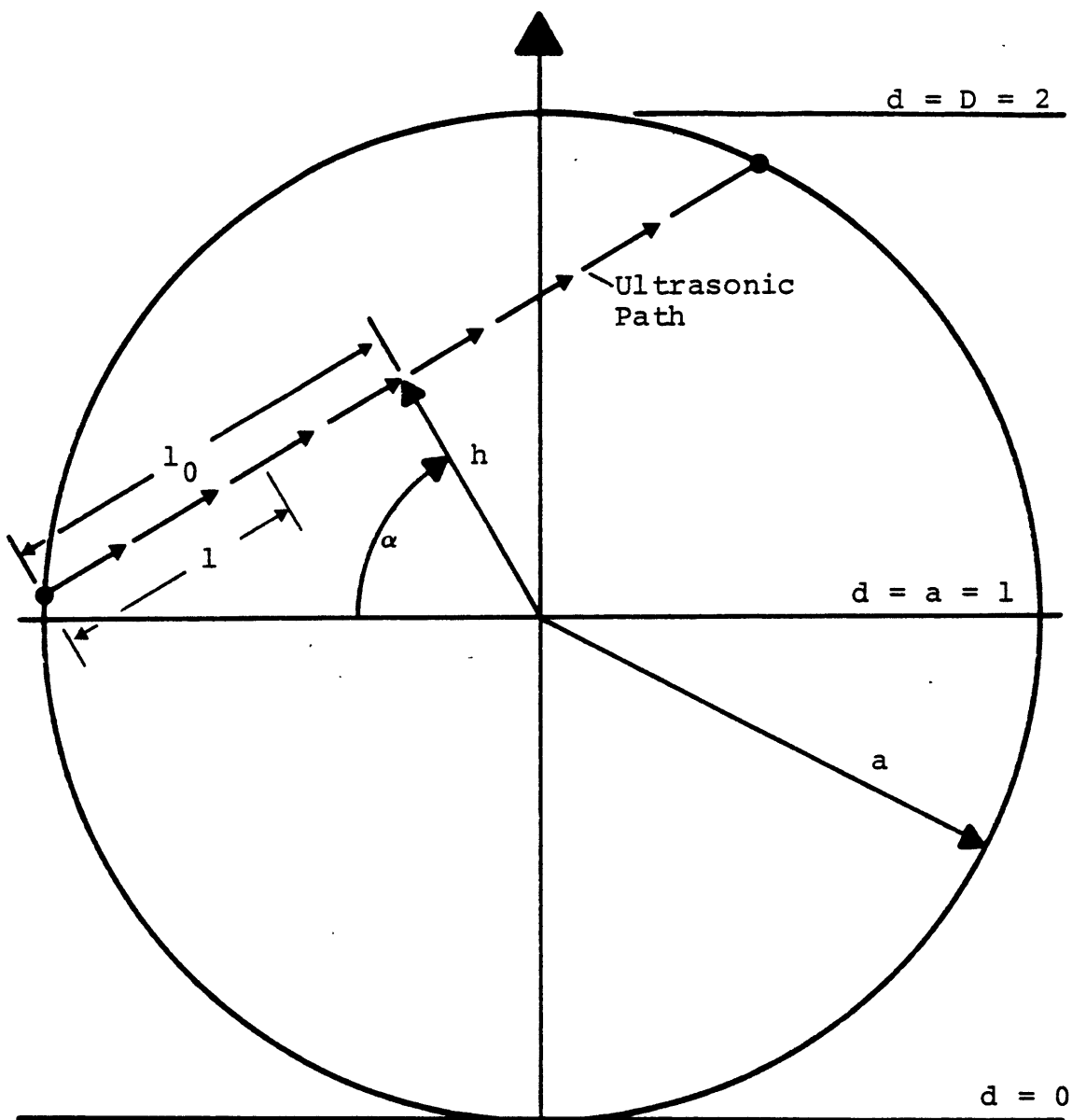
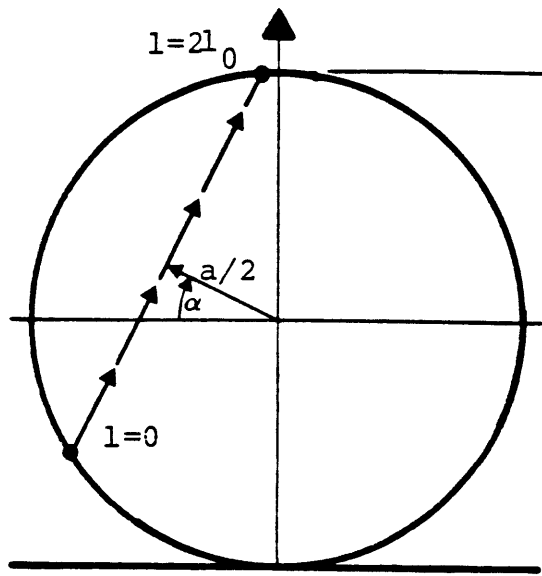
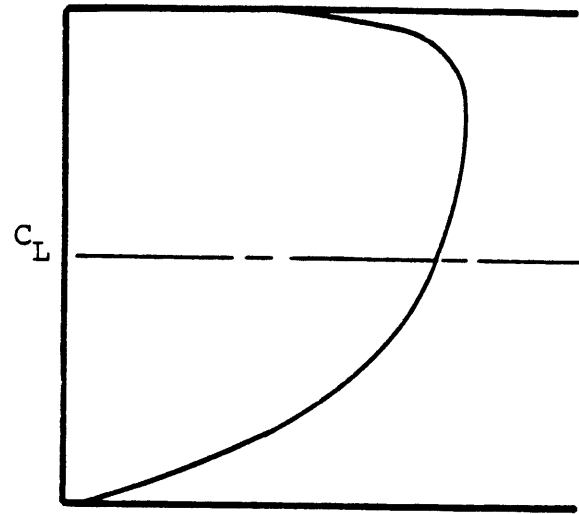


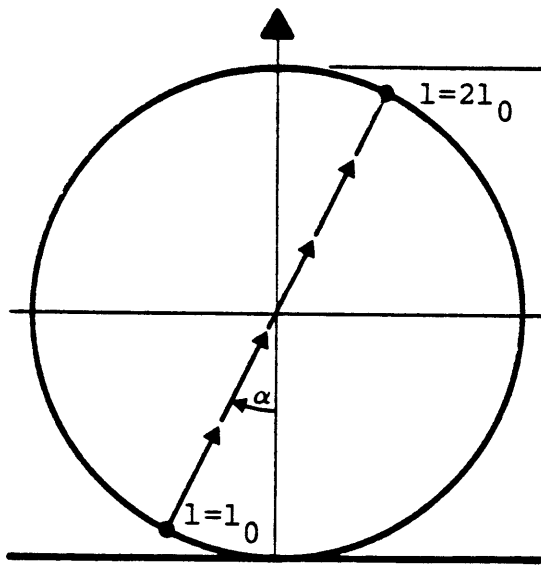
Figure 4.2: Simulation Geometry



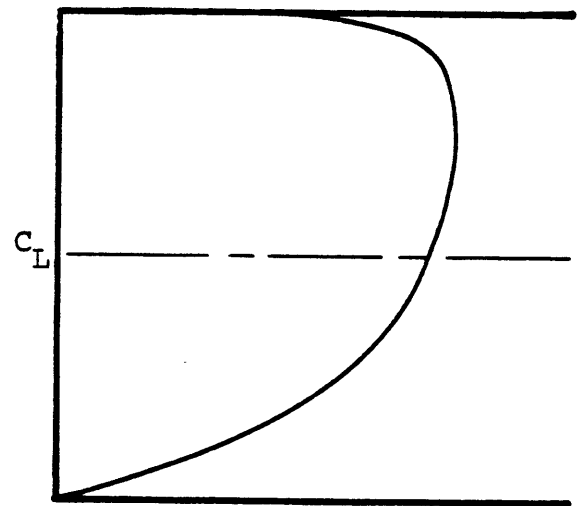
a. Single Midradius Chord



b. Profile



c. Single Diameter



d. Profile (Same as above)

Figure 4.3: Chords of Ultrasonic Interrogation and Simulated Abnormal Velocity Profile

Chapter 5

Experimental Hardware and Procedure

The experimental program was designed to test the accuracy of the double tilted diameter and triple midradius chord ultrasonic configurations against an orifice meter in fully developed flow, and in the abnormal flow downstream of an elbow, at arbitrary angles of rotation relative to these flows.

5.1 The Test Rig

The flow tests were performed in 12 inch nominal diameter pipe using air at ambient temperature and pressure. The test rig is shown schematically in Figure 5.1. A steel ultrasonic metering section was followed by an orifice installation and a blower. The direction of flow was from the ultrasonic test section toward the blower. Upstream of the ultrasonic test section was the inlet section: either a long run of straight pipe, or a short length of straight pipe preceded by an elbow, depending on which velocity profile was required. The centerline of the test rig was approximately 36 inches above floor level.

Twenty diameters of straight PVC pipe were installed upstream of the steel section when it was desired to run tests in a fully developed turbulent flow. A 90 degree elbow was installed 6 or 10 straight diameters upstream of the test section - with another 2 or 4 diameters of straight pipe ahead of the elbow - to produce an abnormal flow situation. The elbow and preceding straight pipe were always oriented vertically. A flow straightener, consisting of approximately 2000 plastic drinking straws packed tightly in a cylindrical galvanized steel container with a standard mesh screen bottom was inserted into the inlet of the test rig for all runs.

Steel was selected for the ultrasonic test section to approximate the direct acoustic coupling between transducers that would occur in actual metering setups. The 52 inch long

steel section was rotatable about its longitudinal axis, supported on four hard rubber casters (See Figure 5.2). The steel section could be fixed in any rotational orientation by tightening a hose clamp which encircled one pair of casters and the pipe. It was possible to rotate the steel section through 135 degrees in 45 degree increments; 45 degree graduations on the steel section were aligned with a scribe mark on the adjoining PVC section. Ports, 2.75 inches in diameter, were bored into the steel section for transducer insertion. At zero degrees test section rotation the transducer ports were facing the ceiling of the lab. The upstream port served for both the triple midradius and tilted diameter configurations. Two downstream ports, each with a removable plug (curved and fitted to match the pipe inside surface) were necessary to accommodate the downstream transducers. The centerline of the downstream port of the triple midradius chord configuration was located 4 degrees tangentially from the centerline of the upstream port because of the wall thickness of the pipe. The positions of the ports were laid out on longitudinal lines scribed onto the pipe outside surface to plus or minus 1/32 inch accuracy. These scribe marks facilitated alignment of the transducer saddles, to be described below.

The orifice metering section, designed according to Reference 12, consisted of 20 diameters of straight PVC pipe downstream of the steel section, a 5.500 inch square edge orifice plate with vena contracta taps, and another 4 diameters of PVC. A 12 inch to 8 inch reducer was coupled to the 8 inch blower inlet by a thick rubber sleeve fastened with a hose clamp.

Alignment of the three main pipe sections of the rig was accomplished by aligning the PVC supports with a chalkline and level, laying the two 20 foot sections of PVC into place, and positioning the steel section between them and adjusting the casters. The width of the gap at the PVC-steel butt joint was approximately 3/32 inch or less. With the steel test section

at zero degrees rotation the external radial misalignment between the steel and PVC pipe sections was plus or minus $3/32$ of an inch. A dial indicator showed that the rotation of the steel section was out of true by plus or minus 0.025 inches. Combining these uncertainties gives a maximum local surface discontinuity, externally, of less than 0.119 inches. A sizing error resulted in the steel pipe being 0.182 inches larger in inside diameter than the PVC pipe. Thus, as the flow passed from the PVC pipe to the steel test section, the end of the steel pipe could have protruded into the flow by as much as 0.028 inches. The maximum outward step the flow could have been forced to take was 0.21 inches. The two pipe sections were simply butted together with no internal bridge over the joint. The difference between the cross sectional areas of the pipe sections was taken into account when the cross sectional average velocity at the steel section was calculated from orifice velocity measurements made in downstream PVC pipe. Sealing of both steel-to-PVC joints was done with window caulk or duct tape.

Flow velocity in the test rig was regulated by two independent means. With the rubber sleeve in place on the blower inlet a hinged gate at the rectangular blower outlet gave continuous velocity adjustment from approximately 15 fps to 25 fps. Removal of the rubber sleeve exposed a 2 inch wide gap between the flow reducer and the blower inlet, reducing the velocity range obtainable through throttling to approximately 5.5 fps to 15 fps. See Figure 5.3.

5.2 Ultrasonic Flowmetering Hardware

The waterproof enclosure housing the electronics was mounted on the wall directly over the steel test section. A hinged door on the front of the enclosure allowed access to the power switch, circuit boards, and two BNC connectors for the transducer cables. Pins on the circuit boards allowed oscilloscope monitoring of the essential flowmetering signals.

Data was sent via an RS232 interface to a DEC lineprinter. A reset switch positioned near the printer readied the flowmeter to accept keyboard commands.

5.2.1 Panametrics' Model C508R (Modified Model 6000)

The Panametrics Model C508R is a prototype ultrasonic flowmetering package containing pulsing and receiving circuitry, received signal conditioning and timing circuitry, and a microprocessor to control data acquisition and processing. The commercial model corresponding to this prototype is presently available as the Model 7100.

As used in the experiments described in this paper the Model C508R functioned as follows: 100 kHz square wave bursts (4 cycles, -180 volts peak to peak, per burst) were sent alternately to the transducers every 0.01 seconds. The acoustic signals received at the opposite transducers were filtered and amplified, and a patent-pending timing method measured the time of flight of each pulse. The microprocessor sent transit time data to an external printer.¹³

5.2.1.1 Pulsing and Receiving

The 100 cycle per second "sync" signal controlling the pulse repetition rate of the meter, and the alternating upstream and downstream received wave packets are shown in Figures 5.4a and 5.4b. The transit time measurement of the upstream and downstream pulses commences on the positive slope of the "sync" pulse. Figure 5.5, an expanded view of Figure 5.4b, shows the shape of the received signal wave packet (the upstream and downstream signals appear to be superimposed because of the persistence of the oscilloscope screen). The raw received signals have been filtered, and amplified with automatic gain control (AGC) which maintains a constant steady-state (still air) amplitude of approximately 3.4 volts. The filtering and AGC operate only within a "receive window" of variable width which must be positioned so that it includes the wave packets of the received signals (See Figure 5.6).

Window position and width are adjusted to reject spurious signals arriving earlier or later than the expected gas-borne signals. The filtered received signal is not disturbed by sharp hammer blows to the pipe.

5.2.1.2 Timing Method

The Model C508R uses a patent-pending timing method to overcome the fundamental difficulty of ultrasonic flowmeters using narrowband high frequency pulses rather than broadband shock pulses: a narrowband received signal has no definite time of arrival. It is evident from the wave packet shown in Figure 5.5 that the transducer requires several cycles to reach peak amplitude, and that the first peak is likely to be indistinguishable from the baseline noise. Because flow turbulence causes large fluctuations in the received signal amplitude a simplistic timing method based on locating the first zero cross of the received wave packet would sometimes detect the first zero cross, sometimes the second or third, leading to errors of multiples of one cycle (10 microseconds).

Part of Panametrics' technique uses a preset voltage threshold which must be reached by an integration of the voltage levels of the positive peaks in the received wave packet before the "stop" gate can be triggered on a subsequent zero cross. The time integration of the received signal forms a sort of staircase, shown in Figure 5.7a, in which the horizontals are lines of constant voltage, and the verticals are lines of high dV/dt . It is not necessary to observe the preset voltage threshold on an oscilloscope directly. It is sufficient to observe a vertical line which Panametrics calls the "integrated threshold," Figure 5.7b. The intersection of this line with the "integration level" staircase marks the threshold level. It is desirable to set the threshold voltage so that it fits within the limits of one of the integration level verticals. The integrated threshold, zero cross, and stop gate signals are superimposed in Figure 5.8, as traces a, b, and c, respectively. It can be seen that

the stop gate is triggered by the vertical of the zero cross signal (verticals indicate zero crosses of the received signal) immediately following the integrated threshold signal.¹³

5.2.1.3 The Non-Fluid Transit Time Component t_w

Both the upstream and downstream pulse transit times measured by the Model C508R contain a non-fluid transit time component, t_w , made up of two parts. The first is the time spent in the coaxial lines, signal processing components, etc; the second and more important part is the time between the reception of the very first part of a pulse at the transducer, and the stop gate signal. Thus, the value of t_w depends largely upon the choice of integration level vertical with which the threshold voltage is set to coincide.¹³ Further information about t_w is presented in Section 5.4.1.1.

5.2.1.4 Cycle Jumping During Pulse Timing

If the integrated threshold voltage has been set to coincide with the center of the third vertical of the integration level staircase under zero flow conditions, it is evident that introducing flow - and hence fluctuations in the amplitude of the AGC signals - will cause no timing error unless the integration level increases so much that the threshold voltage is reached on the second vertical, or decreases so much that the threshold voltage is only reached on the fourth vertical.¹³ Under these extreme, but common, circumstances the stop gate will be triggered by the zero crosses corresponding to the second and fourth integration level verticals, respectively. The result will be timing errors of minus 10 microseconds and plus 10 microseconds, respectively. Typical upstream and downstream transit time distributions are shown in Figure 5.9. A typical upstream or downstream transit time distribution exhibited bimodality or trimodality. There was usually a dominant "true" peak, a secondary peak at plus 10 microseconds, and a tertiary peak at

minus 10 microseconds. Pairs of t_u and t_d values in which both t_u and t_d experienced a cycle jump in the same direction occurred only randomly. Thus, most cycle jumps did not cancel each other out when Δt was calculated. Cycle jumping was the single worst problem encountered during the course of this project. The subject is discussed further under ultrasonic data acquisition in Section 5.4.2, in the recommendations for data acquisition in Section 7.2, and in Appendix A, where some investigations of cycle jumping are described.

5.2.1.5 Data Output Format

The data from the Model C508R was sent via an RS232 interface to a Digital Equipment Decwriter II lineprinter. A sample printout, showing the microprocessor prompts, user inputs, and data output format is shown in Figure 5.10. The data processing program, installed in the Model C508R by means of a PROM, was designed to allow transit time averaging with bad data rejection.

5.2.2 The Transducers

Panametrics C508R sealed piezoelectric transducers were used for all testing. These transducers, shown schematically in Figure 5.11, and in photographs in Figures 5.13 and 5.14, consist of three critical elements: the piezoelectric crystal, an acoustic impedance matching material, and a thin metallic window, all contained within a titanium housing. Traditionally, an obstacle to using piezoelectric crystals to generate and receive acoustic pulses in a gas has been the large acoustic impedance mismatch at the crystal-gas interface, which made energy transfer difficult. The impedance matching material is chosen principally on the basis of its having an acoustic impedance as close as possible to the geometric mean of the crystal and gas impedances.¹⁴

The thin metallic window serves to seal the transducer from moist and/or corrosive environments. The thinner the window, the stronger the received signal. Window and housing

damping is important because ringing limits the pulse repetition frequency.¹⁴

A layer of household plastic wrap stretched tightly over the transducer face can greatly increase received signal strength. This layer of plastic, and perhaps also a film of air trapped beneath it, is thought to act as an external impedance matcher, but the phenomenon is not well understood. A 15 dB increase in received signal amplitude has been reported by Lynnworth;¹⁴ a 22 dB increase was obtained during the course of the present work with the transducers in the double bounce configuration. This large gain was measured within a few minutes of application of the plastic. No measurements were made of the gain after the transducers had been placed in flowing air, which is believed to cause relaxation of the plastic stretched over the transducer face, and a loss of amplification.¹⁵ Lynnworth mentions an air film trapped between the transducer face and the plastic; however it was not the intention of the plastic wrap application procedure described in Section 5.2.2.2 to include air between the plastic and the transducer.

The signal increase due to the plastic wrap is useful in laboratory experiments because it acts as a "pressure multiplier." The amplitude of the received signal increases linearly with the pressure of the metered gas, thus, a gain of 15 dB is equivalent to operating at 68 psig.^{13,14} The plastic wrap would, of course, not be appropriate in a long-term practical application.

The included angle between 3 dB points of the ultrasonic beam is given approximately by

$$\beta \approx \left(\frac{\lambda}{d} \right) \quad (5.1)$$

where:

- λ = Ultrasonic wavelength.
- d = Diameter of the transducer face.

For the transducers used in the present experiments, $\lambda = 0.137$

inches, and $d = 0.75$ inches, so that β is approximately 10 degrees.⁶

5.2.2.1 Transducer Mounting

The two ultrasonic transducers were purchased already mounted on 15 inch long, 1/2 inch diameter stainless steel tubes terminating in male BNC connectors. Two pairs of aluminum saddles were fabricated to hold the transducers rigidly and accurately at the correct angles for the triple midradius and tilted diameter configurations (see Figure 5.12). The angles of the transducer axes with respect to the pipe axis, although maintained at 45 degrees plus or minus two degrees, were not critical. The tangential angles of the transducer axes with respect to a diameter of the pipe, also accurate to within plus or minus two degrees, were critical because they determined whether or not the ultrasonic trajectories were in fact located in the plane of the pipe centerline in the one case, and in three successive midradius planes in the other. The 15 inch stems of the transducers were held in the 1.5 inch pipes protruding from the saddles by Swagelock fittings with Teflon ferrules. Insertion depth of the transducers was fixed using collars with set screws on the transducer stems. See Figure 5.13a. Each transducer could thus be rotated about its longitudinal axis without changing its insertion depth. The underside of each saddle was radiused to fit the outside diameter of the steel pipe; a 1/16 inch soft rubber gasket was glued to the underside of each saddle to serve as an air seal. See Figure 5.13b. The fit of the saddle radii on the outside of the steel section was such that skewing of the saddles was never a problem. The saddles were held firmly in place on the test section by single worm-gear type hose clamps.

5.2.2.2 Application of Plastic Wrap to Transducers

Upon setting up the triple midradius configuration with bare transducers, it was observed that the large percentage of

baseline noise on the post AGC received signal was incapacitating the integration level. It was thus necessary to apply plastic to the transducers to boost the raw received signal. Whereas plastic was not necessary for proper integration in the case of the tilted diameter configuration (probably because of the shorter pathlength), it was applied there, too, for consistency. The plastic wrap used was Purity Supreme Generic brand household wrap, with a measured thickness of 1.5 mils, plus or minus 0.5 mils. Tests showed that Saran brand wrap was not as effective.

The plastic wrap was held taught over the transducer faces with hard plastic collars one inch long which fit the transducer bodies with an easy sliding fit. The transducer housing before and after application of plastic wrap is shown in Figures 5.14a&b. The wrap was applied to each transducer as follows: A portion of a large sheet was pulled tightly over the transducer face. No effort was made to trap air under the plastic, nor was any attempt made to force residual air out from under the plastic. The collar was then pushed partway onto the transducer over the wrap until appreciable force was felt. The wrap protruding from beneath the collar was trimmed off, and the collar was pressed on until the trailing edge of the collar was flush with the transducer face. Visual inspection of the surface of the plastic for tear-through, and maximization of the raw received signal amplitude at each transducer as viewed on an oscilloscope, were used to check the quality of the application.

5.2.2.3 Coaxial Transducer Cables

Ultrasonic velocity measurements made with the triple midradius configuration in fully developed flow and 10 diameters downstream of the elbow were made with RG58U coaxial cables, approximately 6 feet on the upstream transducer and 3 feet on the downstream transducer. When it was noticed that excessive upstream-pulse cycle jumping was occurring, equal lengths (4 feet) of low capacitance RG59U cable were

connected to both transducers. A detailed discussion of cycle jumping is presented in Appendix A.

5.3 Reference Instrumentation

The reference flowmeter used in these experiments was a square edge orifice plate with vena contracta taps, installed in accordance with Reference 12. The minimum number of straight pipe diameters separating the 90 degree elbow from the orifice was 30, including the length of the steel test section and the 6 diameters of PVC between the test section and the elbow.

The pressure drop across the orifice was read in inches of water from an inclined manometer graduated in 0.01 inch increments, and readable to 0.005 inches. The manometer was located directly over the orifice plate. Oscillations on the order of ± 0.01 inches were present at low flowrates, and oscillations of ± 0.02 inches occurred at maximum flow. All readings represent a carefully estimated average of the oscillations. The slope of the manometer was estimated to be accurate to within ± 0.5 percent. The depression of static pressure at the upstream orifice tap with respect to atmospheric pressure (used to correct the barometric pressure in density calculations) was measured using a Magnehelic differential pressure gage with a one inch range, resolveable to 0.01 inches. The pressure depression at the ultrasonic test section was measured on the same gage, which was located over the ultrasonic test section.

Dry bulb temperature was measured in the flowing air at the centerline of the steel test section. A standard laboratory thermometer with a resolution of 0.5 degrees Fahrenheit was used. The difference between dynamic and static temperature at Mach numbers below 0.22 is less than one percent.¹⁹

Wet bulb temperature was taken with a sling psychrometer at the inlet of the test rig. The resolution of the psychrometer was 0.5 degrees Fahrenheit.

Local barometric pressure was read to 0.01 inches from a mercury barometer.

5.4 Experimental Methods

The steps taken to prepare the test rig, ultrasonic hardware, and orifice meter for data acquisition are presented. The data acquisition procedure is described.

5.4.1 Preparations for Data Acquisition

The appropriate inlet section - straight pipe, or elbow plus straight pipe - was laid into place. The steel test section was rotated into the desired angular position relative to the inlet, secured, and the steel-to-PVC joints were sealed. The transducers were covered with plastic wrap and mounted in the appropriate saddle blocks for the desired trajectory. The distance from the center of the face of each transducer to the edge of the saddle facing the opposite transducer was measured with a scale and recorded. The transducer saddles were placed over the ports in the steel section and fastened loosely into place. All velocity tests were performed with the faces of the transducers one-half in and one-half out of the inside diameter of the test section.

Final transducer positioning proceeded as follows: one transducer was connected to the flowmeter electronics to serve as sender, and the other was connected to an oscilloscope to serve as receiver. In the case of the tilted diameter configuration, scribe marks on the saddles indicating their axial centerlines were aligned with the centerline of the transducer ports. One saddle was then firmly tightened, and the other was moved axially along the port centerline until the signal received at the oscilloscope was maximized. That saddle was tightened, and the transducers were rotated in the Swagelock fittings until the received signal was again maximized.

Positioning of the saddles for the triple midradius configuration proceeded similarly, except that the scribe marks

indicating the port centerlines were used only as rough guides, and signal maximization dictated the final saddle locations. Axial and tangential movements of the transducer saddles on the order of one inch were necessary to produce noticeable changes in the amplitude of the received signals. The largest variations in received signal amplitude (on the order of 50 percent of maximum) were caused by rotation of the transducers in the Swagelock fittings.

The distance between the saddles was measured with a tape; this value added to the two measurements of transducer face to saddle edge distance gave the L pathlength.

5.4.1.1 Electronics Adjustments

The burst frequency was set to 100 kHz, which coincided with the center frequency of the transducers. The pulse repetition rate was set at 50 upstream-downstream pairs per second.

Before taking any flowmeasurement data it was necessary to determine t_w , the electronic component of t_1 and t_2 mentioned in Section 5.2.1.3. The manufacturer's instructions were followed. The transducers were clamped in V-blocks and placed opposite each other in a Dexion channel on a table top in still air. Using a tape measure, the transducers were spaced one foot apart and 100 samples of t_1 and t_2 were recorded. This was repeated at a spacing of two feet. A graph of average total transit time versus distance yielded t_w as the y-intercept.¹³

It was necessary to reset the "integrated threshold" level when switching among transducer configurations - direct path, single bounce, triple midradius - because of slight differences in received wave packet shape. While it was easy enough to set the threshold level at the center of a vertical of the "integration level" staircase with zero flow in the rig, this method did not yield a minimum of cycle-jumping. Cycle-jumping was minimized by setting the threshold to the point of minimum jittering as seen on an oscilloscope in

storage mode, while medium to high velocity flow existed in the rig.

Strictly speaking, a "Catch 22" arose at this point: it was necessary to reset the threshold level when the transducer configuration was changed, which implied a change in t_w (See Section 5.2.1.2); yet, it was only possible to measure t_w as described above - in a direct pulse configuration. The problem was actually insignificant: once t_w was known for the direct path, that value was used in the velocity calculations for the other transducer configurations. The likely error thus introduced is slight: at 15 fps an error in t_w of 20 microseconds, or two cycles, gives a velocity error of 0.0003 percent. For maximum accuracy, a fixture would have to be constructed which would duplicate exactly the in situ pulse trajectory, and would allow the transducers to be moved on-axis so that a total transit time versus distance graph could be plotted as described above.

5.4.2 Data Acquisition

Ultrasonic flow measurements were made with the triple midradius chord configuration in fully developed flow, and at 6 and 10 pipe diameters from the 90 degree elbow. Ultrasonic flow measurements were made with the double tilted diameter configuration in fully developed flow and at 6 pipe diameters from the elbow. One ten-flowrate run was also conducted with the latter configuration, in fully developed flow, in which the ultrasonic pulses were reflected from a sheet of rolled roofing material taped onto the bottom of the steel test section. The purpose of this experiment was to test the effect of mild roughness of the reflecting surface on received wave packet shape, and on pulse timing. The received wave packets were not noticeably distorted, nor was pulse timing disturbed. The small but significant amount of the pipe cross sectional area obstructed by the cross section of the roofing material was figured into the steel pipe area to PVC pipe area ratio in the orifice velocity calculation.

Once a transducer configuration and flow pattern had been set up, pairs of ultrasonic and orifice velocity measurements were made at ten different flowrates at each of the rotational positions of the ultrasonic test section: zero, 45, 90, and 135 degrees. In this manner, the orientation of the ultrasonic trajectory with respect to the flow profile was changed, without disturbing the flow profile. The rotational position was fixed during each run of ten ultrasonic and ten orifice velocity measurements. The phrase "ultrasonic velocity measurement" here refers to a group of 300 - 500 individual Δt measurements. A detailed description of making an ultrasonic velocity measurement is presented in the following section. Usually, velocity measurements were made at five different flowrates between 5 fps and 15 fps in the low flow range of the rig, and at five flowrates between 15 fps and 25 fps in the high flow range, in order of increasing flowrate. A typical ten-flowrate run took about 45 minutes, and was conducted as follows:

The ultrasonic flowmeter was switched on and the inclined manometer and Magnehelic gage were zeroed. A number of transit time readings (200-400) were taken at zero flow from which (with the dry-bulb temperature) the ultrasonic pathlength S would be calculated. During tests of the triple midradius configuration in fully developed flow and at 10D downstream of the elbow the dry-bulb temperature was taken only before velocity measurements 1 and 6. Dry bulb temperature was taken for each velocity point for all subsequent runs. Wet-bulb temperature and barometric pressure were taken only before points 1 and 6 for all runs. At each flowrate, the ultrasonic readings were taken (see below), ΔP_{oa} and ΔP_{ta} were read from the Magnehelic, and h_w was read from the inclined manometer.

5.4.2.1 Making an Ultrasonic Velocity Measurement

Ultrasonic transit time measurements were taken iteratively at each flowrate setting. Each time the flowrate

was reset, single upstream pulse-downstream pulse pairs were sampled with no data rejection to establish by eye the location of the prominent peak in the distribution of Δt values. A typical Δt distribution histogram (maximum flowrate) is shown in Figure 5.9c. Once the approximate location of the prominent peak was established, the microprocessor was instructed to average 100 t values falling within plus or minus 5 microseconds of the estimated "true" average Δt value. At low velocities, all Δt values fell within this window. The tolerance on data rejection was set at plus or minus 5 microseconds because this would allow data to be taken from the dominant peak in the transit time distribution without interference from neighboring, overlapping peaks at plus or minus 10 microseconds (i.e., plus or minus one cycle).

However, as the flowrate was increased and cycle jumping commenced it became increasingly difficult to locate by eye the dominant peak in the distribution of Δt values. Approaching maximum flow, the proper decade of the true peak was most easily located by comparison with the Δt value corresponding to the previous, lower flowrate. Having estimated the peak location, the microprocessor was instructed to average 100 samples falling within plus or minus 5 microseconds of the peak. Because the peaks were broad and tended to blend into each other, the position of the data acquisition window on the peak influenced the value of the 100-point averages. Positioning the 10 microsecond wide window became an iterative procedure in which two parameters were minimized simultaneously: 1) The total number of samples required to yield 100 which fell inside the window, and 2) the difference between the center value of the rejection window and the 100 point averaged Δt value. When the acquisition window had been satisfactorily positioned, three to five 100-point averages were calculated (three to five 100-point averages were also made at each low flowrate); a cumulative average was calculated by hand later.

5.4.2.2 A Comparison of Triple Midradius Chord and Double Tilted Diameter Cycle Jumping

It was suspected for quite a while before the final ultrasonic flowmeasurements were completed that cycle jumping would occur more frequently with the triple midradius chord configuration than with the double tilted diameter configuration. There were several reasons for this suspicion. The first was that the "raw" received signals in the triple midradius chord configuration were weaker than the double tilted diameter "raw" received signals: signal boosting using plastic wrap on the transducers was necessary for proper timing circuitry functioning with the former configuration but not with the latter. To use the Model C508R in the triple midradius chord configuration, it was believed, was pushing the system to its limits. It was felt also that the longer pathlength of this configuration would allow flow turbulence more opportunity to cause received signal attenuation, and amplitude fluctuation from signal to signal.

These prejudices against the triple midradius chord configuration were partially shaken when flowmetering data was taken with both configurations six pipe diameters downstream of the elbow. The double tilted diameter, previously considered the more stable configuration, did in fact exhibit considerable cycle jumping in this abnormal flow, although data acquisition was conducted successfully. The supposedly less stable triple midradius chord configuration also exhibited considerable cycle jumping, but with this configuration, too, data was taken successfully.

In an attempt to compare the relative frequencies of triple midradius chord and double tilted diameter cycle jumping quantitatively, graphs were made in which the number of Δt readings rejected as unacceptable (per average of 100 acceptable readings) during data acquisition was plotted as a function of reference velocity. The number of Δt values rejected was taken as being roughly equal to the number of

cycle jumps. Figure 5.15 is a comparison of the amount of data rejected by the two flowmetering configurations in fully developed flow, and Figure 5.16 is a comparison of data rejection by the two configurations in the flow six diameters from the elbow.

In Figure 5.16 the double tilted diameter and triple midradius chord data rejection curves are nearly the same. Regrettably, the prejudice against the triple midradius chord configuration prompted a decision not to attempt data acquisition six diameters from the elbow at more than about four-fifths of maximum flow. Even so, the conclusion to be drawn from Figure 5.16 seems to be that in terms of cycle jumping the two configurations were equally stable.

The same conclusion cannot be drawn from Figure 5.15, however. There are clearly two trends according to which the double tilted diameter data was being rejected (plotted as solid round points and solid square points). The triple midradius chord data rejection curve follows the double tilted diameter trend of higher data rejection. It should be recalled (Section 5.4.1.1) that cycle jumping for a given configuration could be lessened by adjusting the integrated threshold voltage setting to minimize the number of cycle jumps viewed on an oscilloscope. It is easy to believe that the trend of lower double tilted diameter data rejection in Figure 5.15 (solid square points) represents a more carefully chosen integrated threshold setting than the trend of greater data rejection (solid round points). It is reasonable to assume that with this optimum threshold setting in use, all of the double tilted diameter data rejection would follow the trend of lower data rejection. Thus, it is not possible to conclude from Figure 5.15 that the double tilted diameter and triple midradius chord configurations are equally stable with respect to cycle jumping.

5.5 Data Analysis and Reduction

All ultrasonic flow measurements were compared to orifice

flow measurements in terms of the area averaged velocity, V_{avg} , at the steel test section. Data reduction for both flowmeters was performed on a programmable calculator.

5.5.1 Reduction of Ultrasonic Data

The ultrasonic measurement of V_{avg} , denoted V_{us} , was calculated from

$$V_{avg,us} = V_{us} = V_{ln} \left(\frac{1}{m} \right) \quad (5.2)$$

where:

- V_{ln} = Line averaged velocity.
- m = Profile correction factor.

The profile correction factor used for all triple midradius chord configuration measurements was unity. For the double tilted diameter configuration the Kivilis Reynolds number dependent correction factor was used (See Section 3.1). The Reynolds number was based on the line averaged velocity measurement. The line averaged velocity was calculated using

$$V_{ln} = \frac{S^2}{L\Delta t} \left[\left(1 + \left(\frac{c\Delta t}{S} \right)^2 \right)^{1/2} - 1 \right] \quad (5.3)$$

where:

- S = total ultrasonic pathlength.
- L = axial component of ultrasonic pathlength.
- Δt = cumulative transit time average.
- c = speed of sound.

The speed of sound, c , was calculated from^{20,21}

$$c = (49.05) \sqrt{T_d(^{\circ}F) + 459.7} \quad (f/s) \quad (5.4)$$

where:

- T_d = dry bulb temperature.

The total ultrasonic pathlength, S , was computed using¹

$$S = (t_0 - t_w) * c \quad (5.5)$$

where:

- t_0 = Average total transit time in still air.
- t_w = Non-fluid component of t_0 .
- c = Speed of sound, as above.

5.5.2 Accuracy of Ultrasonic Velocity Measurements

The line averaged velocity, V_{ln} , can be calculated from a linearized version of Equation 5.3:

$$V_{ln} \approx \frac{c^2 \Delta t}{2L} \quad (5.6)$$

This linearization introduces a maximum error of ± 0.02 percent in the calculation of V_{ln} at 25 feet per second, while making clear the dependence of V_{ln} on c , Δt , and L .

The tolerance on c is ± 0.1 percent, one-half the tolerance on the dry bulb temperature in degrees Rankine.

The measurements of L were made to $\pm 1/16$ inch. The average length of the L path for the double tilted diameter configuration was 24.4 inches, and the average length of L in the case of the triple midradius chord configuration was 31.8 inches. The percent tolerances are ± 0.26 percent and ± 0.20 percent, respectively.

Percent tolerances on Δt were calculated from the standard deviation provided by the flowmeter. The worst-case tolerances on the Δt values at minimum and maximum flowrate, for both flowmetering configurations, and for all flow situations, are presented in Table 5.1.

The validity of assigning a standard deviation to a 100 measurement sample centered on what might well be an erroneous peak in a distribution of Δt values seems questionable. As far as the data acquisition techniques used in the present work are concerned, however, this objection can be dealt with

as follows: that the data acquisition window was in fact positioned on the dominant peak in a given transit time distribution is proved by the fact that no 100 measurement average involved rejection of more than 91 measurements (out of 191 total). That the dominant peak in the transit time distributions coincided with the "true" Δt value was proved after the data was plotted; a 10 microsecond error in Δt would have resulted in a 46 percent velocity error at minimum flowrate, and a 13 percent velocity error at maximum flowrate. No such large, random velocity errors occurred.

The overall tolerances on the measurements of V_{1n} were calculated using¹

$$X = \sqrt{\sum (a_i x_i)^2} \quad (5.7)$$

where:

- X = Overall tolerance associated with the measurement.
- x_i = Percent tolerance on an individual variable.
- a_i = Exponent of individual variable.

The worst-case overall tolerances on the V_{1n} measurements for both flowmetering configurations turned out to be the same as the overall tolerances on Δt , to one decimal accuracy.

5.5.3 Orifice Meter Data Reduction

The mass flowrate in pounds mass per hour through the orifice plate was given by¹²

$$\dot{m} = (F_r) (F_a) (Y) (I) (D_u)^2 \sqrt{h_w \rho_u} \quad (5.8)$$

Average velocity at the ultrasonic test section was calculated using^{1,12}

$$V_{avg,o} = V_o = 2.410 \left(\frac{P_u}{P_t} \right) \left(\frac{D_u}{D_t} \right)^2 \sqrt{\frac{h_w}{\rho_u}} (F_r) \quad (5.9)$$

where:

- F_r = Reynolds number factor (dimensionless); value at $Re = 30,000$, 1.009; value at $Re = 150,000$, 1.001; linear interpolation used to determine intermediate values.
- F_a = Area factor (dimensionless); value, 1.000.
- Y = Expansion factor (dimensionless); value, 0.995.
- I = Principal meter constant (dimensionless); value, 47.549.
- D_u = Inside diameter of PVC pipe at upstream pressure tap; 11.84 inches.
- D_t = Inside diameter of steel test section; 12.026 inches.
- P_u = Static pressure at upstream tap (inches Hg).
- P_t = Static pressure at ultrasonic test section (inches Hg).
- h_w = Differential pressure across orifice (inches of water).
- ρ_u = Density of flowing air at upstream tap (lbm/ft^3).

The static pressure at the ultrasonic test section was calculated by subtracting the pressure depression at the test section from the local barometric pressure.

The air density at the upstream pressure tap was calculated using the following equations²²

$$\rho_u = \frac{70.73(P_u - .378P_p)}{R(T_d + 459.7)} \quad (5.10)$$

$$P_p = P_e - P_u(T_d - T_w)/2700 \quad (5.11)$$

$$P_u = P_b - \Delta P_{oa}/13.6 \quad (5.12)$$

$$P_e = 0.000296T_w^2 - 0.0159T_w + 0.41 \quad (5.13)$$

where:

- P_p = Partial pressure (inches Hg).
- P_u = Static pressure at upstream tap (inches Hg).
- P_e = Saturation vapor pressure (inches Hg).
- ΔP_{oa} = Static pressure depression at upstream tap (inches of water).

- P_b = Barometric pressure (inches Hg).
- T_d = Dry bulb temperature (degrees F).
- T_w = Wet bulb temperature (degrees F).
- R = Gas constant; value, 53.35 ((ft-lbf)/(lbm-degrees R)).

5.5.4 Accuracy of Orifice Meter Measurements

The tolerances on the individual factors in Equation 5.9 were as follows:

- F_r : Presented in graphical form with resolution of ± 0.1 percent.
 - F_a : Presented in graphical form with resolution of ± 0.02 percent.
 - Y : Presented in graphical form with resolution of ± 0.1 percent.
 - I : Tabulated value; accuracy stated to be ± 0.2 percent.
 - D_u : Measured to $\pm 1/32$ inch, or ± 0.26 percent.
 - D_t : Measured to ± 0.003 inch, or ± 0.03 percent.
 - P_u and P_t : Accuracy determined by tolerance on barometric pressure of ± 0.01 inch, or ± 0.03 percent.
 - h_w : Accuracy determined by water density uncertainty of ± 0.1 percent; manometer oscillations at maximum flowrate of ± 0.02 inches, and oscillations at minimum flowrate of ± 0.01 inches - yielding tolerances of ± 0.25 percent and ± 2.3 percent, respectively; and the ± 0.5 percent tolerance on the slope of the incline. The combined tolerances are ± 0.6 percent at maximum flowrate, and ± 2.4 percent at minimum flowrate.
 - ρ_u : Accuracy stated in the ASHRAE tables to be ± 0.5 percent.
- Combining the uncertainties given above using equation 5.7 yields overall tolerances on the test section velocity measured by the orifice meter of ± 1.0 percent at maximum flowrate, and ± 2.5 percent at minimum flowrate.

Table 5.1 Uncertainties Associated with Δt Measurements and Ultrasonic Velocity Measurements at Maximum and Minimum Flowrates

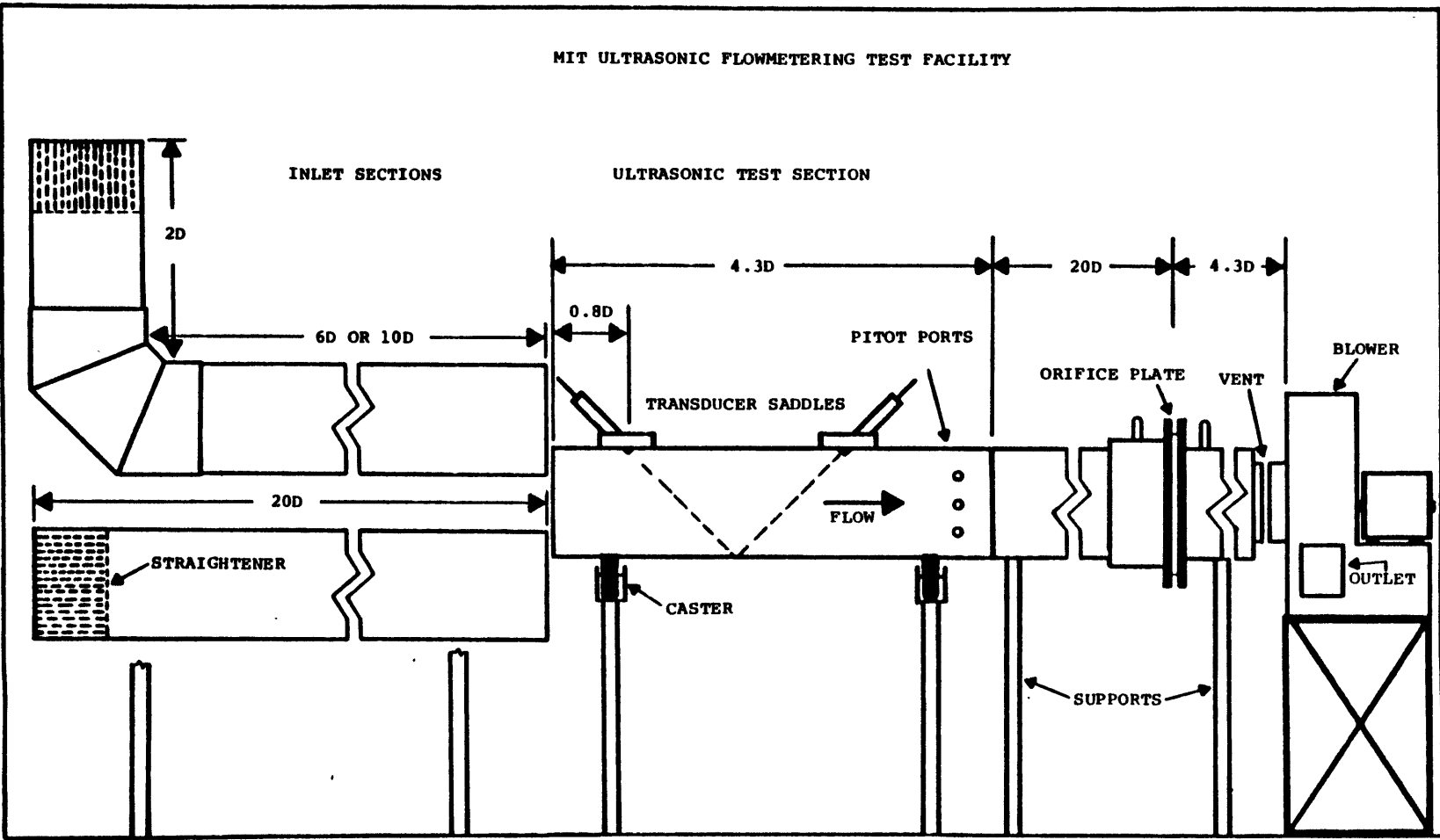
(I) Triple Midradius Chord Configuration

Inlet Section	Uncertainty at Maximum Flowrate (% of reading)	Uncertainty at Minimum Flowrate (% of reading)
20D straight	1.9	2.7
Elbow/10D straight	2.9	3.3
Elbow/6D straight	3.1	4.4

(II) Double Tilted Diameter Configuration

Inlet Section	Uncertainty at Maximum Flowrate (% of reading)	Uncertainty at Minimum Flowrate (% of reading)
20D straight	2.1	2.7
Elbow/6D straight	3.3	5.2
20D straight/roofing	1.9	2.4

Figure 5.1: Schematic of M.I.T. Test Facility



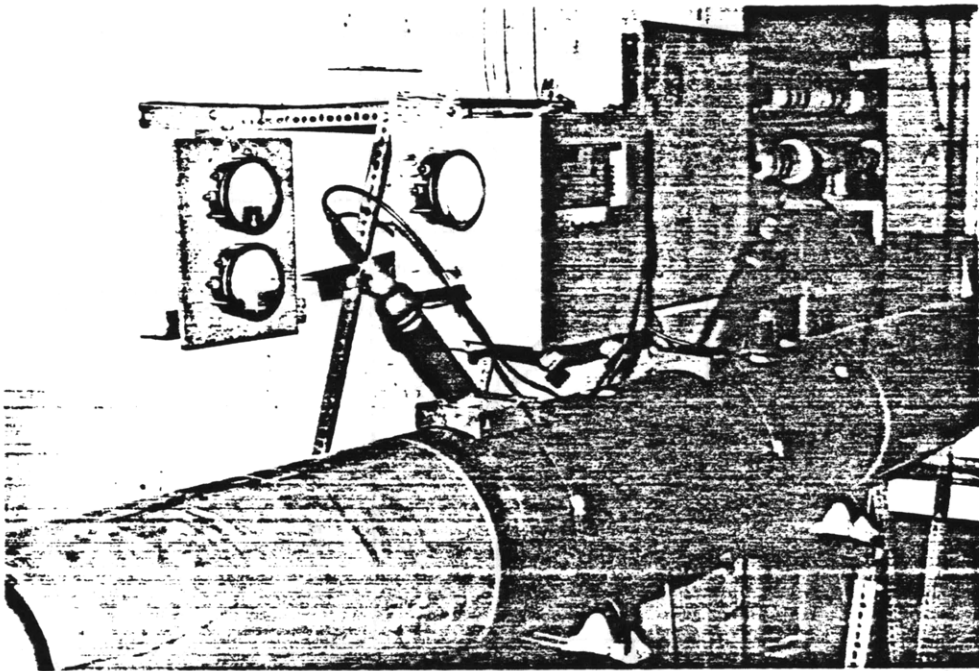


Figure 5.2: Photograph of Ultrasonic Test Section

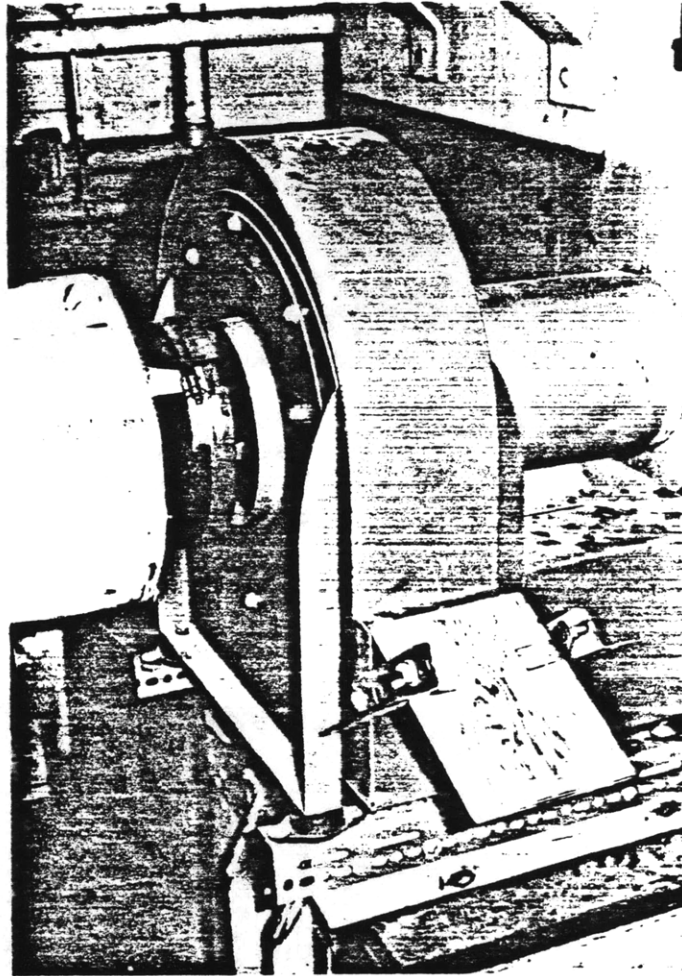


Figure 5.3: Photograph of Blower Outlet

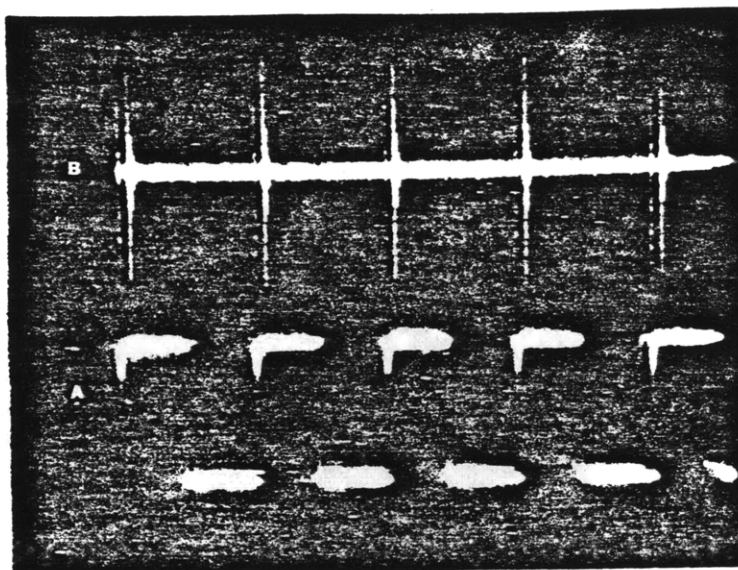


Figure 5.4: a. Oscillogram of "Sync" Signal
b. Oscillogram of Alternating
Upstream and Downstream Received
Signals

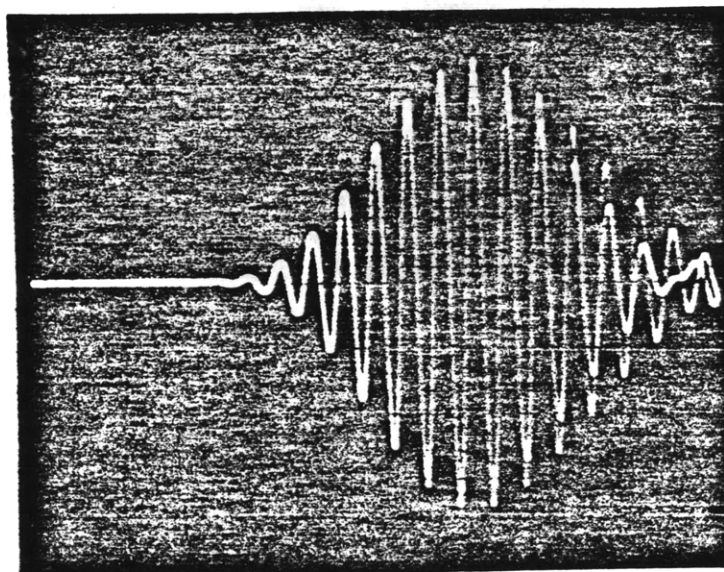


Figure 5.5: Oscillogram of Received Signal
(Expanded)

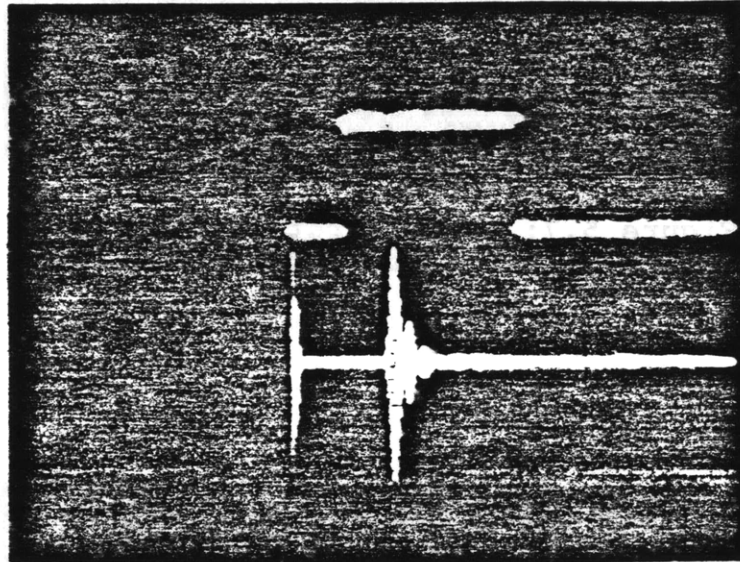


Figure 5.6: Oscillogram of Received Signal and Filtering Window

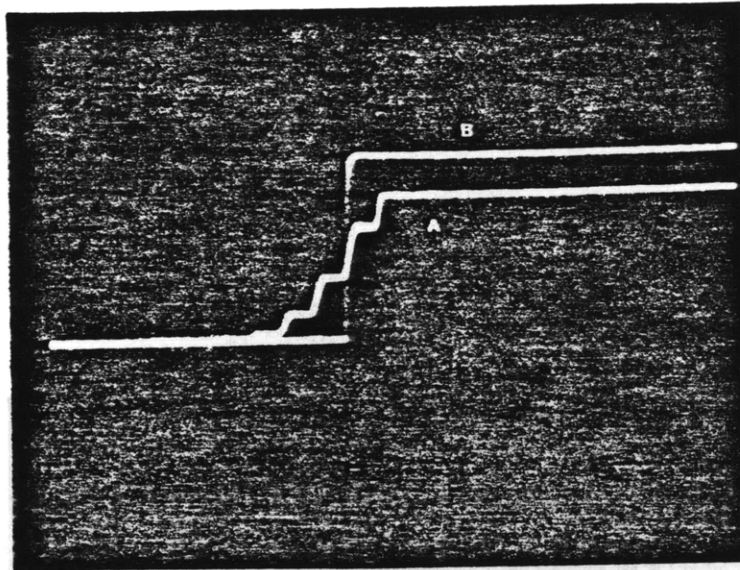


Figure 5.7: a. Integration Level
b. Integrated Threshold

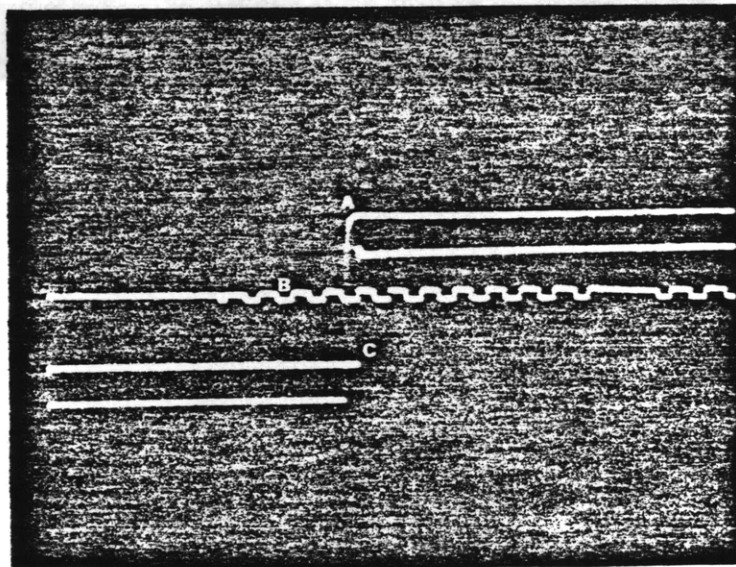


Figure 5.8: a. Integrated Threshold
b. Zero Cross Signal
c. "Stop" Signal

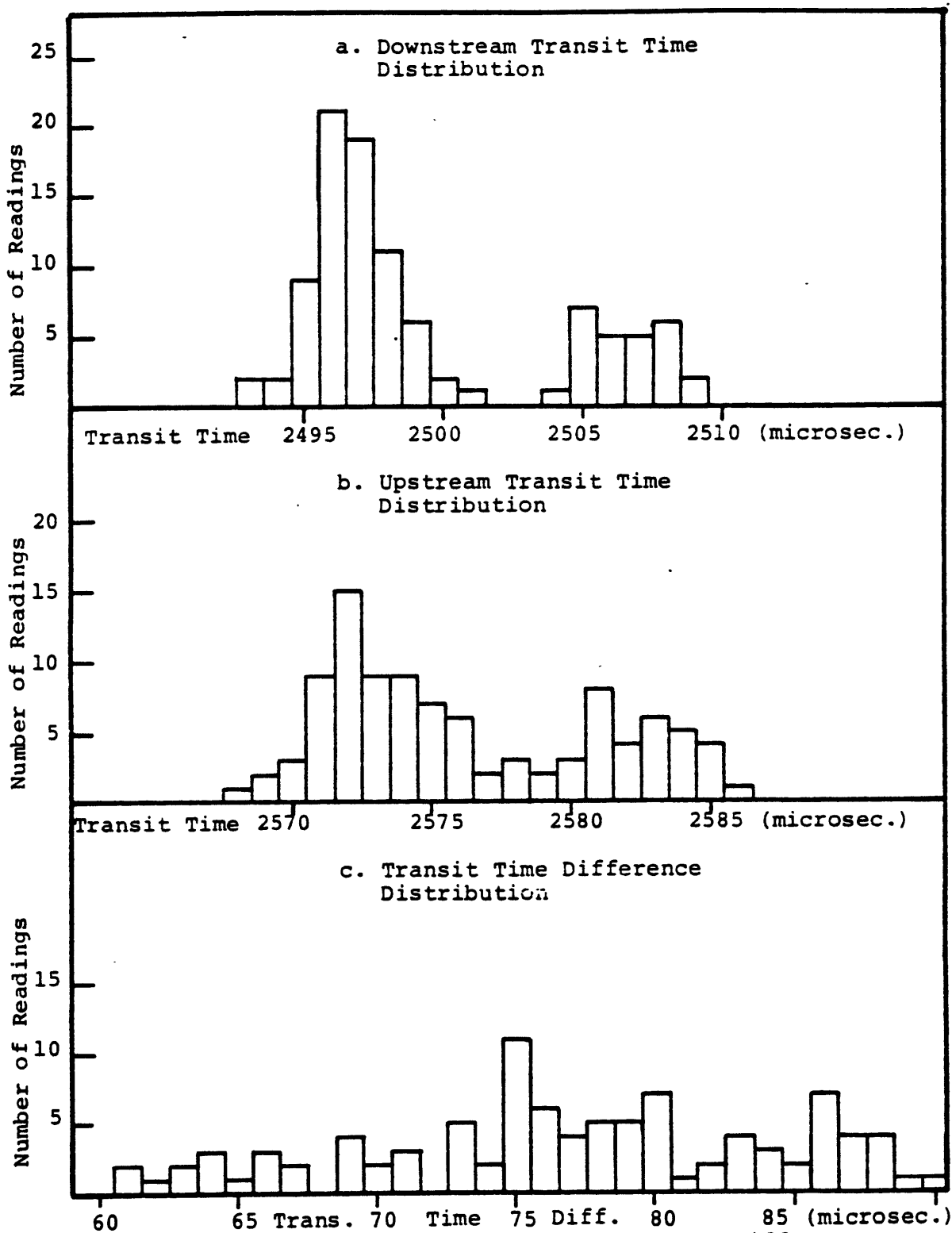


Figure 5.9: Transit Time and Transit Time Difference Distributions

```

ENTER SAMPLE SIZE (1-255) 1
ENTER MAXIMUM DELTA-T (MICROSECONDS) 200
ENTER MINIMUM DELTA-T(MICROSECONDS)
#   T1 MEAN   T2 MEAN   T1 - T2   DT MEAN   SIGMA   MAX DEV
0001 00033078 00032450 00000628 000628.00 000000.00 000000.00
0001 00033088 00032453 00000635 000635.00 000000.00 000000.00
0001 00033076 00032463 00000613 000613.00 000000.00 000000.00
0001 00033103 00032452 00000651 000651.00 000000.00 000000.00
0001 00033164 00032459 00000705 000705.00 000000.00 000000.00
0001 00033070 00032456 00000614 000614.00 000000.00 000000.00

ENTER SAMPLE SIZE (1-255) 100
ENTER MAXIMUM DELTA-T (MICROSECONDS) 67
ENTER MINIMUM DELTA-T(MICROSECONDS) 57
#   T1 MEAN   T2 MEAN   T1 - T2   DT MEAN   SIGMA   MAX DEV
0159 00033083 00032442 00000595 000641.11 000020.91 -000068.45
0151 00033084 00032443 00000663 000640.57 000017.82 -000065.67
0154 00033086 00032444 00000651 000641.64 000019.07 -000063.37

ENTER SAMPLE SIZE (1-255) 100
ENTER MAXIMUM DELTA-T (MICROSECONDS) 69
ENTER MINIMUM DELTA-T(MICROSECONDS) 59
#   T1 MEAN   T2 MEAN   T1 - T2   DT MEAN   SIGMA   MAX DEV
0114 00033092 00032448 00000667 000643.44 000020.74 -000052.15
0128 00033094 00032448 00000669 000645.60 000019.92 -000041.42
0115 00033094 00032448 00000650 000646.05 000020.40 -000049.86

ENTER SAMPLE SIZE (1-255) 100
ENTER MAXIMUM DELTA-T (MICROSECONDS) 70
ENTER MINIMUM DELTA-T(MICROSECONDS) 60
#   T1 MEAN   T2 MEAN   T1 - T2   DT MEAN   SIGMA   MAX DEV
0108 00033093 00032446 00000650 000647.00 000020.88 000057.22
0124 00033094 00032445 00000662 000649.08 000022.35 -000047.75
0119 00033092 00032444 00000618 000647.40 000021.27 000048.75

```

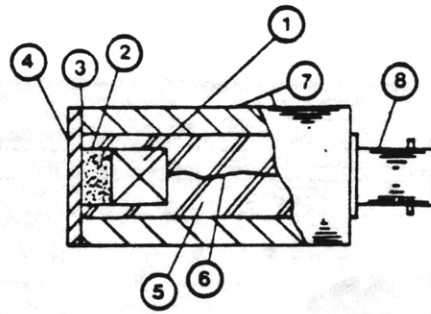


Fig. 1. Schematic cross section of basic elements of sealed and matched transducer. 1) Piezoelectric element. 2) Quarter-wave matcher. 3) Metallurgical seal. 4) Thin window. 5) Insulating potting. 6) Lead wire. 7) Housing sleeve. 8) Electrical connector.

Figure 5.11: Schematic of Transducer¹⁴

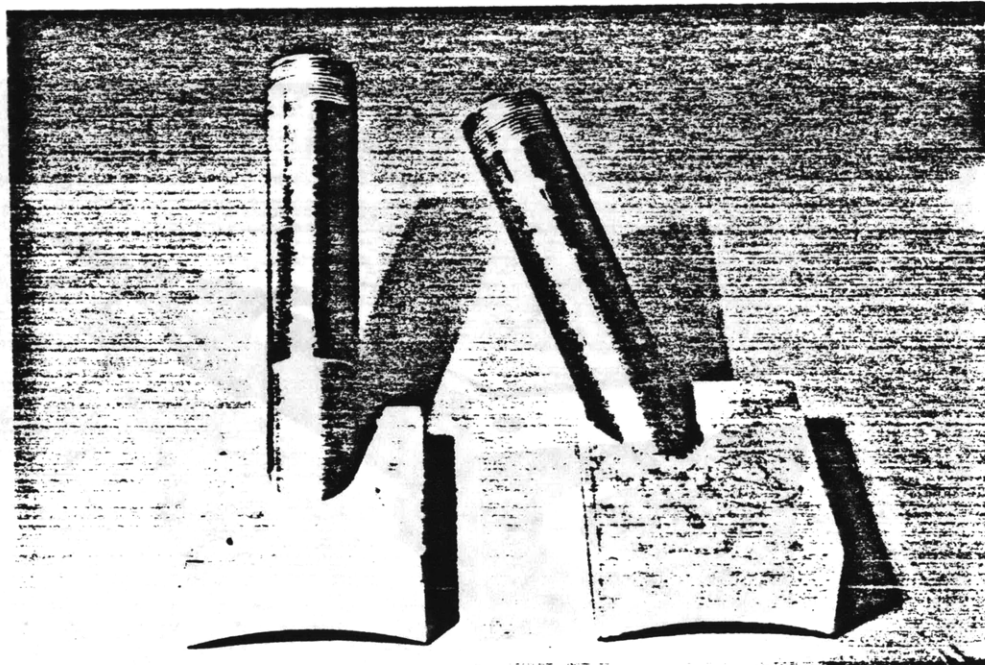


Figure 5.12: 1. Double Tilted Diameter Transducer Saddle
r. Triple Midradius Chord Transducer Saddle

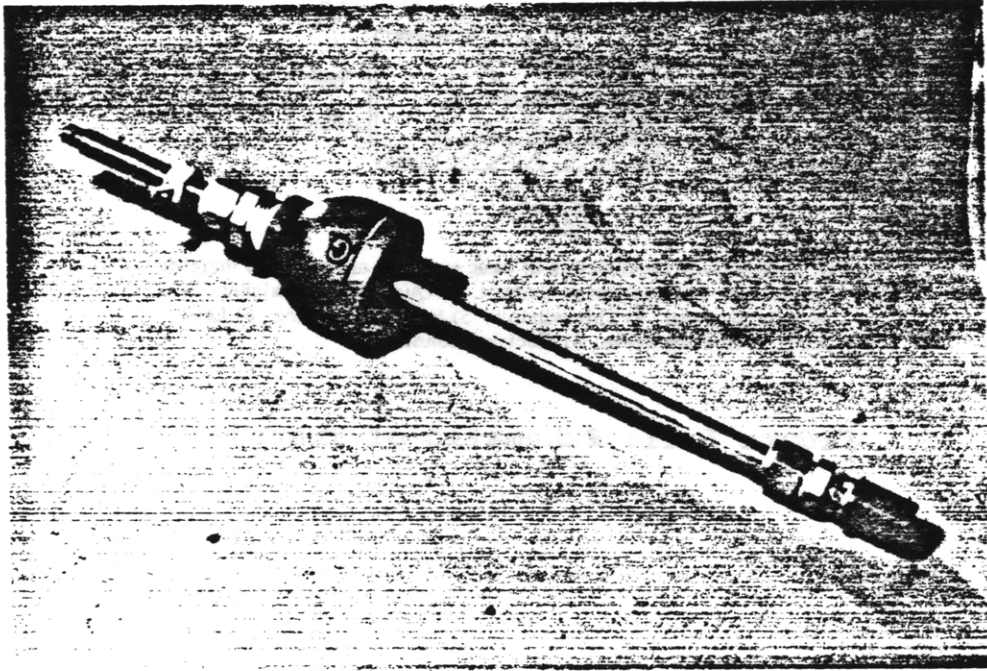


Figure 5.13a: Transducer with Locking Collar and Fittings

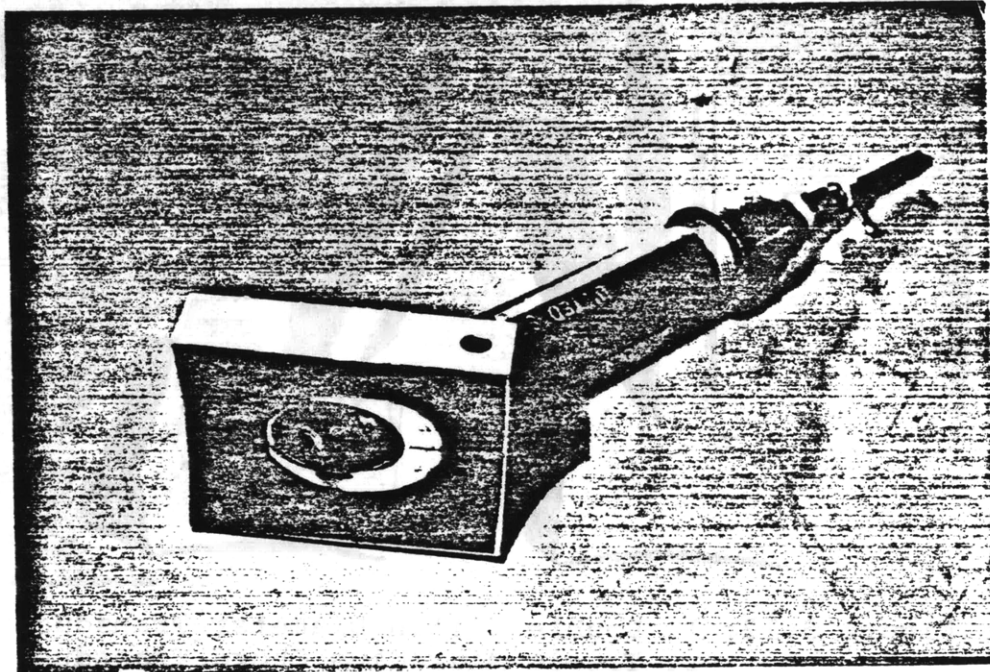


Figure 5.13b: Transducer Mounted in Saddle

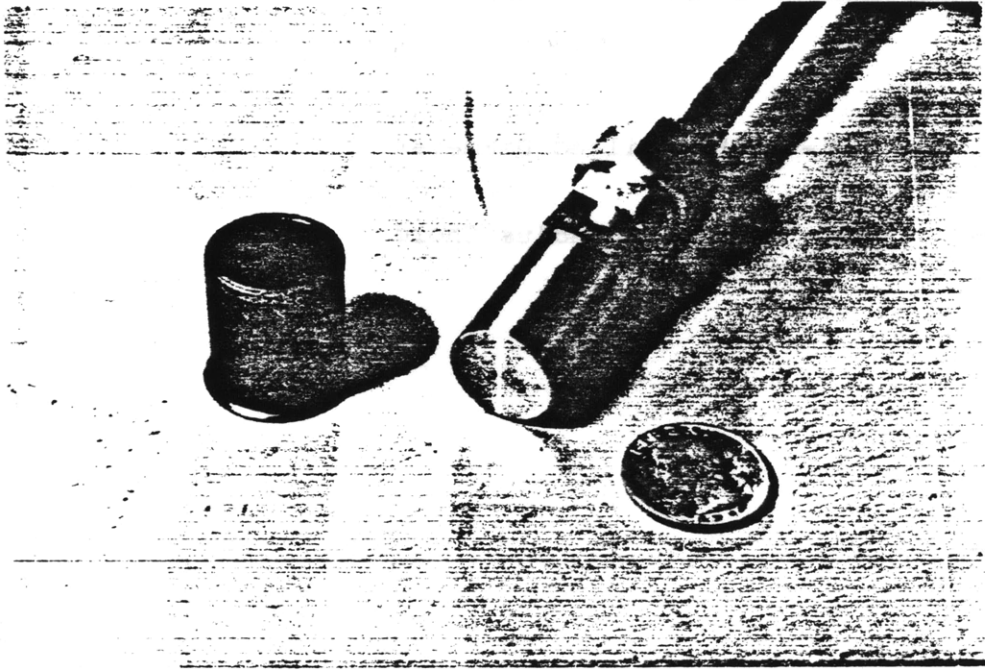


Figure 5.14a: Transducer with Plastic Collar Removed

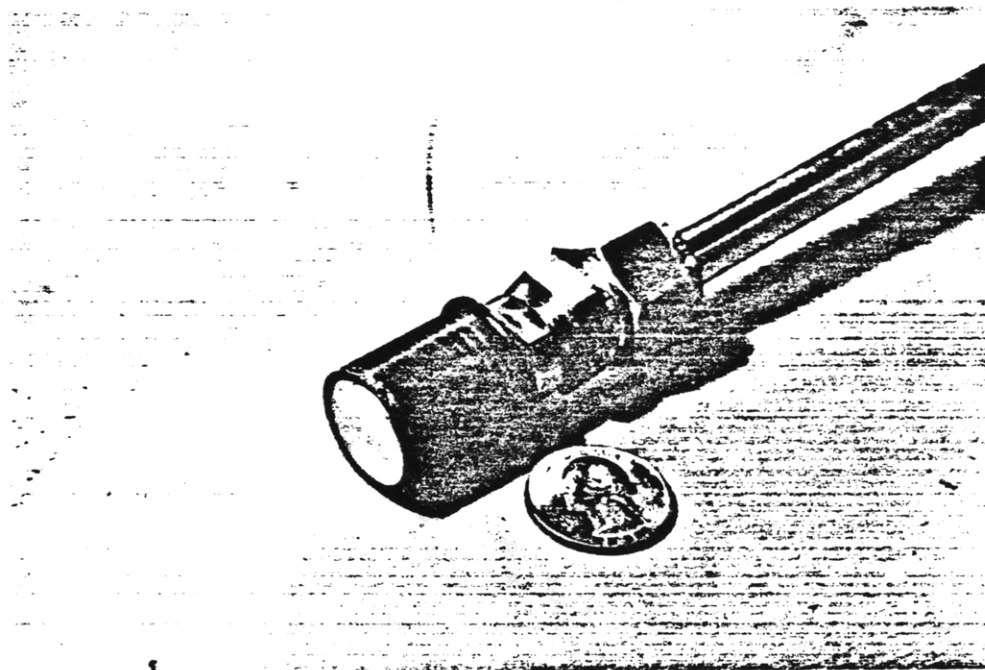


Figure 5.14b: Transducer and Plastic Collar with Plastic Wrap in Place

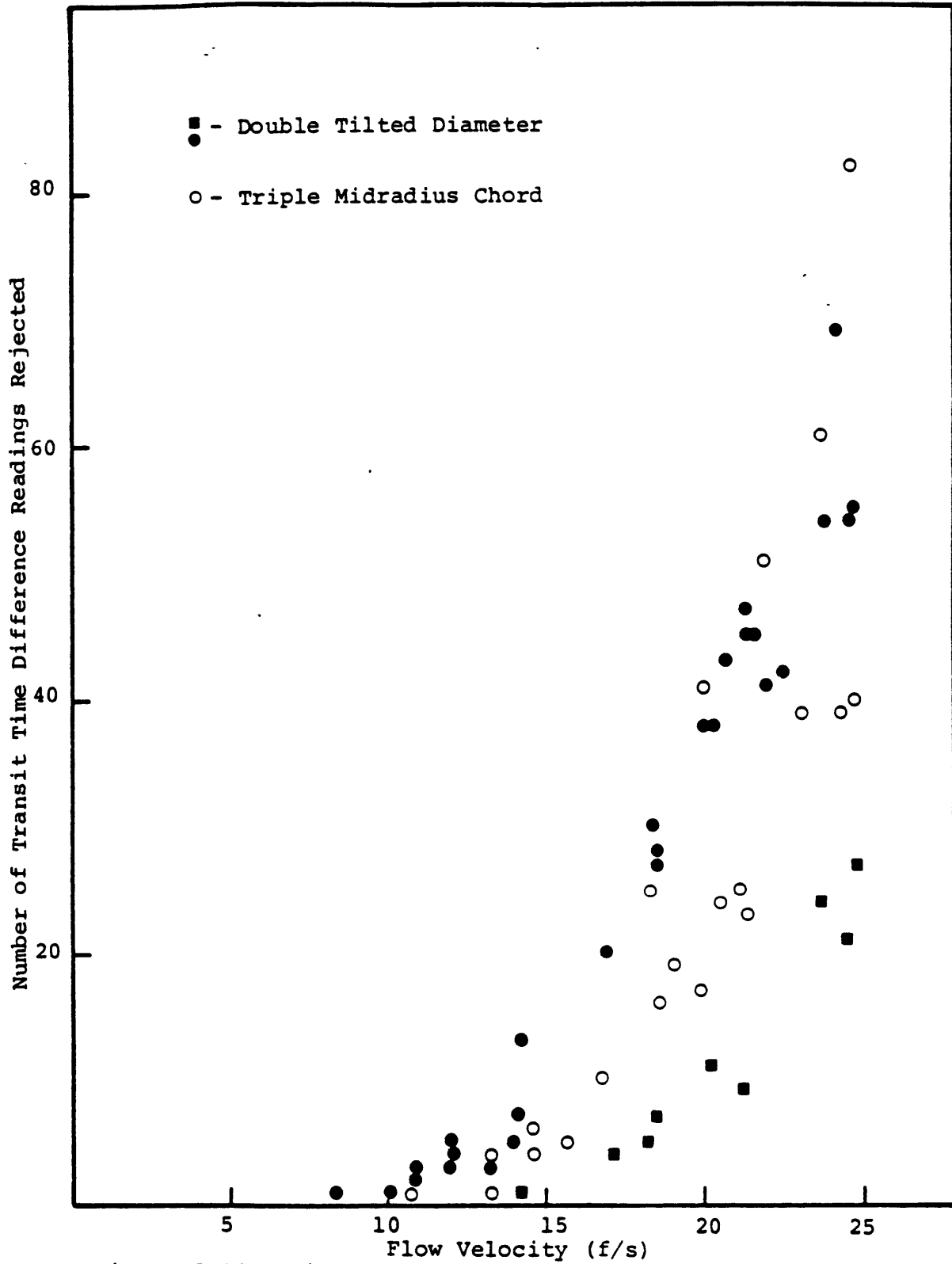


Figure 5.15: Triple Midradius Chord and Double Tilted Diameter Data Rejection Versus Velocity in Fully Developed Flow

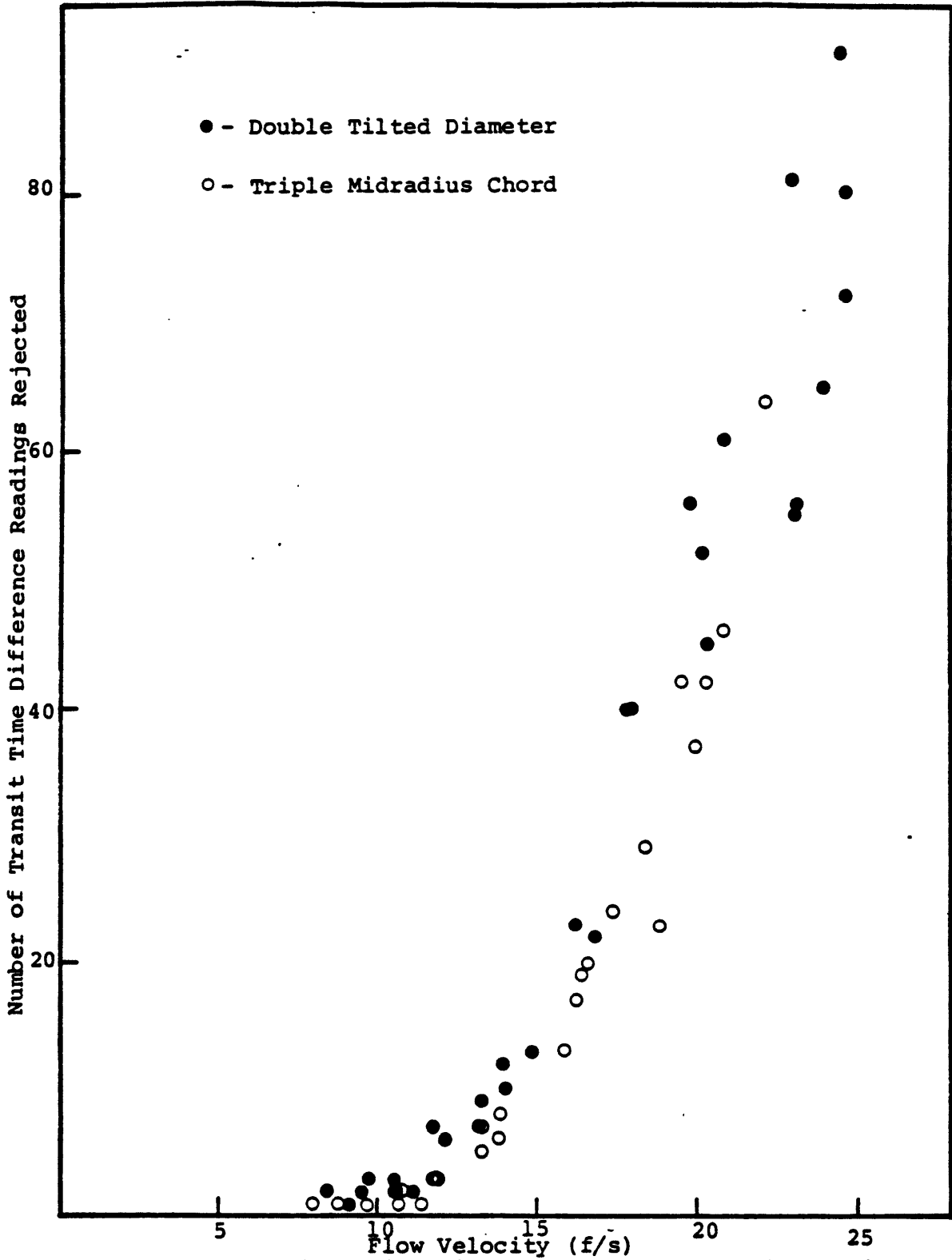


Figure 5.16: Triple Midradius Chord and Double Tilted Diameter Data Rejection Versus Velocity in the Abnormal Flow 6D From Elbow

Chapter 6

Ultrasonic Flowmetering Results

The ultrasonic flowmeasurements made in the test rig were compared with the orifice meter flow measurements in terms of the average velocity over the cross section of the ultrasonic test section, V_{avg} . The ultrasonic measurements of V_{avg} were denoted V_{us} ; the orifice measurements of V_{avg} were denoted V_o . The results of the flowmetering tests are presented in Tables 6.1 and 6.2, and also in Figures 6.1 - 6.6 as plots of V_{us} versus V_o .

The information tabulated for both flowmetering configurations in each type of flow includes the best fit slope of V_{us} versus V_o at each rotational position of the test section, and the maximum percent-of-reading error of the ultrasonic flowmeter (taking the orifice as absolute standard) at each rotational position. Each of the graphs, Figures 6.1 - 6.6, presents the flowmetering data taken with one of the two ultrasonic configurations in one type of flow, at all rotational positions of the ultrasonic test section. The circular points represent zero degrees test section rotation, with the tops of the transducer saddles facing the ceiling of the lab; the square points represent 45 degrees test section rotation, the upright triangular points 90 degrees, and the inverted triangular points 135 degrees.

6.1 Triple Midradius Chord Results

The velocity measurements made with the triple midradius chord configuration agree with orifice velocity measurements to well within the combined uncertainties on both velocity measurements. See Table 6.1 and Figures 6.1 - 6.3. If a temperature correction is made for 5 data points taken in fully developed flow at 90 degrees rotation of the ultrasonic test section (See note below), the maximum percent of reading errors in each type of flow are as follows; 2.0 percent at 6 pipe diameters from the elbow, 1.6 percent at 10 pipe

diameters from the elbow, and 1.3 percent in fully developed flow. The triple midradius chord configuration is thus not subject to abnormal flow induced errors. It is satisfying to see that the accuracy of this configuration in the test rig is very close to that predicted numerically (See Chapter 4).

(A note must be made here concerning the measurements made in fully developed flow with the ultrasonic test section at 90 degrees rotation, (See Figure 6.1, upright triangular points). The upper five data points, which were the first points taken at 90 degrees test section rotation, deviate greatly from the lower five points in the same run. The dry bulb temperature recorded prior to taking the questionable data was 72 degrees Fahrenheit. The lower five data points, taken subsequently, show superb agreement with the orifice measurements, and with the ultrasonic measurements made at other rotations of the test section. The dry bulb temperature recorded prior to taking this data was 75 degrees Fahrenheit. If the upper five ultrasonic and orifice velocity values are re-calculated using a temperature of 75 degrees they, too, are in agreement with the orifice.

This temperature correction is by no means ad hoc. It is justifiable on the grounds that all other runs conducted in the test area show that the ambient temperature in the vicinity of the rig was at least 75 degrees, and that during no other ten flowrate run does the dry bulb temperature undergo a variation as large as 3 degrees. (Dry bulb temperature was taken at every velocity measurement during later runs, to prevent errors like this one). The low temperature reading can be explained by noting that the data points in question were the first taken on that day, and that the thermometer was brought to the test area from a cooler part of the lab. The corrected results are presented in parentheses in Table 6.1.)

6.2 Double Tilted Diameter Configuration Results

As expected of any ultrasonic flowmetering configuration

that interrogates the flow along a single chord, the double tilted diameter configuration was found to be subject to abnormal profile induced errors in the abnormal flow 6 pipe diameters downstream of the elbow. See Figure 6.5, and Table 6.2. The maximum variation of the slopes of the V_{us} and V_o plots between two test section rotational positions was 5.5 percent; this is very close to the numerical prediction. The slope of V_{us} versus V_o averaged over the four test section rotational positions was 0.955, and the maximum percent of reading error was 9.2 percent. This poor overall agreement with the orifice was not predicted numerically, probably because of symmetry in the numerically generated abnormal profile.

Most surprising were the poor results obtained with the double tilted diameter configuration in what was thought to be axisymmetric fully developed flow. See Figure 6.4, and Table 6.1. The maximum percent of reading error was 7.3 percent; the maximum difference between slopes of V_{us} versus V_o plots at the different test section rotations was 8.6 percent; the average of all V_{us} versus V_o slopes was 1.038. Because the individual V_{us} versus V_o plot at each test section rotation was very linear, with little data scatter, the large discrepancies among the slopes of the V_{us} versus V_o plots representing the different test section rotations is attributed to unexpected profile asymmetries existing in the flow.

The single test in which the pulses in double tilted diameter configuration were reflected off of rolled roofing material showed that mild roughness of the reflecting surface did not cause velocity measurement errors. See Figure 6.6.

Table 6.1
 Ultrasonic Flowmetering Results
 Triple Midradius Chord Configuration

(I) Inlet Section: Twenty Diameters Straight Pipe

Date	Test Section Rotation (degrees)	Best Fit Slope	Maximum Error (% of reading)
3-11	0	1.008	0.9
3-11	45	1.010	0.9
3-12	90	0.967 (1.006)	2.4 (0.6)
3-12	135	1.011	1.3

(II) Inlet Section: Ninety Degree Elbow with 10 Diameters
 Straight Pipe

Date	Test Section Rotation (degrees)	Best Fit Slope	Maximum Error (% of reading)
3-3	0	1.012	1.2
3-5	45	1.017	1.4
3-3	90	1.002	1.6
3-5	135	1.012	1.4

(III) Inlet Section: Ninety Degree Elbow with 6 Diameters
 Straight Pipe

Date	Test Section Rotation (degrees)	Best Fit Slope	Maximum Error (% of reading)
6-26	0	1.029	2.0
6-26	45	1.022	1.6
6-26	90	1.009	1.8
6-26	135	1.027	1.9

Table 6.2
 Ultrasonic Flowmetering Results
 Double Tilted Diameter Configuration

(I) Inlet Section: Twenty Diameters Straight Pipe

Date	Test Section Rotation (degrees)	Best Fit Slope	Maximum Error (% of reading)
6-16	0	1.090	7.3
6-23	0	1.017	3.0
6-23	45	1.034	2.6
6-19	90	1.004	1.8
6-23	90	1.020	1.4
6-23	135	1.060	4.1

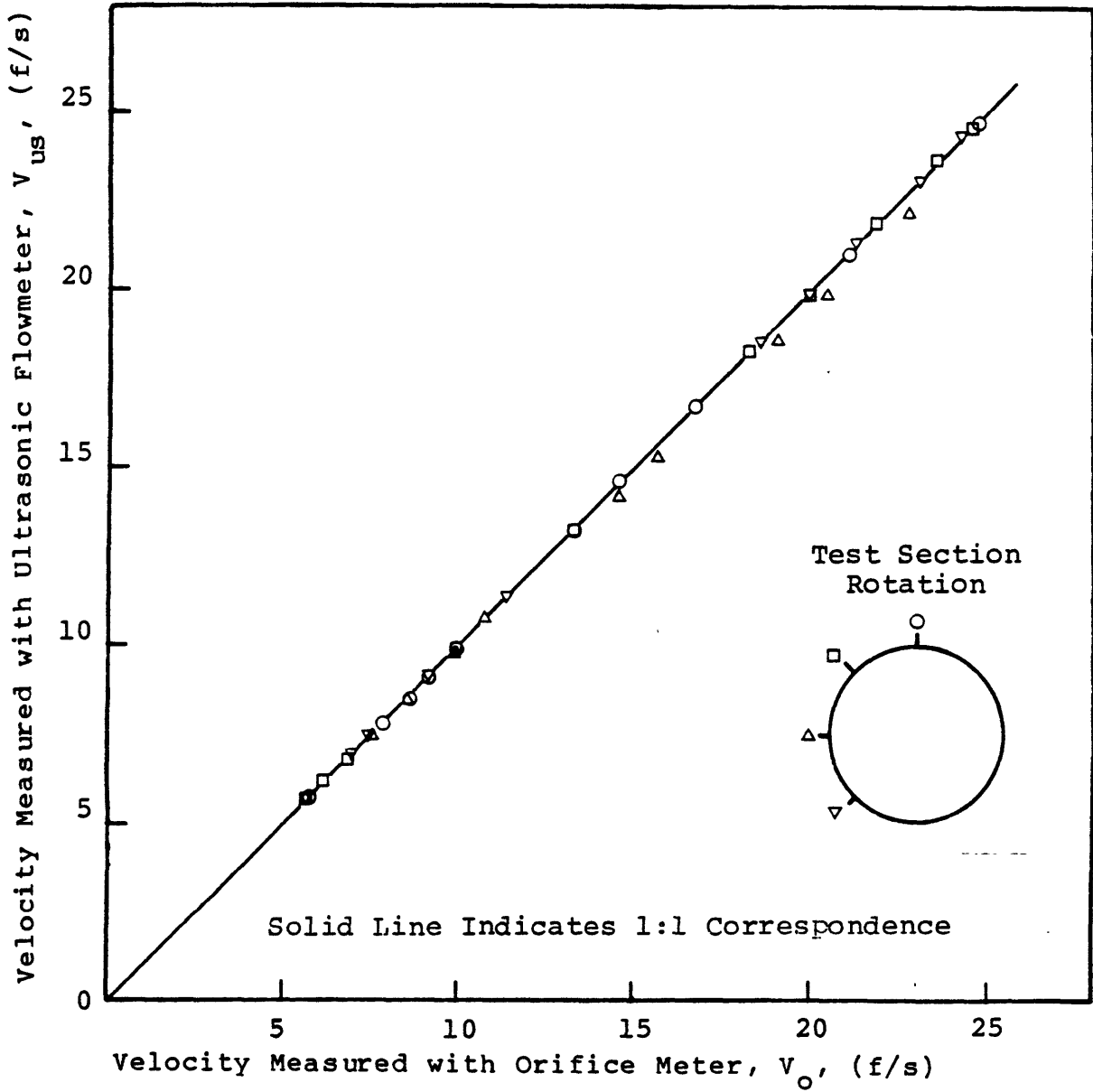
(II) Inlet Section: Ninety Degree Elbow with 6 Diameters
 Straight Pipe

Date	Test Section Rotation (degrees)	Best Fit Slope	Maximum Error (% of reading)
6-15	0	0.991	5.9
6-24	45	0.945	8.4
6-15	90	0.936	8.5
6-24	135	0.946	9.2

(III) Inlet Section: Twenty Diameters Straight Pipe
 Pulses Reflected From Roofing
 Material

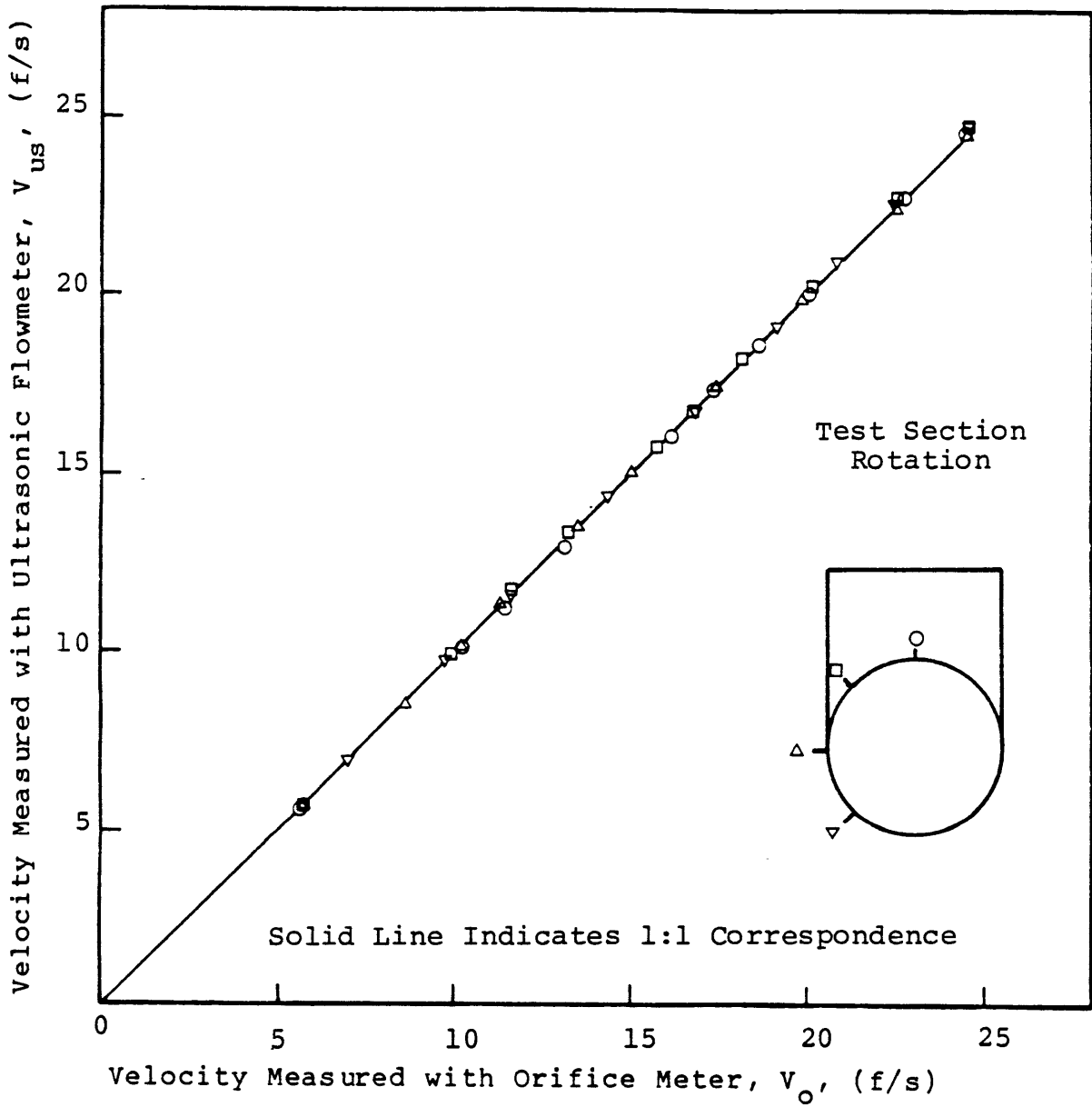
Date	Test Section Rotation (degrees)	Best Fit Slope	Maximum Error (% of reading)
6-25	0	0.993	0.8

Figure 6.1



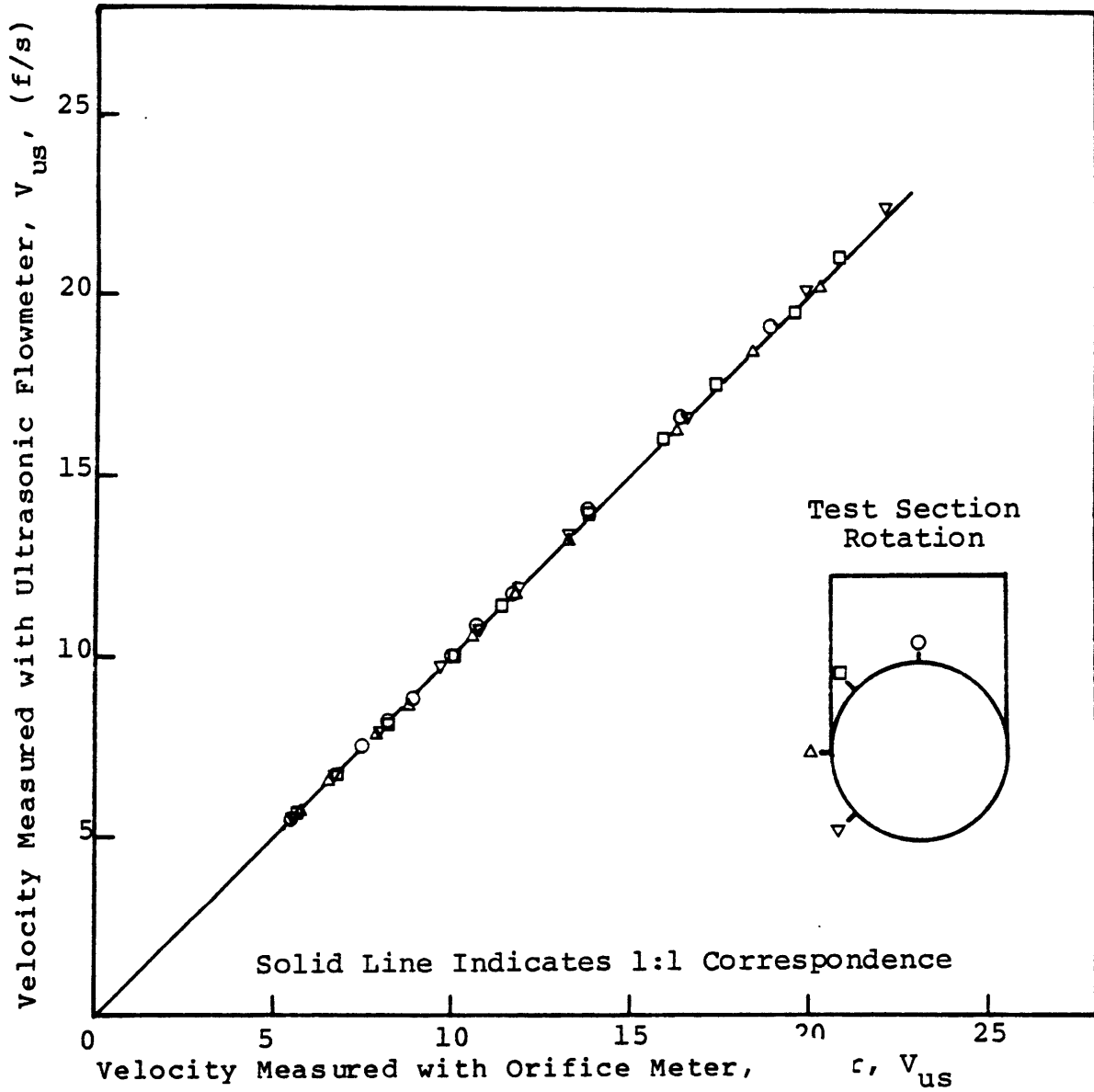
Area Averaged Velocity Measurements
Triple Midradius Ultrasonic Flowmeter Compared to Orifice
20D Straight Pipe at Test Section Inlet

Figure 6.2



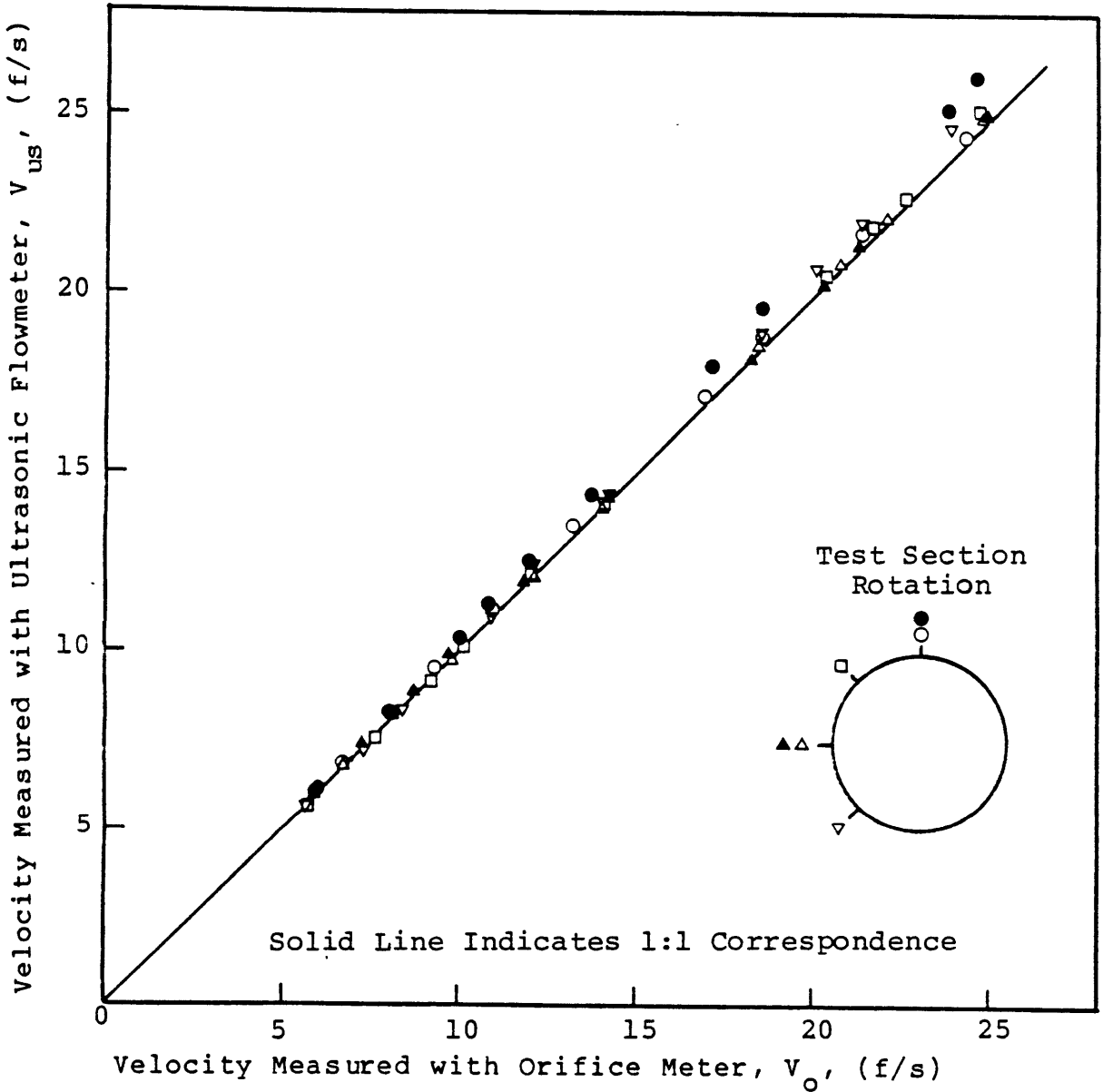
Area Averaged Velocity Measurements
Triple Midradius Ultrasonic Flowmeter Compared to Orifice
90 Degree Elbow 10D from Test Section Inlet

Figure 6.3



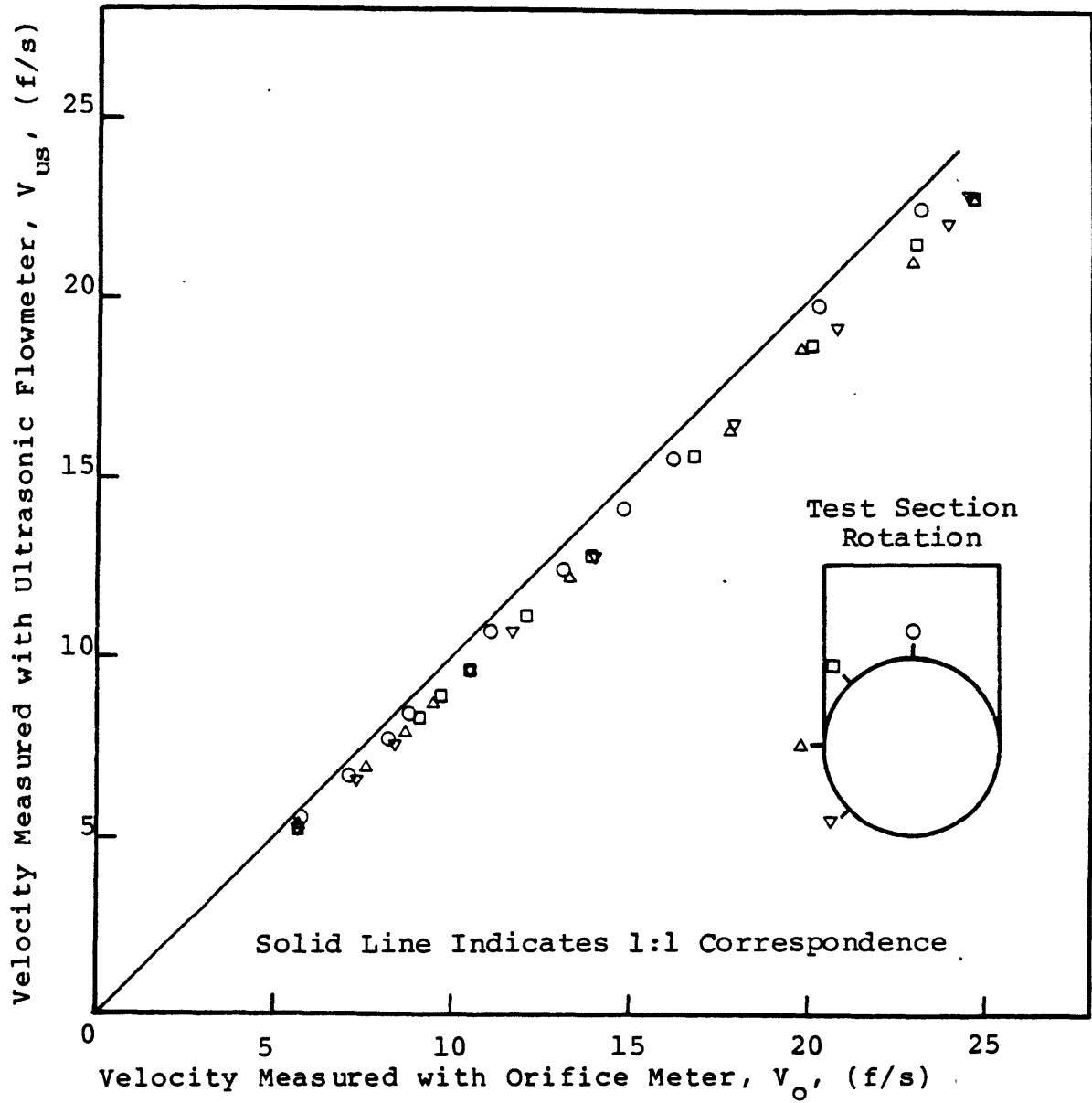
Area Averaged Velocity Measurements
 Triple Midradius Ultrasonic Flowmeter Compared to Orifice
 90 Degree Elbow 6D from Test Section Inlet

Figure 6.4



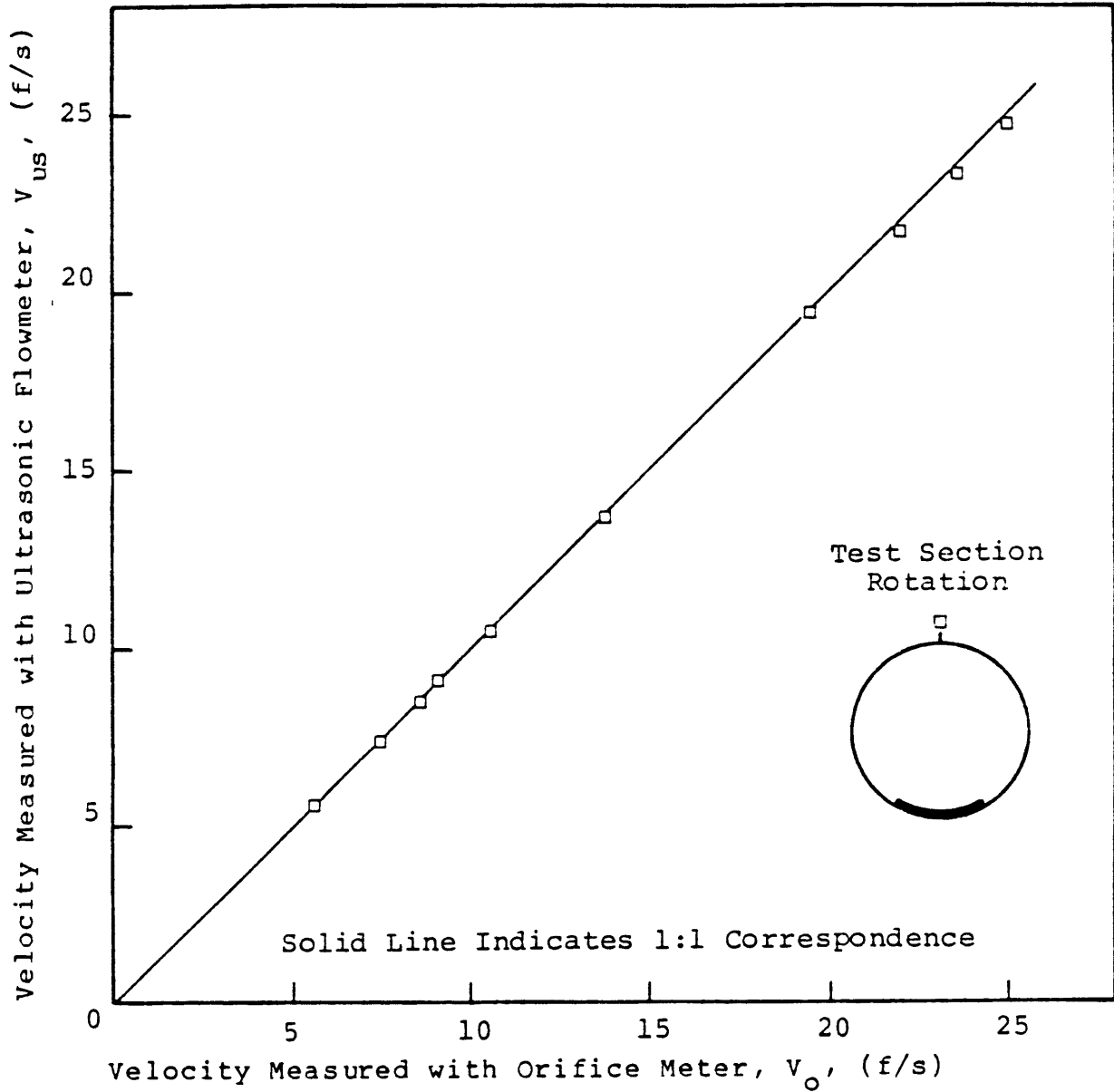
Area Averaged Velocity Measurements
 Double Tilted Diameter Ultrasonic Flowmeter Compared to Orifice
 20D Straight Pipe at Test Section Inlet

Figure 6.5



Area Averaged Velocity Measurements
Double Tilted Diameter Ultrasonic Flowmeter Compared to Orifice
90 Degree Elbow 6D from Test Section Inlet

Figure 6.6



Area Averaged Velocity Measurements
 Double Tilted Diameter Ultrasonic Flowmeter Compared to Orifice
 20D Straight Pipe at Test Section Inlet
 Pulse Reflected from Rolled Roofing Material

Chapter 7

Conclusions and Recommendations

Presented in this chapter are conclusions based on the results of the ultrasonic flowmetering tests conducted in the M.I.T. test facility. Also presented are recommendations for continued testing of the double tilted diameter and triple midradius chord flowmetering configurations in the field, along with brief recommendations for data acquisition procedures.

7.1 Conclusions

1) The results of the M.I.T. ultrasonic flowmetering tests in fully developed flow and in the abnormal flow downstream of a ninety degree elbow show that the triple midradius chord configuration is more accurate - compared with an orifice meter - in all types of flow, and at any rotational orientation relative to an abnormal velocity profile, than the double tilted diameter configuration. The M.I.T. reference instrumentation was not sufficiently accurate to show whether or not the triple midradius chord configuration is capable of meeting Consolidate Edison's accuracy requirement of ± 0.5 percent of yearly totalized flow (See Recommendations).

2) No firm conclusion can be made about the relative stability of the received acoustic signals in the two configurations, although there is some indication that turbulence may cause larger fluctuations and greater attenuation of the triple midradius chord received signals, based on M.I.T. tests in which received signal amplitude and fluctuation were measured for each configuration over a large range of flowrates. Nor can a conclusion about relative received signal stability be made based on the number of transit time readings rejected during data acquisition with each configuration. It is certain that the raw signals received with the triple midradius configuration are weaker

than those received with the double tilted diameter configuration, a necessary result of the longer pathlength in the former case.

3) Tests in which received signal amplitude was measured for each configuration at maximum flow indicate that the signals received at the upstream transducer are weaker than those received at the downstream transducer. A flow effect is believed to be the cause of this discrepancy.

7.2 Recommendations

1) It is recommended that the M.I.T. flowmetering tests be repeated in the field with both ultrasonic trajectories. The tests should be made in what is believed to be fully developed turbulent flow, and in the abnormal flow downstream of an elbow; the M.I.T. procedure of placing the ultrasonic flowmetering configuration at different rotational orientations relative to both of these flows, at the same axial location in the pipe, should be followed. Such tests are needed to verify that the triple midradius trajectory is not subject to profile induced errors, and that the double tilted diameter trajectory is subject to profile induced errors. Further, tests of the triple midradius chord ultrasonic flowmeter against a calibrated reference meter are recommended to establish whether or not this ultrasonic flowmeter will meet Con Edison's accuracy requirement.

2) Field tests in high velocity flow (greater than 25 fps), in a large diameter main (greater than 12 in), at pressures above atmospheric are necessary to resolve the question of relative amplitude stability of the signals received with the two ultrasonic flowmetering configurations. Highly turbulent flow acting on the acoustic signals over long pathlengths should bring out a relative amplitude instability, if it exists. High line pressure is necessary so that plastic wrap need not be applied to the transducers for signal

amplification. The plastic wrap is believed to be a partial cause of fluctuation of the received signals.¹⁵

3) It is recommended that ultrasonic flowmetering electronics with separate automatic gain control on the upstream and downstream channels be used. "Dual AGC," as this feature is called, allows cycle jumping of both channels to be minimized; a unit with a single AGC circuit allows cycle jumping to be minimized on only one channel - upstream or downstream.

4) It is recommended that upstream and downstream transit times, rather than t be used in flow calculations. The flow equation based on the transit time difference, Δt , is not as accurate as the equations based on t_u and t_d . Also, in flowmetering situations where cycle jumping occurs frequently, it is much easier to locate the true upstream and downstream transit times than to locate the true Δt value.

Appendix A
An Experimental Investigation into Factors Affecting Received
Signal Amplitude

A.1 Introduction

Serious investigation into cycle jumping began when it was found to be nearly impossible to take data four pipe diameters downstream of the 90 degree elbow because of 10 microsecond jumping of Δt . It was at this point that the first histograms of upstream and downstream transit time distributions were made. Representative transit time distribution plots are shown in Figures 5.9a&b. It was noted that the upstream and downstream transit time distributions each exhibited bimodality or trimodality, usually a strong "true" peak with a secondary peak at plus 10 microseconds, and a tertiary peak at minus 10 microseconds. The striking feature was that the dominant peak in the downstream distributions tended in nearly all cases to be significantly stronger than the dominant peak in the upstream distributions. The upstream transit time values were jumping plus 10 microseconds more frequently.

In Section 5.2.1.4, random cycle jumping of plus 10 microseconds was linked to weakness of the received signal which causes the integration level "staircase" formed from that signal to require an extra step - and hence an extra 10 microseconds - to reach the preset voltage threshold arming the "stop" gate. When it is considered that the downstream and upstream integration levels must each in turn reach the same preset voltage threshold to trigger the stop gate, it becomes clear that in the case of the transit time distributions described above the upstream AGC signals must have been weaker on average than the downstream AGC signals.

A cause for the relative weakness of the upstream AGC signals was sought among acoustic and electronic possibilities. Switching upstream and downstream transducers, physically reversing the steel test section, and switching

electronics channels had no effect on histogram shape. Tests in which the transducers - normally positioned with their faces one-half in and one-half out of the flow - were inserted well into the flow, or completely withdrawn into the saddles also had no effect on histogram shape. A two-dimensional theoretical investigation into the relative magnitudes of upstream and downstream ultrasonic beam focusing or defocusing caused by beam rotation in high velocity gradients, was begun. The purpose of the study was to see whether the upstream pulses might be weakened by defocusing, while the downstream pulses were strengthened by focusing. This study is presented in Appendix B.

The higher capacitance of the longer coaxial cable connecting the upstream transducer to the electronics was temporarily believed to cause the upstream signal weakness. The elbow was moved to six diameters upstream of the steel test section and equal lengths of low capacitance coaxial cable were put between the transducers and the electronics. Lower turbulence at six diameters from the elbow lessened cycle jumping, and thereby greatly facilitated data acquisition. The disparity between upstream and downstream transit time histogram shape persisted, however. At this point, a quantitative investigation of factors affecting received signal amplitude was begun.

A.2 Objectives

The experimental hypothesis was that weaker upstream received signals were causing the upstream transit time measurements to jump plus 10 microseconds more frequently than the downstream transit time measurements.

The primary objectives of the experiments were, first, to verify that the upstream received signals in flowing air were on average weaker than the downstream received signals and, second, to find the cause of the relative upstream signal weakness.

A tertiary objective was to answer the following

question: if flow effects were found to be the cause of the relative upstream signal weakness, would the triple midradius chord configuration received pulses undergo more attenuation than the double tilted diameter pulses because of the longer pathlength and additional reflection of the former configuration? This objective has to do with settling the question of relative stability of the two flowmetering configurations with respect to cycle jumping as discussed in Section 5.4.2.2.

A.3 Methods

A Nicolet 206 digital recording oscilloscope was used to measure the positive peak amplitude of individual received wave packets. The measurements involved primarily the AGC signals, although some measurements were made of the received signal amplitude with the receiving transducer connected directly to the oscilloscope. Groups of twenty to fifty - usually fifty - random upstream signal amplitude measurements, and twenty to fifty random downstream signal amplitude measurements were taken using the single-sweep feature of the oscilloscope. From each set of amplitude measurements an average and standard deviation were calculated. Several sets of amplitude measurements were made with both the double tilted diameter, and the triple midradius chord configurations at maximum flowrate. See Table A.1. The upstream and downstream transducers - including the coaxial cables - were reversed several times during these tests. Sets of only upstream received signal amplitude measurements were taken with both transducer configurations at different flowrates, to give an idea of the dependence of received signal amplitude and amplitude fluctuation on velocity. See Table A.2 and Figures A.1 and A.2.

A.4 Results and Conclusions

It was discovered early in these experiments that a preferred transmit-receive direction existed between the

transducers in still air. The still air AGC signal received at transducer A was always stronger than the still air AGC signal received at transducer B, irrespective of transducer placement in the pipe, coaxial cable capacitance, or the electronics channel to which the transducers were connected. The still air peak to peak voltage difference was approximately 0.1 - 0.2 volts out of 3.0 - 3.4 volts. Tests in which the upstream and downstream transducers were switched while transit time data was taken showed that the preferred still air transmit-receive direction was not the cause of the histogram shape discrepancy.

It was noticed also that doubling or tripling the length of coaxial cable between a transducer and the electronics had no effect on the amplitude of the still air AGC signal. The same length of cable when connected between a receiving transducer and the oscilloscope caused considerable received signal attenuation.

The numerical results of the tests made at maximum flowrate, presented in Table A.1, show that in 7 out of 10 cases the upstream received signals were weaker, on average, than the downstream received signals. In 8 out of 10 cases, the difference between the zero-flow signal amplitude and the average maximum-flow signal amplitude was greater for the upstream received signals. A received signal amplitude difference caused by a change of interrogation direction has also been found by Lynnworth and Matson.²³ Weaker upstream signals can thus be said to be the cause of the more frequent plus 10 microsecond cycle jumping of the upstream transit times. Because the downstream received signals are stronger independent of transducer firing direction, connecting cable length, and other mechanical and electronic parameters, the received signal strength difference is believed to be caused by a flow effect. New model ultrasonic flowmeters such as the Panametrics 7100 are equipped with dual AGC circuits which compensate automatically for the discrepancy between the upstream and downstream signals.⁸

Zero-flow received signal amplitude minus average received signal amplitude with flow was plotted versus flow velocity, for both transducer configurations. This graph (Figure A.1) shows the average signal strength decreasing with velocity. A plot of the standard deviation of the received signal amplitude versus flow velocity (Figure A.2) shows an increase in fluctuation level with increasing velocity.

There is some indication that the triple midradius chord configuration may be more sensitive to flow velocity and turbulence than the double tilted diameter configuration: The triple midradius chord received signals seem to undergo greater attenuation, and to be more highly fluctuating, as velocity increases (See Figures A.1 and A.2). Further received signal amplitude measurements will have to be made with both configurations at higher velocities than attainable in the present test rig before it can be concluded that timing difficulties will arise with the triple midradius configuration at high velocity.

Measurements of received signal amplitude made with and without plastic wrap over the transducers are inconclusive as to whether the plastic increases or decreases the amplitude fluctuation level. Lynnworth has reported increased amplitude fluctuation with plastic wrap in use, which he attributes to the plastic being sucked away from the transducer face by the flowing air.¹⁵

Table A.1: Upstream and Downstream Received Signal Amplitude Measurements at Maximum Flowrate

	AGC	Date	Plastic Wrap	Best V = 0 Signal	A ₀	\bar{A}	A ₀ - \bar{A}	σ	σ (%)	No. of Samples
										Reading
⊙	NO	6-7	NO	us	4.0 mV	3.35 mV	.65 mV	.89 mV	26	50
				✓ ds	4.3 mV	4.16 mV	.14 mV	.67 mV	16	Peak-Peak
⊙	NO	6-7	No	us	5.85 mV	5.11 mV	.74 mV	.80 mV	16	50
				✓ ds	5.95 mV	5.82 mV	.13 mV	1.07 mV	18	pk-pk
⊙	Yes	6-8	Yes	✓ us	—	1.34 V	—	.24 V	18	30
				ds	—	1.38 V	—	.29 V	21	+ peak
	Yes	6-10	Yes	✓ us	1.72 V	1.17 V	.55 V	.30 V	25	+ peak
				ds	1.62 V	1.48 V	.14 V	.31 V	21	50
	Yes	6-10	Yes	us	1.41 V	.94 V	.47 V	.22 V	24	50
				✓ ds	1.64 V	1.45 V	.19 V	.30 V	21	+ peak
⊙	Yes	6-11	Yes	✓ us	1.63 V	1.42 V	.21 V	.27 V	19	50
				ds	1.45 V	1.24 V	.21 V	.22 V	18	+ peak
	Yes	6-11	Yes	us	1.39 V	1.24 V	.15 V	.24 V	19	50
				✓ ds	1.60 V	1.41 V	.19 V	.25 V	18	+ peak
	Yes	6-11	Yes	✓ us	1.70 V	1.49 V	.21 V	.29 V	19	50
				ds	1.53 V	1.33 V	.20 V	.21 V	16	+ peak
	Yes	6-14	No	✓ us	1.61 V	1.31 V	.30 V	.25 V	19	50
				ds	1.25 V	1.17 V	.08 V	.23 V	19	+ peak





	Date	Vel.	A_0	\bar{A}	$A_0 - \bar{A}$	σ	σ/\bar{A}
	6-16	5.9	1.77	1.76	.01	.098	5.6
	6-16	9.8	1.79	1.70	.09	.139	8.2
	6-16	14.6	1.76	1.62	.14	.189	12
	6-16	19.5	1.74	1.53	.21	.23	15
	6-20	21.0	1.80	1.53	.27	.23	15
	6-20	22.0	1.80	1.52	.28	.19	12.7
	6-20	23.3	1.81	1.49	.32	.26	17
	6-20	25.7	1.79	1.44	.35	.20	14
	6-19	6.0	1.74	1.72	.02	.09	5.5
	6-19	10.0	1.76	1.68	.08	.14	8.2
	6-19	14.9	1.75	1.60	.15	.18	11
	6-19	19.9	1.75	1.55	.20	.24	15
	6-20	20.7	1.73	1.52	.21	.27	18
	6-20	22.0	1.74	1.51	.23	.31	20.7
	6-20	23.5	1.77	1.41	.36	.30	21
	6-20	25.7	1.74	1.36	.38	.28	20

Table A.2: Upstream Received Signal Amplitude Measurements at Different Flowrates

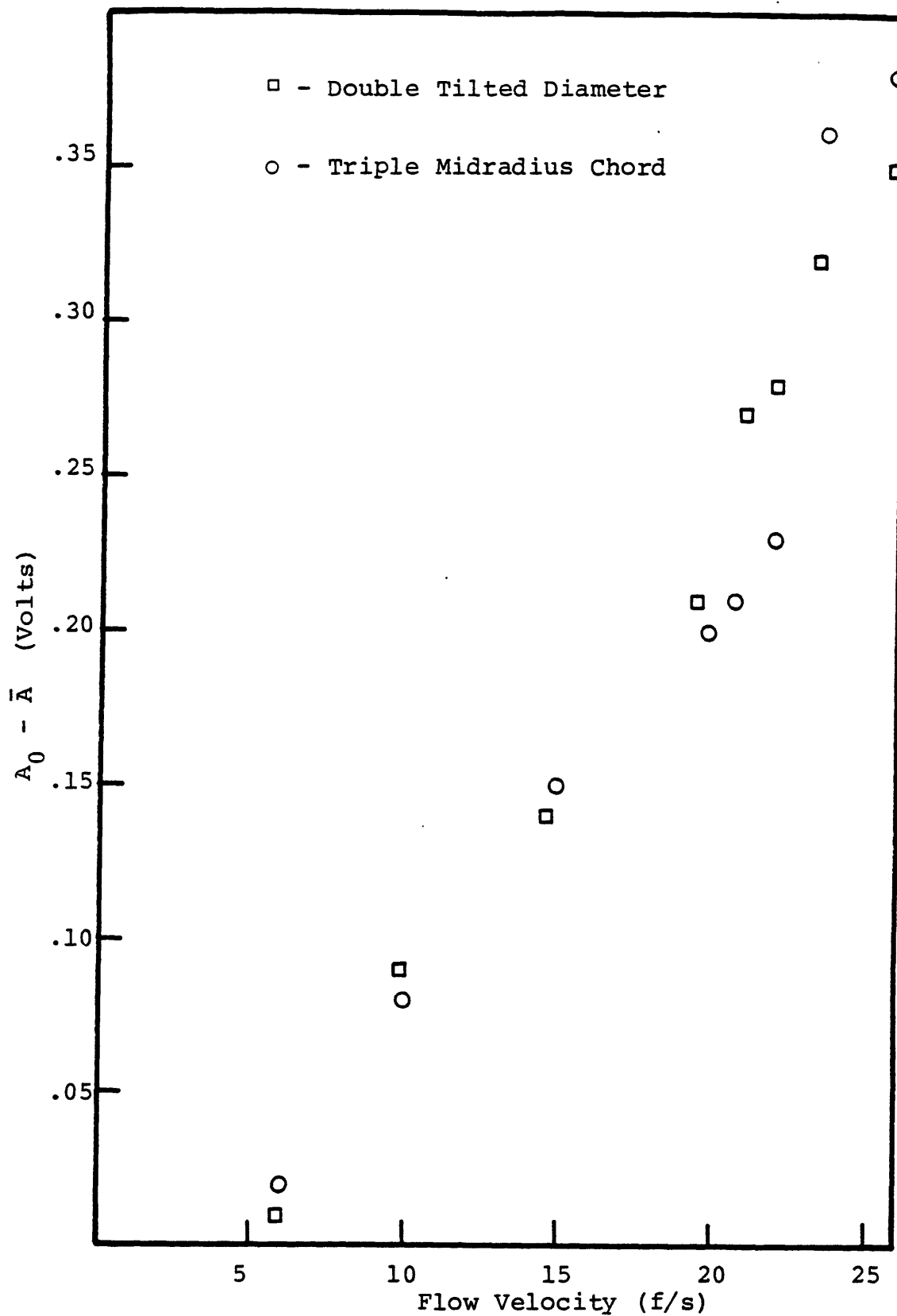


Figure A.1: Zero-Flow Received Signal Amplitude Minus Received Signal Amplitude with Flow Versus Flow Velocity

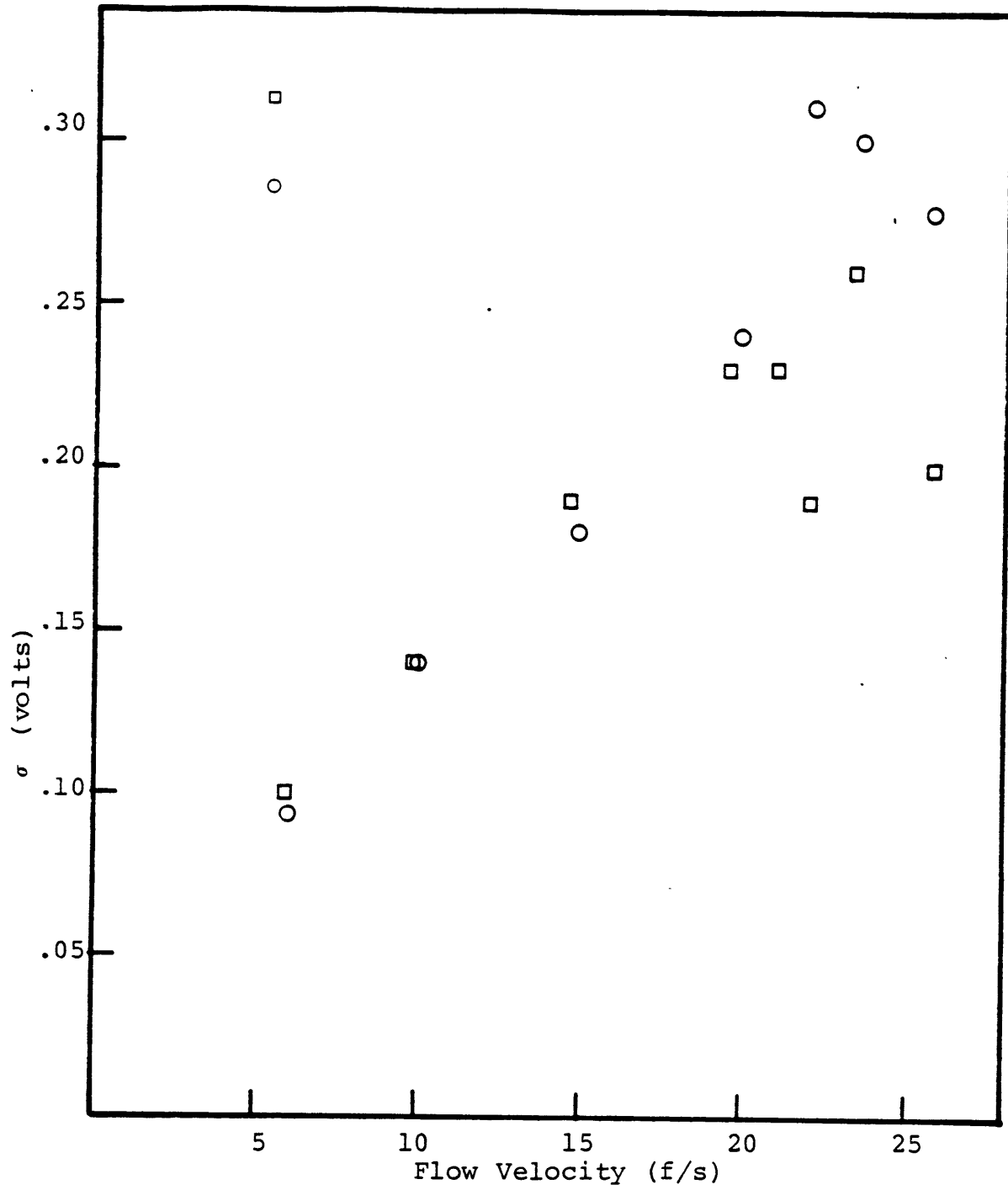


Figure A.2: Standard Deviation of Received Signal Amplitude Versus Flow Velocity

Appendix B

The Effect of Velocity Gradients on Ultrasonic Beam Angle

Appendix A describes how measurements were made which showed that the acoustic signals received at the downstream transducer with flow were stronger, on average, than the signals received at the upstream transducer. It was decided that the signal strength difference was caused by flow effects, because it existed independently of which transducer was located upstream or downstream, of coaxial cable capacitance, and of other mechanical and electronic considerations. A promising explanation of the signal strength difference - which according to this model was a combination of downstream signal strengthening and upstream signal weakening - was focusing of the downstream ultrasonic beam, and defocusing of the upstream ultrasonic beam. Using a two-dimensional plane wave model of a propagating ultrasonic pulse, it was postulated that rotation of the wave front due to velocity gradients would cause the ultrasonic beam to curve as it traversed the pipe. "Beam" refers to the path traced out by the extreme edges of a plane wave front of finite width. The edges of the beam would trace identical curves, separated initially by a perpendicular distance equal to the width of the transducer face. The perpendicular distance between the curves would - in the downstream case - decrease as the wave front propagated across the flow, as shown in Figure B.1. The thickness of the region of high velocity gradient has been greatly exaggerated in this figure. Hence, the downstream beam would undergo focusing. Similarly, divergence would occur between the sides of the upstream beam. It was reasoned that if a large amount of focusing or defocusing occurred in the region of high velocity gradient near the pipe wall where the wave entered the flow, the convergence or divergence of the beam would persist across the region of low velocity gradient in the core of the flow, and would not be removed as the wave front traversed the thin

region of high velocity gradient on the opposite side of the pipe. Thus, the focusing or defocusing would not be negated by the symmetry of the flow, and would persist to the receiving transducer.

The rotation of a differential element of a wave front as it traverses a velocity gradient is shown schematically in Figure B.2. In the case shown, the differential wavefront element undergoes rotation through a differential angle $d\theta$. The upper edge of the element is acted on by an average velocity $u + du$, and the lower edge of the element is acted upon by an average velocity u . Using the approximations listed on the diagram, the resulting expression for $d\theta$, in terms of the velocity gradient du/dy is:

$$d\theta \approx \frac{\sin^2\theta}{c \cos\theta} \left(\frac{du}{dy} \right) dy \quad (\text{B.1})$$

This expression is valid only for small changes in θ . Cook and Moffatt⁵ who were interested in wave rotation to explain the deviation of shock pulse trajectories from a straight line, derived a similar expression for $d\theta$ in terms of dt .

To get a feeling for the size of the change in θ in the M.I.T. test rig, $d\theta$ as given by Equation B.1 was integrated from one pipe wall to the centerline taking θ_0 as 45 degrees. The flow velocity u in terms of radial distance y was computed from the three term universal velocity distribution law,²⁵ using the parameters of the M.I.T. test rig with an average velocity of 25 fps. Differentiation yielded the velocity gradients in the three regions of the flow from the wall to the centerline. The integration showed that either edge of an upstream or downstream beam would undergo rotation of only 1.1 degrees. Thus, the sides of an initially parallel beam remain essentially parallel. The convergence (or divergence) shown greatly exaggerated in Figure B.1 is in fact negligible. This model cannot be said to explain the signal strength discrepancy.

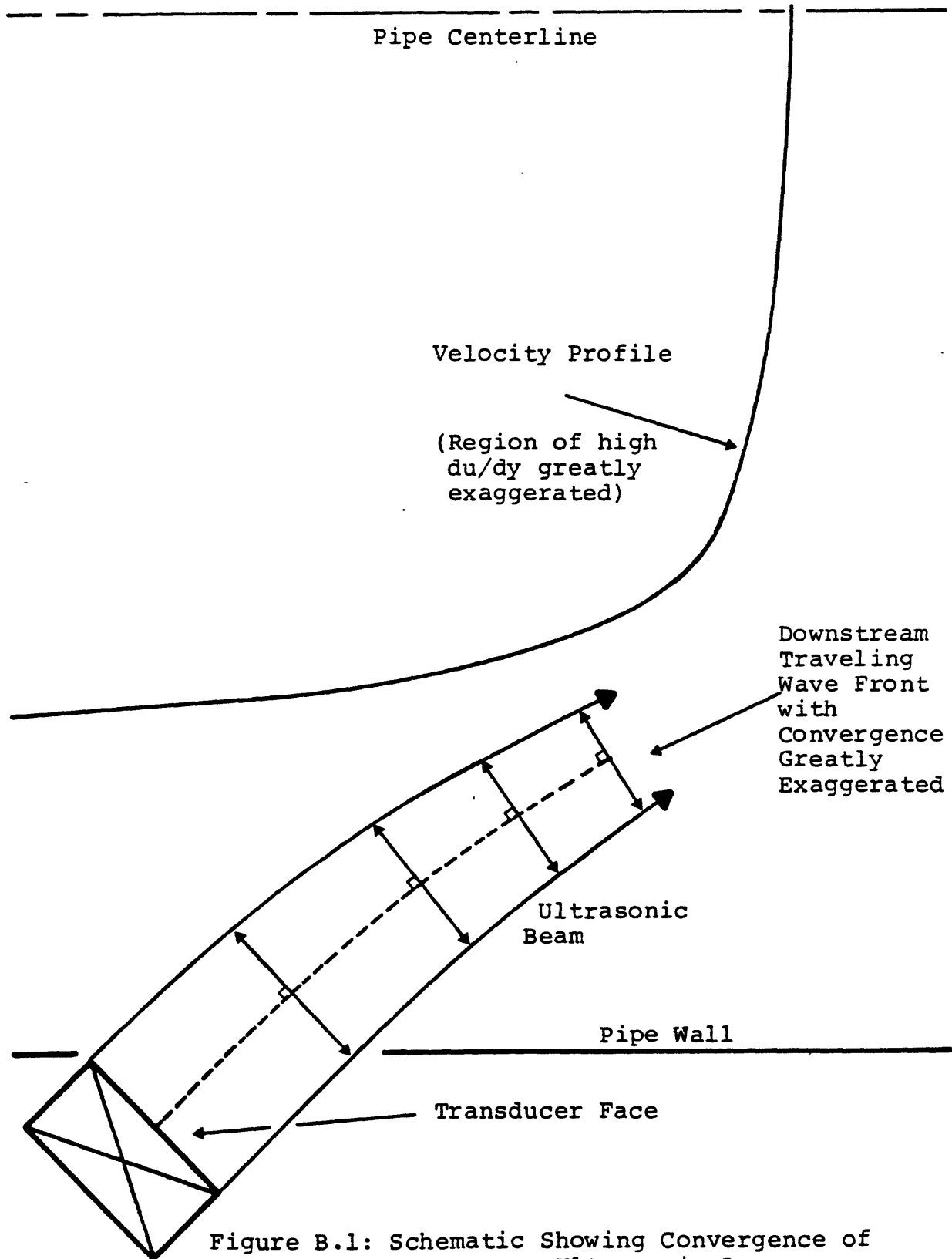
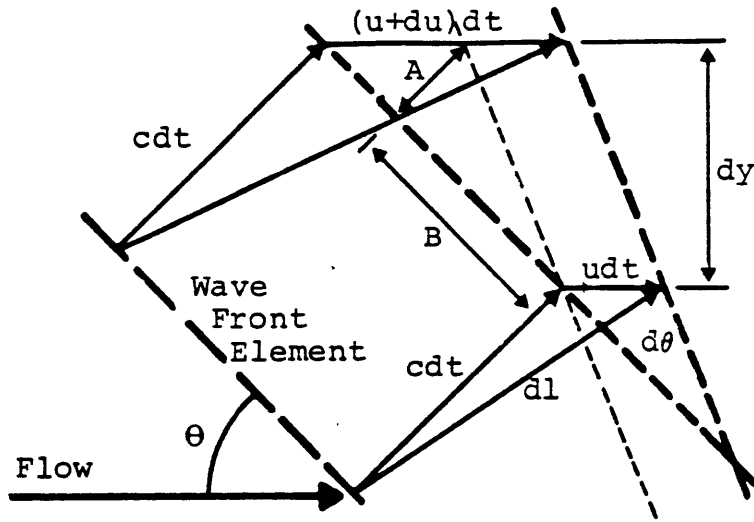


Figure B.1: Schematic Showing Convergence of Downstream Ultrasonic Beam



$$dl \approx \frac{dy}{\cos\theta}, \quad dt \approx \frac{dl}{c+u\sin\theta} \quad \longrightarrow \quad dt \approx \frac{dy}{(c+u\sin\theta)\cos\theta}$$

$$A = du\,dt\,\sin\theta \quad B \approx \frac{dy}{\sin\theta}$$



$$\tan d\theta \approx d\theta \approx \frac{du\,dt\,\sin\theta}{\left(\frac{dy}{\sin\theta}\right)} \quad \longrightarrow \quad d\theta \approx \frac{\sin^2\theta}{c\cos\theta} \left(\frac{du}{dy}\right) dy$$



Figure B.2: Wave Element Rotation Diagram


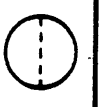
Appendix C
Ultrasonic Flowmetering Data

The following pages contain all information necessary to reproduce the ultrasonic and orifice velocity measurements shown graphically in Chapter 6. The following notation is used:



- T_0 = Zero flow dry bulb temperature, used to calculate the speed of sound C_0 for S path measurement (degrees F.).
- c_0 = Speed of sound used as stated above (f/s).
- $(t_0 - t_w)$ = Average of 200-400 upstream and downstream transit time measurements, minus the non-fluid component, t_w (microseconds). Used to calculate S pathlength.
- S = Total ultrasonic pathlength (ft.).
- L = Axial component of S (ft.).
- T_d = Dry bulb temperature (degrees F.).
- T_w = Wet bulb temperature (degrees F.).
- P_b = Barometric pressure (in. Hg).
- Δt = Transit time difference (microseconds).
- ΔP_{oa} = Pressure depression at orifice (in. water).
- ΔP_{ta} = Pressure depression at ultrasonic test section (in. water).
- h_w = Pressure differential across orifice plate (in. water).
- V_{us} = Average velocity over cross section of ultrasonic test section as measured by ultrasonic flowmeter (f/s).
- V_o = Average velocity over cross section of ultrasonic test section calculated from orifice measurements (f/s).



Date			20D Strt. Pipe ✓	D from Elbow	Test Sect. Rotation	Note			
3-11					0°				
T_0		c_0		$t_0 - t_w$		S		L	
77		1136.21		3294.43		3.743		2.682	
Run	T_d	T_w	P_b	Δt	h_w	ΔP_{oa}	ΔP_{ta}	V_{us}	V_o
1	79	68	29.63	41.05	1.296	.20	.19	9.92	9.94
2				37.57	1.089	.17	.16	9.08	9.12
3				35.26	.969	.16	.15	8.52	8.60
4				32.30	.806	.14	.13	7.80	7.84
5				23.69	.43	.09	.08	5.72	5.75
6				54.79	2.29	.32	.30	13.2	13.2
7				60.34	2.765	.38	.36	14.6	14.5
8				102.31	7.99	.99	.94	24.7	24.6
9				86.80	5.78	.75	.70	21.0	20.9
10				69.21	3.66	.48	.46	16.7	16.7



Date			20D Strt. Pipe ✓	D from Elbow	Test Sect. Rotation 45°	Note			
T_0	c_0		$t_0 - t_w$		S	L			
Run	T_d	T_w	P_b	\dot{t}	h_w	ΔP_{oa}	ΔP_{ta}	V_{us}	V_o
3-11	77	1136.21		3294.43		3.743	2.682		
1	7.7	65	29.64	102.23	7.91	.98	.93	24.6	24.4
2				98.41	7.33	.91	.87	23.7	23.5
3				90.95	6.26	.80	.76	21.9	21.7
4				83.06	5.20	.68	.63	20.0	19.8
5				75.89	4.37	.57	.54	18.3	18.2
6				55.31	2.325	.32	.30	13.3	13.3
7				23.55	.42	.08	.08	5.67	5.66
8				25.78	.50	.09	.09	6.20	6.17
9				28.27	.61	.11	.10	6.80	6.82
10				41.30	1.296	.20	.19	9.94	9.91


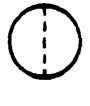
Date			20D Strt. Pipe ✓	D from Elbow	Test Sect. Rotation	Note * Temperature Correction (See Text)			
3-12					90°				
T_0 76		c_0 1135.23		$t_0 - t_w$ 3299.6		S 3.746		L 2.682	
Run	T_d	T_w	P_b	Δt	h_w	ΔP_{oa}	ΔP_{ta}	V_{us}	V_o
1	72 (75)	61	30.38	59.56	2.785	.38	.35	14.2 (14.3)	14.55 (14.30)
2				63.95	3.20	.43	.40	15.25 (15.34)	15.60 (15.32)
3				77.80	4.75	.62	.58	18.55 (18.66)	18.98 (18.65)
4				83.45	5.45	.71	.66	19.90 (20.01)	20.33 (19.98)
5				93.28	6.78	.87	.82	22.24 (22.37)	22.67 (22.29)
6	75	63	30.39	44.96	1.567	.23	.22	10.78	10.72
7				40.91	1.312	.20	.19	9.81	9.81
8				35.58	.995	.16	.15	8.53	8.56
9				31.20	.768	.13	.12	7.48	7.53
10				23.61	.44	.08	.08	5.70	5.70


* V_{us} and V_o values in parentheses were calculated using a corrected T_d value of 75° F. (See text).



Date			20D Strt. Pipe ✓	D from Elbow	Test Sect. Rotation 135°	Note			
T ₀ 76		c ₀ 1135.23		t ₀ - t _w 3299.6		S 3.746		L 2.682	
Run	T _d	T _w	P _b	Δt	h _w	ΔP _{oa}	ΔP _{ta}	V _{us}	V _o
1	75	63	30.39	23.77	.44	.08	.08	5.70	5.70
2				28.96	.647	.11	.10	6.95	6.91
3				31.21	.755	.13	.12	7.49	7.46
4				38.51	1.14	.18	.17	9.24	9.16
5				47.61	1.742	.26	.24	11.4	11.3
6	76	62	30.39	101.69	8.01	.99	.93	24.4	24.2
7				96.26	7.20	.91	.85	23.1	22.9
8				88.89	6.145	.79	.74	21.4	21.2
9				83.32	5.34	.70	.68	20.0	19.8
10				77.33	4.655	.61	.57	18.6	18.5



Date			20D Strt. Pipe	D from Elbow	Test Sect. Rotation	Note			
3-3				10	0°				
T_0 77		c_0 1136.3		$t_0 - t_w$ 3290.5		S 3.739		L 2.685	
Run	T_d	T_w	P_b	Δt	h_w	ΔP_{oa}	ΔP_{ta}	V_{us}	V_o
1	77	66	29.91	101.89	7.91	1.05	1.00	24.5	24.3
2				94.50	6.84	.94	.89	22.7	22.6
3				83.25	5.31	.75	.70	20.0	19.9
4				77.11	4.57	.65	.60	18.6	18.5
5				71.93	3.96	.56	.53	17.3	17.2
6				66.47	3.42	.49	.46	16.0	16.0
7				53.94	2.23	.34	.32	12.9	13.0
8				46.71	1.70	.27	.26	11.2	11.3
9				41.99	1.34	.22	.21	10.1	10.1
10				23.22	.41	.09	.08	5.58	5.58


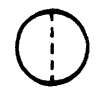
Date			20D Strt. Pipe	D from Elbow	Test Sect. Rotation	Note			
3-5				10	45°				
T_0	c_0	$t_0 - t_w$	S	L					
76	1135.23	3291.6	3.737	2.682					
Run	T_d	T_w	P_b	Δt	h_w	ΔP_{oa}	ΔP_{ta}	V_{us}	V_o
1	78	67	29.99	102.46	7.97	1.06	1.01	24.7	24.4
2				94.08	6.72	.93	.87	22.7	22.4
3				83.85	5.36	.76	.71	20.2	20.0
4				75.19	4.315	.61	.57	18.2	18.0
5				69.15	3.67	.52	.49	16.7	16.6
6				65.01	3.23	.46	.44	15.7	15.6
7				55.09	2.31	.35	.32	13.3	13.2
8				48.28	1.76	.27	.26	11.7	11.5
9				41.18	1.29	.21	.20	9.94	9.85
10				23.66	.43	.09	.08	5.71	5.71



Date			20D Strt. Pipe	D from Elbow	Test Sect. Rotation	Note			
3-3				10	90°				
T_0 77		c_0 1136.3		$t_0 - t_w$ 3290.5	S 3.739	L 2.685			
Run	T_d	T_w	P_b	Δt	h_w	ΔP_{oa}	ΔP_{ta}	V_{us}	V_o
1	77	68	29.91	23.66	.42	.09	.08	5.74	5.65
2				35.44	.96	.17	.16	8.52	8.51
3				42.04	1.35	.22	.21	10.1	10.1
4				46.85	1.67	.27	.25	11.3	11.2
5				56.14	2.42	.36	.34	13.5	13.5
6				65.52	3.00	.44	.41	15.0	14.9
7				72.38	4.01	.57	.54	17.4	17.3
8				82.16	5.17	.73	.69	19.8	19.7
9				93.31	6.68	.92	.87	22.4	22.4
10				101.59	7.92	1.05	1.00	24.4	24.4



Date		20D Strt. Pipe	D from Elbow	Test Sect. Rotation	Note				
3-5			10	135°					
T_0	c_0	$t_0 - t_w$	S	L					
76	1135.23	3291.6	3.737	2.682					
Run	T_d	T_w	P_b	Δt	h_w	ΔP_{oa}	ΔP_{ta}	V_{us}	V_o
1	76	65	30.01	23.61	.42	.09	.08	5.67	5.63
2				29.14	.64	.12	.11	7.00	6.93
3				40.44	1.245	.20	.19	9.72	9.65
4				48.40	1.775	.28	.28	11.6	11.5
5				59.53	2.72	.40	.38	14.3	14.2
6				69.49	3.72	.53	.50	16.7	16.7
7				79.39	4.82	.69	.64	19.1	18.9
8				87.09	5.76	.81	.76	20.9	20.7
9				93.68	6.69	.93	.87	22.5	22.3
10				102.67	7.97	1.07	1.01	24.7	24.3



Date			20D Strt. Pipe	D from Elbow	Test Sect. Rotation	Note			
G-26				G	0°				
T_0 77		c_0 1136.27		$t_0 - t_w$ 3199.43	S 3.635	L 2.578			
Run	T_d	T_w	P_b	Δt	h_w	ΔP_{oa}	ΔP_{ta}	V_{us}	V_o
1	76.8	69	29.72	21.86	.388	.09	.08	5.47	5.44
2	76.9			29.79	.726	.14	.13	7.46	7.44
3	77.1			32.72	.875	.16	.15	8.20	8.16
4	77.2			35.30	1.025	.18	.17	8.84	8.84
5	77.7			39.99	1.30	.22	.20	10.03	9.94
6	78.1	71	29.71	42.89	1.497	.25	.23	10.8	10.6
7	78.1			46.76	1.78	.29	.27	11.7	11.6
8	77.9			55.78	2.495	.38	.35	14.0	13.7
9	77			66.15	3.525	.52	.49	16.6	16.3
10	76.7			76.15	4.65	.67	.63	19.1	18.7



Date			20D Strt. Pipe	D from Elbow	Test Sect. Rotation		Note		
G-26				6	45°				
T_0 77		c_0 1136.27		$t_0 - t_w$ 3201.1		S 3.637		L 2.578	
Run	T_d	T_w	P_b	Δt	h_w	ΔP_{oa}	ΔP_{ta}	V_{us}	V_o
1	77.1	71.5	29.70	22.53	.415	.09	.09	5.64	5.64
2	76.9			26.86	.590	.12	.11	6.73	6.72
3	77			32.50	.877	.16	.15	8.14	8.17
4	77.5			40.04	1.315	.22	.21	10.0	10.0
5	77.8			45.34	1.695	.27	.26	11.4	11.3
6	77	70	29.70	55.50	2.485	.38	.35	13.9	13.7
7	76.5			63.89	3.31	.49	.46	16.0	15.81
8	76.7			69.89	3.955	.57	.54	17.5	17.3
9	76.9			78.27	4.94	.71	.67	19.6	19.3
10	77			84.04	5.675	.80	.76	21.0	20.7



Date			20D Strt. Pipe	D from Elbow	Test Sect. Rotation	Note			
6-26				G	90°				
T_0 77.8		c_0 1137.11		$t_0 - t_w$ 3200.73	S 3.640	L 2.578			
Run	T_d	T_w	P_b	Δt	h_w	ΔP_{oa}	ΔP_{ta}	V_{us}	V_o
1	76.6	68	29.70	22.81	.428	.09	.09	5.71	5.72
2	76.5			25.85	.555	.11	.11	6.47	6.51
3	76.9			31.14	.815	.15	.14	7.80	7.88
4	77			34.46	1.015	.18	.17	8.63	8.79
5	77.2			41.76	1.46	.24	.23	10.5	10.5
6	77.9	68	29.70	46.75	1.825	.29	.27	11.7	11.7
7	77.3			52.72	2.298	.35	.33	13.2	13.2
8	76.1			64.78	3.475	.50	.48	16.2	16.2
9	76			73.66	4.44	.64	.60	18.4	18.3
10	76			80.82	5.40	.76	.73	20.2	20.2



Date			20D Strt. Pipe	D from Elbow	Test Sect. Rotation	Note			
6-26				6	135°				
T_0		c_0		$t_0 - t_w$	S		L		
76.8		1136.06		3202.53	3.638		2.578		
Run	T_d	T_w	P_b	Δt	h_w	ΔP_{oa}	ΔP_{ta}	V_{us}	V_o
1	75.5	66	29.72	22.22	.407	.09	.08	5.50	5.57
2	75.8			26.67	.585	.12	.11	6.66	6.67
3	76.1			31.65	.833	.15	.14	7.91	7.95
4	76.1			38.76	1.25	.21	.20	9.69	9.61
5	76.9			42.84	1.515	.25	.23	10.7	10.7
6	77.6	68	29.72	47.32	1.835	.29	.28	11.9	11.8
7	76.5			53.40	2.327	.35	.33	13.4	13.2
8	76			66.51	3.595	.53	.49	16.6	16.5
9	76			80.62	5.19	.74	.70	20.1	19.8
10	76			89.65	6.43	.91	.86	22.4	22.0



Date			20D Strt. Pipe ✓	D from Elbow	Test Sect. Rotation	Note			
6-16					0°				
T_0 77.3		c_0 1136.58		$t_0 - t_w$ 2475.4	S 2.814	L 2.00			
Run	T_d	T_w	P_b	Δt	h_w	ΔP_{oa}	ΔP_{ta}	V_{us}	V_o
1	75.5	67	30.23	86.00	8.00	1.04	.98	26.1	24.3
2	76			83.18	7.51	.98	.93	25.2	23.6
3	77			64.44	4.54	.63	.58	19.6	18.4
4	76.6			59.42	3.88	.54	.50	18.0	17.0
5	76.6			47.58	2.50	.38	.34	14.4	13.6
6	77.5	67	30.22	41.15	1.87	.28	.26	12.5	11.8
7	77.8			37.15	1.545	.24	.22	11.3	10.7
8	78			33.98	1.32	.21	.20	10.3	9.93
9	78			27.05	.84	.14	.14	8.20	7.94
10	77.5			20.14	.48	.10	.09	6.09	6.00



Date			20D Strt. Pipe ✓	D from Elbow	Test Sect. Rotation	Note			
6-23					0°				
T_0	c_0	$t_0 - t_w$	S	L					
79.9	1139.33	2485.2	2.831	2.029					
Run	T_d	T_w	P_b	Δt	h_w	ΔP_{oa}	ΔP_{ta}	V_{us}	V_o
1	78.8	71	29.96	20.19	.45	.09	.09	6.03	5.86
2	79			22.75	.58	.11	.10	6.80	6.64
3	79.2			27.44	.847	.15	.14	8.21	8.02
4	80			31.50	1.125	.19	.18	9.45	9.24
5	80.2			37.06	1.56	.25	.23	11.1	10.9
6	80	73	29.96	45.01	2.29	.34	.32	13.5	13.1
7	79.8			56.90	3.72	.53	.49	17.1	16.8
8	80			62.37	4.48	.62	.58	18.8	18.4
9	81			71.80	5.91	.82	.77	21.7	21.1
10	81.5			80.74	7.64	1.01	.95	24.4	24.0



Date			20D Strt. Pipe ✓	D from Elbow	Test Sect. Rotation	Note			
6.23					45°				
T_0	c_0	$t_0 - t_w$	S	L					
81	1140.49	2486.25	2.836	2.029					
Run	T_d	T_w	P_b	Δt	h_w	ΔP_{oa}	ΔP_{ta}	V_{us}	\dot{V}_o
1	81.1	67	29.96	18.64	.42	.09	.08	5.59	5.66
2	81			24.84	.747	.14	.13	7.45	7.54
3	81.6			30.22	1.092	.18	.17	9.09	9.10
4	82			33.44	1.33	.22	.20	10.1	10.0
5	82			40.07	1.89	.29	.27	12.1	11.9
6	81.5	68	29.96	46.87	2.60	.38	.36	14.1	14.0
7	81.5			67.98	5.405	.75	.70	20.5	20.2
8	82			72.44	6.11	.84	.79	21.9	21.5
9	82			75.25	6.60	.89	.84	22.7	22.3
10	82.1			82.86	7.93	1.04	.98	25.1	24.5



Date			20D Strt. Pipe ✓	D from Elbow	Test Sect. Rotation	Note			
6-19					90°				
T_0 82.1		c_0 1141.65		$t_0 - t_w$ 2459.3	S 2.808	L 2.00			
Run	T_d	T_w	P_b	Δt	h_w	ΔP_{oa}	ΔP_{ta}	V_{us}	V_o
1	81.1	76.5	29.72	19.68	.450	.1	.09	5.90	5.89
2	82.0			23.89	.665	.13	.12	7.15	7.16
3	82.7			28.84	.980	.17	.16	8.68	8.69
4	83.2			32.15	1.215	.20	.19	9.67	9.67
5	83.5			38.84	1.78	.27	.26	11.7	11.7
6	83.4	76	29.72	46.68	2.59	.38	.35	14.1	14.1
7	83.5			59.36	4.26	.59	.55	18.1	18.1
8	83.7			65.55	5.26	.72	.67	20.1	20.1
9	83.2			69.29	5.81	.79	.74	21.2	21.1
10	83.6			80.82	7.95	1.03	.97	24.8	24.7



Date			20D Strt. Pipe ✓	D from Elbow	Test Sect. Rotation 90°	Note			
T_0	c_0		$t_0 - t_w$		S	L			
6-23	82°	1141.55	2480.05	2.831	2.029				
Run	T_d	T_w	P_b	Δt	h_w	ΔP_{oa}	ΔP_{ta}	V_{us}	V_o
1	81.9	72	29.96	19.66	.455	.10	.09	5.91	5.90
2	81.8			22.24	.586	.12	.11	6.68	6.69
3	82			26.76	.860	.15	.14	8.05	8.09
4	82.4			32.22	1.25	.2	.2	9.71	9.75
5	82.7			39.92	1.91	.29	.27	12.0	12.0
6	82	70	29.96	46.30	2.55	.37	.35	14.0	13.9
7	82			61.30	4.42	.62	.58	18.5	18.3
8	82.1			68.94	5.61	.78	.73	20.8	20.6
9	82.5			73.20	6.32	.86	.81	22.1	21.9
10	82.8			82.13	7.95	1.05	.99	24.9	24.6



Date				20D Strt. Pipe ✓	D from Elbow	Test Sect. Rotation 135°	Note		
T ₀		c ₀		t ₀ - t _w		S		L	
82.8		1142.39		2478.95		2.832		2.029	
Run	T _d	T _w	P _b	Δt	h _w	ΔP _{oa}	ΔP _{ta}	V _{us}	V _o
1	81.5	71	29.95	18.53	.41	.09	.08	5.56	5.60
2	81.5			24.11	.697	.13	.12	7.24	7.30
3	82.0			27.56	.907	.16	.15	8.29	8.31
4	82.4			36.20	1.547	.25	.23	10.9	10.8
5	82.9			41.16	1.92	.30	.28	12.4	12.1
6	81.6	70	29.95	47.70	2.62	.38	.36	14.4	14.1
7	82			62.69	4.45	.62	.59	18.9	18.4
8	82			68.33	5.24	.73	.69	20.7	19.9
9	82.2			72.86	5.93	.82	.77	22.0	21.2
10	82.8			81.10	7.39	.98	.93	24.6	23.7

Date			20D Strt. Pipe	D from Elbow	Test Sect. Rotation	Note			
6-15				6	0°				
T_0 76.5	c_0 1135.74	$t_0 - t_w$ 2532.3	S 2.876	L 2.089					
Run	T_d	T_w	P_b	Δt	h_w	ΔP_{oa}	ΔP_{ta}	V_{us}	V_o
1	76	59	30.00	19.00	.445	.10	.09	5.48	5.79
2	78			23.13	.655	.12	.12	6.70	7.07
3	77.5			26.4	.88	.16	.15	7.65	8.13
4	78			28.9	1.03	.18	.17	8.38	8.79
5	78			36.77	1.63	.26	.25	10.68	11.0
6	77	66	29.99	42.70	2.26	.34	.32	12.38	13.0
7	77			48.73	2.88	.42	.40	14.14	14.7
8	77			53.37	3.47	.50	.47	15.49	16.1
9	77			68.03	5.45	.78	.73	19.78	20.2
10	77			77.3	7.10	.97	.91	22.48	23.0

Date			20D Strt. Pipe	D from Elbow	Test Sect. Rotation	Note			
6-24				6	45°				
T_0 77.9		c_0 1137.22		$t_0 - t_w$ 2488.78		S 2.830		L 2.029	
Run	T_d	T_w	P_b	Δt	h_w	ΔP_{oa}	ΔP_{ta}	V_{us}	V_o
1	77.2	70	30.03	17.56	.43	.09	.09	5.23	5.71
2	77.6			27.73	1.075	.18	.17	8.28	9.01
3	77.9			29.84	1.246	.21	.20	8.91	9.68
4	78			32.25	1.446	.24	.22	9.64	10.4
5	78.2			37.24	1.92	.30	.28	11.1	12.0
6	77.9	69	30.03	42.86	2.53	.38	.35	12.8	13.8
7	77.8			52.00	3.71	.53	.50	15.6	16.7
8	77.9			62.39	5.306	.75	.70	18.7	20.0
9	77.5			71.90	7.01	.96	.90	21.5	22.9
10	77.9			76.18	8.00	1.06	1.01	22.8	24.5

Date			20D Strt. Pipe	D from Elbow	Test Sect. Rotation	Note			
6-15				6	90°				
T_0 78		c_0 1137.33		$t_0 - t_w$ 2530.6		S 2.878	L 2.089		
Run	T_d	T_w	P_b	Δt	h_w	ΔP_{oa}	ΔP_{ta}	v_{us}	v_o
1	77	66	29.99	18.18	.43	.09	.09	5.25	5.70
2	77.5			23.93	.76	.14	.13	6.93	7.57
3	78			27.38	.995	.18	.16	7.94	8.66
4	78.5			29.92	1.19	.20	.19	8.69	9.47
5	78			33.21	1.46	.24	.23	9.64	10.5
6	78.5	67	29.99	41.87	2.33	.35	.33	12.2	13.2
7	78.5			56.10	4.16	.60	.58	16.3	17.7
8	78.5			63.80	5.18	.75	.70	18.6	19.7
9	78.5			71.85	6.90	.95	.91	21.0	22.7
10	79			77.92	7.96	1.08	1.03	22.7	24.4

Date			20D Strt. Pipe	D from Elbow	Test Sect. Rotation	Note			
6-24				6	135°				
T_0	c_0	$t_0 - t_w$	S	L					
77.0	1136.27	2491.25	2.831	2.029					
Run	T_d	T_w	P_b	Δt	h_w	ΔP_{oa}	ΔP_{ta}	V_{us}	V_o
1	76.9	69	30.05	17.53	.428	.09	.08	5.21	5.69
2	77			22.07	.695	.13	.12	6.57	7.24
3	77			25.58	.925	.16	.15	7.63	8.34
4	77.8			31.97	1.44	.23	.22	9.56	10.4
5	78			35.74	1.796	.28	.26	10.7	11.6
6	77.6	70	30.05	42.83	2.57	.38	.36	12.8	13.9
7	77.4			55.27	4.25	.61	.57	16.5	17.8
8	77.3			63.95	5.72	.80	.75	19.2	20.7
9	77.1			73.65	7.585	1.02	.96	22.1	23.8
10	77.2			76.37	7.90	1.06	1.00	22.9	24.3

Date			20D Strt. Pipe ✓	D from Elbow	Test Sect. Rotation 0°	Note See below *			
T ₀ 78.0		c ₀ 1137.33		t ₀ - t _w 2446.53		S 2.783	L 1.984		
Run	T _d	T _w	P _b	Δt	h _w	ΔP _{oa}	ΔP _{ta}	V _{us}	V _o
1	77.2	72	29.77	18.25	.393	.09	.08	5.55	5.55
2	77.9			24.26	.71	.13	.12	7.40	7.45
3	77.9			27.75	.927	.16	.15	8.48	8.50
4	78.1			29.62	1.06	.18	.17	9.05	9.09
5	78.2			34.43	1.427	.23	.22	10.5	10.5
6	78.0	72.5	29.77	44.77	2.42	.35	.33	13.7	13.7
7	78.1			63.13	4.835	.67	.63	19.4	19.4
8	78.0			70.87	6.16	.84	.79	21.7	21.9
9	78.1			76.09	7.09	.95	.90	23.3	23.5
10	78.1			80.50	7.98	1.04	.99	24.7	24.9

* Pulses reflected from rolled roofing material.
See text.

References

1. Bender, Donald A., "An Ultrasonic Flowmeter for Gases," Master's Thesis, M.I.T. (Oct, 1982).
2. Lynnworth, L.C., U.S. Patent 4,103,551 (1978).
3. Annubar Flow Measurement, Industrial Line, catalog, Dieterich Standard Corporation, Boulder, CO (1978).
4. Ken, of Massa Products, Inc., telephone conversation with the Author (May 6, 1983).
5. Cook, F. Bert and Moffatt, E., "Flow Meter for High Pressure Gases Using Sonic Pulses," in Advances in Instrumentation, I.S.A. International Instrumentation and Automation Conference (Oct, 1974).
6. Smalling, J.W. and Braswell, L.D., with Lynnworth, L.C. and Wallace, D.R., "Flare Gas Ultrasonic Flowmeter," in Proceedings, Thirty-Ninth Annual Symposium on Instrumentation for the Process Industries, Dept. of Chemical Engineering, Texas A&M University (Jan, 1984).
7. Nolan, M.E. and O'Hair, J.G., "The Development of a Multipath Ultrasonic Flowmeter for the Measurement of High Pressure Gas Flows," I.G.R.C./A23-83, given at the International Gas Research Conference, London (June, 1983).
8. Lynnworth, L.C., of Panametrics, Inc., Waltham, MA, private communication with the Author (Aug, 23, 1984).
9. Kivilis, S.S., and Reshetnikov, V.A., "Hydromechanical Error in Ultrasonic Flowmeters," translated from Izmeritel'naya Tekhnika, in Measurement Techniques (a publication of the Academy of Sciences of the U.S.S.R.), No. 11 (Nov, 1965), pp. 1057-1059.
10. Lynnworth, L.C., "Selected Alternatives to Conventional Ultrasonic Flowmeter Cell Designs," Proceedings, Ultrasonics International Conference and Exhibition, Brighton, U.K. (June, 1977).
11. Fox, R.W. and McDonald, A.T., Introduction to Fluid Mechanics, Second Edition, Wiley, New York (1978).
12. A.S.M.E. Research Committee on Fluid Meters, Flowmeter Computation Handbook, A.S.M.E., New York (1961).
13. Lynnworth, L.C., et. al., of Panametrics, Inc., Waltham, MA, private communications with the Author (Spring 1983-Fall 1984).

14. Lynnworth, L.C., Patch, D.R., and Mellish, W.C., "Impedance-Matched Metallurgically Sealed Transducers," I.E.E.E. Transactions on Sonics and Ultrasonics, Vol. SU-31, No. 2 (March 1984), pp. 101-104.
15. Lynnworth, L.C., of Panametrics, Inc., Waltham, MA, private communication with the Author (Aug, 28, 1984).
16. Munk, W.D., "The Ultrasonic Flowmeter - a New Approach to Gas Measurement," Pipe Line Industry (April, 1983), pp. 65-68.
17. Pederson, N.E., Bradshaw, J.E., Lynnworth, L.C., and Morel, P.R., "A New Ultrasonic Flowmeter for the Natural Gas Industry," N.B.S. Special Publication 484, Proceedings of the Symposium on Flow in Open Channels and Closed Conduits, N.B.S., Gaithersburg, MD, February, 1977 (Issued Oct, 1977).
18. Baker, R.C., and Thompson, E.J., "A Two Beam Ultrasonic Phase-Shift Flowmeter," in Fluid Flow Measurement in the Mid-1970's, Vol. 2, Proceedings of a Conference Held at the National Engineering Laboratory, Spencer, E.A. and Ramsay, W.J., Editors, Her Majesty's Stationery Office, Edinburgh (April, 1975), pp. 571-582.
19. Doebelin, E.O., Measurement Systems: Application and Design, McGraw-Hill, New York (1966), p. 568.
20. Weast, R.C., Ed., C.R.C. Handbook of Chemistry and Physics, Sixty-Second Edition, C.R.C. Press, Boca Raton, Florida (1981), p. E-50.
21. Anderson, J.D., Jr., Modern Compressible Flow, McGraw-Hill, New York (1982), p. 48.
22. A.S.H.R.A.E. Standard 51-75, "Laboratory Methods of Testing Fans for Rating Purposes," Technical Report, American Society of Heating, Refrigeration, and Air Conditioning Engineers (1972).
23. Lynnworth, L.C., and Matson, J.E., U.S. Patent application No. 518,344, "Integrated Threshold Arming Method and Apparatus," (July 29, 1983).
24. McShane, J.L., "Ultrasonic Flowmeters," in Advances in Instrumentation, I.S.A. International Instrumentation and Automation Conference (Oct, 1974).
25. Rohsenow, W.M., and Choi, H.Y., Heat, Mass, and Momentum Transfer, Prentice-Hall, NJ (1961), p. 72.
26. Mertens, H., of Consolidated Edison, Gas Engineering Dept., comment at project meeting, M.I.T. (Nov, 1983).

27. Nguyen, T.H. and Lynnworth, L.C., "Zigzag Flowcells," in Proceedings of the Ultrasonics Symposium, (Oct. 31, Nov. 1, 2, 1983).